Title
Secondary Organic Aerosol Formation From Aromatic Hydrocarbon

Author
Tang, Ping

Publication Date
2013

UNIVERSITY OF CALIFORNIA
RIVERSIDE

Secondary Organic Aerosol Formation From Aromatic Hydrocarbons

A Dissertation submitted in partial satisfaction
of the requirements for the degree of

Doctor of Philosophy

in

Chemical and Environmental Engineering

by

Ping Tang

August 2013

Dissertation Committee:
Dr. David R. Cocker III, Chairperson
Dr. Akua Asa-Awuku
Dr. Roya Behreini

This Dissertation of Ping Tang is approved:

____

____

____
Committee Chairperson

University of California, Riverside

Acknowledgements

With my graduate study approaching the end, I would like to show my gratitude to many individuals who have given me the professional guidance and personal support during the past four and a half years. This dissertation would not have been possible without them.

First, I would like to thank my advisor, Prof. David Cocker for his excellent guidance, caring, patience, and providing me with a flexible atmosphere for doing research. Not only did I gain technical knowledge and professional capability from him, but I also improved my skills in research, writing and presentation. His positive attitude made my five years in his research group exciting and fun. In addition to scientific knowledge and technical skills, He has given me a number of opportunities to mentor students and collaborate with others, which were critical in my professional development.

I would like to show my gratitude to the previous and current graduate students for their assistance and advice. Dr. Quentin Malloy, Dr. Li Qi, Dr. Christopher Clark and Dr. Shunsuke Nakao joined in the Atmospheric Processes Lab before me and patiently trained me on a number of experimental techniques and instrument troubleshooting. Especially, during the four years working with Dr. Nakao, he always gave me his best suggestions and patient help. Thanks must also be given to graduate students, Dr. Xiaochen (Esther) Tang, current students, Ms. Chia-Li (Candice) Chen and Mr. Derek Price for contributing to keep the chamber running, as well as some of the data processing for this work. Also, several undergraduate students helped the operation of the instruments and data processing during my graduate study. Thanks should be given to Mr. Eric Praske, Ms. Lorelei Adams, Mr. Thomas Kwan, Ms. Sarah Bates, Mr. Dylan Switzer, Mr. Gary Liu, and Mr. Ali Roohani. Completion of this work will not have happened without the assistance and support of CE-CERT staff members, including but not limited to Mr. Kurt Bumiller, Mr. Charles Bufalino, Mr. Dennis Fitz, Ms. Kathy Cocker, and Mr. Todd Ambriz.

I would like to thank my advisory committee Dr. Akua Asa-Awuku and Dr. Roya Behreini for their time and advice during developing this dissertation. Dr. Paul Ziemann, Dr. Jingsong Zhang and Dr. Yushan Yan gave me valuable comments during my proposal defense. In addition, thanks should be given to W.M. Keck Foundation, National Science Foundation, UCR- Department of Chemical and Environmental Engineering and UCR Dissertation Year Program.

Last but not least, I would also like to give special thanks to my loved parents and husband. Even though you may not understand exactly what I have been doing, I could not have gotten here without your support. Thank you for being there for me all the time, and encouraging me to get out of those tense and stressed moments.

The text of this dissertation, in part, is a reprint of the material as is appears in Nakao *et al.* (Atmospheric Environment 68, 273–277, 2012). The co-author listed in that publication directed and supervised the research which forms the basis for this dissertation.

ABSTRACT OF THE DISSERTATION

Secondary Organic Aerosol Formation From Aromatic Hydrocarbons

by

Ping Tang

Doctor of Philosophy, Graduate Program in Chemical and Environmental Engineering
University of California, Riverside, August 2013
Dr. David R Cocker III, Chairperson

Secondary organic aerosol (SOA) from 17 aromatic hydrocarbons is explored in depth for simulated atmospheric photooxidation conditions. The overall objective of this study is to improve our understanding of the chemical and physical processes leading to SOA formation for aromatic systems and identify the key critical parameters necessary to accurately predict SOA formation.

SOA formation potential under low-NO_X atmospheric conditions is found to decrease as the carbon number of parent aromatic hydrocarbon increases while no aerosol formation trends are observed with carbon number for no-NO_X systems. This trend is attributed to the formation of greater fractions of low vapor pressure ring-retaining products from the lighter aromatic hydrocarbons. SOA chemical composition, measured using the Aerodyne High-resolution Time-of-Flight Mass Spectrometer (HR-ToF-AMS), is evaluated for both low-NO_X and no-NO_X conditions. Generally, aerosol formed in this study is observed to be less oxidized than ambient SOA. It is further observed that aerosol formed from aromatics with less substituents attached to the ring has a lower m/z 43 to m/z 44 ratio and a higher O/C ratio, which indicates that lighter aromatic precursors produced a more oxidized SOA than the heavier aromatic precursors. SOA Volatility further supports the observations that lower vapor pressure and more oxidized products of SOA are produced from lighter compounds. A recently proposed empirical relationship between SOA density and elemental ratio (O/C and H/C) is evaluated against real-time density measurements in an effort to extend the applicability of the empirical relationship to aromatic SOA.

Finally, a gas-phase reaction model (SAPRC-11) is used to predict the OH and HO_2 levels present for the different aromatic oxidation systems. Generally, it is observed that aerosol formation decreased with increasing $[OH]/[HO_2]$ ratios for both low NO_X and no-NO_X experiments. This trend is possibly attributed to fragmentation of intermediate compounds to form organics with higher volatility in OH radical abundant environments. It is expected that $[OH]/[HO_2]$ ratio can be utilized to help improve the extrapolation of environmental chamber results to prediction of ambient SOA from aromatic precursors.

Table of Contents

List of Tables

List of Figures

1 Introduction

1.1 Introduction of Dissertation

Atmospheric aerosols are defined as a suspension of liquid or solid particles in air. They are formed from a wide variety of natural and anthropogenic sources. Particles emitted directly from sources such as biomass burning, combustion of fossil fuels and cooking operation are called primary organic aerosol (POA). Additionally, the atmospheric photooxidation of volatile organic compounds (VOCs) can lead to products that have sufficiently low vapor pressure to partition between the gas and particulate phase. Organic particulate arising from this path is referred to as secondary organic aerosol (SOA), which accounts for approximately 70% of organic carbon mass globally (Hallquist *et al.*, 2009; Lanz *et al.*, 2007a; Turpin and Huntzicker, 1995; Q. Zhang *et al.*, 2005).

The impact of organic aerosols on both human health (Davidson *et al.*, 2005; Harrison and Yin, 2000) and global climate (Andreae and Crutzen, 1997; Haywood and Boucher, 2000) has long been recognized. However, there are significant uncertainties to fully understanding the health and climate effects of atmospheric aerosols because of a lack of knowledge of their sources, composition, properties and formation mechanism.

The traditional view of SOA formation is dominated by the oxidation of a few classes of VOCs (mostly monoterpenes and aromatics), followed by partitioning of gas-phase semi-volatile organics between the gas-e and particle-phase (Odum *et al.*, 1996; Pankow, 1994). A number of laboratory studies (e.g., Atkinson *et al.*, 1989; Calvert *et al.*, 2002; Griffin *et al.*, 1999; Hurley *et al.*, 2001; Odum *et al.*, 1997) have quantified SOA formation from individual precursors for integration into atmospheric chemical transport models. However, recent studies have suggested that current models informed by chamber measurements often predict far less SOA than is observed (de Gouw *et al.*, 2005; Heald *et al.*, 2005; Kleinman *et al.*, 2008; Volkamer *et al.*, 2006). Several key factors including differences between chamber experiments and atmosphere conditions, incomplete treatment of SOA chemistry (uncertainties in heterogeneous and multiphase reactions) and omission of additional SOA precursors in models are identified as reasons for the model-measurement discrepancies (Kroll and Seinfeld, 2008)

Aromatic hydrocarbons are an important class of anthropogenic VOCs in the urban area and are estimated to contribute up to 50-70% of the SOA formation in the urban atmosphere (Na *et al.*, 2004). SOA formation from photooxidation of aromatics hydrocarbons has long been a focus of SOA research. SOA yields are generally found to decrease as NO_X increases (Hurley *et al.*, 2001; Johnson *et al.*, 2004; Ng *et al.*, 2007; Song *et al.*, 2005; Wyche *et al.*, 2009). But for most chamber experiments, the NO_X level and relative concentrations radical oxidants (OH, HO_2 and RO_2) are not comparable to the atmosphere conditions, which might result in a different radical chemistry and thus aerosol formation.

Additionally, some chamber experiments have focused on identifying the molecular composition of the oxidation products from aromatic SOA, and have offered detailed molecular mechanisms for the formation of various chemical species (Forstner *et al.*, 1997; Griffin *et al.*, 2002; Jang and Kamens, 2001; Kleindienst *et al.*, 2004). Recent studies (Aiken *et al.*, 2008; Chhabra *et al.*, 2010; Ng *et al.*, 2010) using Aerodyne High Resolution Time-of-Flight Aerosol Mass Spectrometer (HR-ToF-MS) compared experiments and ambient measurement, found that chamber SOA was less oxidized than ambient aerosols. Sato *et al.* (2010) further observed that aromatic structure impacts SOA chemical composition.

Despite considerable studies of the oxidation chemistry of aromatic hydrocarbons, the basic underlying mechanisms of SOA formation and growth from aromatic precursors remain poorly understood. Studies have showed that only 10% or less of aromatic SOA mass can be identified using current analytical techniques (Cocker *et al.*, 2001; Hamilton *et al.*, 2005; Sato *et al.*, 2007), which makes the development of explicit mechanisms of aromatic SOA formation impractical.

The objective of this study is to improve our understanding of SOA formation from aromatics and the critical parameters needed to accurately predict SOA formation in the absence of detailed chemical product information. This goal is achieved by conducting a careful series of photooxidation experiments of 17 different individual aromatic hydrocarbons under widely varying conditions. A large and more accurate experimental database is provided to improve the performance of gas-phase prediction model, SAPRC-11; SAPRC-11 is then utilized to estimate radical levels present during aromatic photooxidation.

Chapter 2 investigates the SOA formation potential from the photooxidation of 17 different aromatic hydrocarbons under low-NO_X conditions. SOA yield curves, developed by Odum *et al.* (1996), is used to describe the aerosol formation. Aerosol formation in this study is compared with previous aromatic photooxidation experiments; differences in SOA yield are addressed by comparing the experimental conditions between experiments, including NO_X level, preexisting aerosol mass, temperature and light intensity. A strong correlation between SOA yield and the carbon number of aromatic precursors is observed in our study; possible reasons are provided.

Chapter 3 explores the bulk chemical composition of SOA formed from different aromatic precursors using data measured by Aerodyne HR-ToF-AMS. Experiments are carried out under low-NO_X and no-NO_X conditions are compared. Van-Krevelen diagrams are employed to investigate the oxidation process of SOA in different aromatic photooxidation systems. A direct comparison of key organic signals at m/z 43 ($C_2H_3O^+$) and m/z 44 (CO_2^+) in HR-ToF-AMS measurements is carried out using the Ng *et al.* (2010) triangle plot; an obvious trend between aromatic structure and SOA chemical composition is observed. In addition, the structural impact on chemical composition is also correlated with the volatility of SOA.

Chapter 4 extends the Chapter 3 study of bulk chemical composition of aromatic secondary aerosols to include SOA density prediction.. Elemental ratios (O/C and H/C) of SOA formed from the oxidation of 23 different volatile organic compounds (VOC) are used to estimate the density of aerosols using the method recently proposed by Kuwata *et al.* (2012). The estimation is then compared with density measurements by aerosol particle mass analyzer-scanning mobility particle sizer (APM-SMPS); the estimation method is shown to predict SOA density within 20% error.

Chapter 5 applies model predictions by SAPRC-11 to explain the variation of SOA yield and chemical composition under low-NO_X and no-NO_X conditions in individual aromatic photooxidation systems. The OH and HO_2 radical both closely relates to gas phase oxidation process; OH concentration is constrained by experimentally observed hydrocarbon decay and HO_2 is predicted by the SAPRC-11 model. Generally, $[OH]/[HO_2]$ ratio is found to be highly related to SOA yield for aromatic hydrocarbons; more aerosols are formed in lower $[OH]/[HO_2]$ environment. $[OH]/[HO_2]$ ratio is suggested as a metric to aid in extrapolation of chamber experimental data to the ambient environment.

1.2 References

Aiken, A.C., DeCarlo, P.F., Kroll, J.H., Worsnop, D.R., Huffman, J.A., Docherty, K.S., Ulbrich, I.M., Mohr, C., Kimmel, J.R., Sueper, D., Sun, Y., Zhang, Q., Trimborn, A., Northway, M., Ziemann, P.J., Canagaratna, M.R., Onasch, T.B., Alfarra, M.R., Prevot, A.S.H., Dommen, J., Duplissy, J., Metzger, A., Baltensperger, U., Jimenez, J.L., 2008. O/C and OM/OC Ratios of Primary, Secondary, and Ambient Organic Aerosols with High-Resolution Time-of-Flight Aerosol Mass Spectrometry. Environ. Sci. Technol. 42, 4478–4485.

Andreae, M.O., Crutzen, P.J., 1997. Atmospheric Aerosols: Biogeochemical Sources and Role in Atmospheric Chemistry. Science 276, 1052–1058.

Atkinson, R., Aschmann, S.M., Arey, J., Carter, W.P.L., 1989. Formation of ring-retaining products from the OH radical-initiated reactions of benzene and toluene. International Journal of Chemical Kinetics 21, 801–827.

Calvert, J.G., Atkinson, R., Becker, K.H., Kamens, R.M., Seinfeld, J.H., 2002. The Mechanisms of Atmospheric Oxidation of the Aromatic Hydrocarbons. Oxford University Press, New York.

Chhabra, P.S., Flagan, R.C., Seinfeld, J.H., 2010. Elemental analysis of chamber organic aerosol using an aerodyne high-resolution aerosol mass spectrometer. Atmos. Chem. Phys. 10, 4111–4131.

Cocker III, D.R., Mader, B.T., Kalberer, M., Flagan, R.C., Seinfeld, J.H., 2001. The effect of water on gas–particle partitioning of secondary organic aerosol: II. m-xylene and 1,3,5-trimethylbenzene photooxidation systems. Atmospheric Environment 35, 6073–6085.

Davidson, C.I., Phalen, R.F., Solomon, P.A., 2005. Airborne Particulate Matter and Human Health: A Review. Aerosol Science and Technology 39, 737–749.

De Gouw, J.A., Middlebrook, A.M., Warneke, C., Goldan, P.D., Kuster, W.C., Roberts, J.M., Fehsenfeld, F.C., Worsnop, D.R., Canagaratna, M.R., Pszenny, A. a. P., Keene, W.C., Marchewka, M., Bertman, S.B., Bates, T.S., 2005. Budget of organic carbon in a polluted atmosphere: Results from the New England Air Quality Study in 2002. Journal of Geophysical Research: Atmospheres 110, n/a–n/a.

Forstner, H.J.L., Flagan, R.C., Seinfeld, J.H., 1997. Secondary Organic Aerosol from the Photooxidation of Aromatic Hydrocarbons: Molecular Composition. Environ. Sci. Technol. 31, 1345–1358.

Griffin, R.J., Cocker, D.R., Flagan, R.C., Seinfeld, J.H., 1999. Organic aerosol formation from the oxidation of biogenic hydrocarbons. Journal of Geophysical Research: Atmospheres 104, 3555–3567.

Griffin, R.J., Dabdub, D., Kleeman, M.J., Fraser, M.P., Cass, G.R., Seinfeld, J.H., 2002. Secondary organic aerosol 3. Urban/regional scale model of size- and composition-resolved aerosols. Journal of Geophysical Research: Atmospheres 107, AAC 5–1–AAC 5–14.

Hallquist, M., Wenger, J.C., Baltensperger, U., Rudich, Y., Simpson, D., Claeys, M., Dommen, J., Donahue, N.M., George, C., Goldstein, A.H., Hamilton, J.F., Herrmann, H., Hoffmann, T., Iinuma, Y., Jang, M., Jenkin, M.E., Jimenez, J.L., Kiendler-Scharr, A., Maenhaut, W., McFiggans, G., Mentel, T.F., Monod, A., Prévôt, A.S.H., Seinfeld, J.H., Surratt, J.D., Szmigielski, R., Wildt, J., 2009. The formation, properties and impact of secondary organic aerosol: current and emerging issues. Atmos. Chem. Phys. 9, 5155–5236.

Hamilton, J.F., Webb, P.J., Lewis, A.C., Reviejo, M.M., 2005. Quantifying small molecules in secondary organic aerosol formed during the photo-oxidation of toluene with hydroxyl radicals. Atmospheric Environment 39, 7263–7275.

Harrison, R.M., Yin, J., 2000. Particulate matter in the atmosphere: which particle properties are important for its effects on health? Science of The Total Environment 249, 85–101.

Haywood, J., Boucher, O., 2000. Estimates of the direct and indirect radiative forcing due to tropospheric aerosols: A review. Reviews of Geophysics 38, 513–543.

Heald, C.L., Jacob, D.J., Park, R.J., Russell, L.M., Huebert, B.J., Seinfeld, J.H., Liao, H., Weber, R.J., 2005. A large organic aerosol source in the free troposphere missing from current models. Geophysical Research Letters 32, n/a–n/a.

Hurley, M.D., Sokolov, O., Wallington, T.J., Takekawa, H., Karasawa, M., Klotz, B., Barnes, I., Becker, K.H., 2001. Organic Aerosol Formation during the Atmospheric Degradation of Toluene. Environ. Sci. Technol. 35, 1358–1366.

Jang, M., Kamens, R.M., 2001. Characterization of Secondary Aerosol from the Photooxidation of Toluene in the Presence of NO_X and 1-Propene. Environ. Sci. Technol. 35, 3626–3639.

Johnson, D., Jenkin, M.E., Wirtz, K., Martin-Reviejo, M., 2004. Simulating the Formation of Secondary Organic Aerosol from the Photooxidation of Toluene. Environ. Chem. 1, 150–165.

Kleindienst, T.E., Conver, T.S., McIver, C.D., Edney, E.O., 2004. Determination of Secondary Organic Aerosol Products from the Photooxidation of Toluene and their Implications in Ambient PM 2.5. Journal of Atmospheric Chemistry 47, 79–100.

Kleinman, L.I., Springston, S.R., Daum, P.H., Lee, Y.-N., Nunnermacker, L.J., Senum, G.I., Wang, J., Weinstein-Lloyd, J., Alexander, M.L., Hubbe, J., Ortega, J., Canagaratna, M.R., Jayne, J., 2008. The time evolution of aerosol composition over the Mexico City plateau. Atmos. Chem. Phys. 8, 1559–1575.

Kroll, J.H., Seinfeld, J.H., 2008. Chemistry of secondary organic aerosol: Formation and evolution of low-volatility organics in the atmosphere. Atmospheric Environment 42, 3593–3624.

Kuwata, M., Zorn, S.R., Martin, S.T., 2012. Using Elemental Ratios to Predict the Density of Organic Material Composed of Carbon, Hydrogen, and Oxygen. Environ. Sci. Technol. 46, 787–794.

Lanz, V.A., Alfarra, M.R., Baltensperger, U., Buchmann, B., Hueglin, C., Prévôt, A.S.H., 2007. Source apportionment of submicron organic aerosols at an urban site by factor analytical modelling of aerosol mass spectra. Atmos. Chem. Phys. 7, 1503–1522.

Na, K., Sawant, A.A., Song, C., Cocker, D.R., 2004. Primary and secondary carbonaceous species in the atmosphere of Western Riverside County, California. Atmospheric Environment 38, 1345–1355.

Ng, N.L., Canagaratna, M.R., Zhang, Q., Jimenez, J.L., Tian, J., Ulbrich, I.M., Kroll, J.H., Docherty, K.S., Chhabra, P.S., Bahreini, R., Murphy, S.M., Seinfeld, J.H., Hildebrandt, L., Donahue, N.M., DeCarlo, P.F., Lanz, V.A., Prévôt, A.S.H., Dinar, E., Rudich, Y., Worsnop, D.R., 2010. Organic aerosol components observed in Northern Hemispheric datasets from Aerosol Mass Spectrometry. Atmos. Chem. Phys. 10, 4625–4641.

Ng, N.L., Kroll, J.H., Chan, A.W.H., Chhabra, P.S., Flagan, R.C., Seinfeld, J.H., 2007. Secondary organic aerosol formation from m-xylene, toluene and benzene. Atmospheric Chemistry and Physics 7, 3909–3922.

Odum, J.R., Hoffmann, T., Bowman, F., Collins, D., Flagan, R.C., Seinfeld, J.H., 1996. Gas/Particle Partitioning and Secondary Organic Aerosol Yields. Environ. Sci. Technol. 30, 2580–2585.

Odum, J.R., Jungkamp, T.P.W., Griffin, R.J., Flagan, R.C., Seinfeld, J.H., 1997. The Atmospheric Aerosol-Forming Potential of Whole Gasoline Vapor. Science 276, 96–99.

Pankow, J.F., 1994. An absorption model of the gas/aerosol partitioning involved in the formation of secondary organic aerosol. Atmospheric Environment 41, Supplement, 75–79.

Sato, K., Hatakeyama, S., Imamura, T., 2007. Secondary organic aerosol formation during the photooxidation of toluene: NO_X dependence of chemical composition. J Phys Chem A 111, 9796–9808.

Sato, K., Takami, A., Isozaki, T., Hikida, T., Shimono, A., Imamura, T., 2010. Mass spectrometric study of secondary organic aerosol formed from the photo-oxidation of aromatic hydrocarbons. Atmospheric Environment 44, 1080–1087.

Song, C., Na, K., Cocker, D.R., 2005. Impact of the Hydrocarbon to NO_X Ratio on Secondary Organic Aerosol Formation. Environ. Sci. Technol. 39, 3143–3149.

Turpin, B.J., Huntzicker, J.J., 1995. Identification of secondary organic aerosol episodes and quantitation of primary and secondary organic aerosol concentrations during SCAQS. Atmospheric Environment 29, 3527–3544.

Volkamer, R., Jimenez, J.L., San Martini, F., Dzepina, K., Zhang, Q., Salcedo, D., Molina, L.T., Worsnop, D.R., Molina, M.J., 2006. Secondary organic aerosol formation from anthropogenic air pollution: Rapid and higher than expected. Geophysical Research Letters 33, n/a–n/a.

Wyche, K.P., Monks, P.S., Ellis, A.M., Cordell, R.L., Parker, A.E., Whyte, C., Metzger, A., Dommen, J., Duplissy, J., Prevot, A.S.H., Baltensperger, U., Rickard, A.R., Wulfert, F., 2009. Gas phase precursors to anthropogenic secondary organic aerosol: detailed observations of 1,3,5-trimethylbenzene photooxidation. Atmos. Chem. Phys. 9, 635–665.

Zhang, Q., Worsnop, D.R., Canagaratna, M.R., Jimenez, J.L., 2005. Hydrocarbon-like and oxygenated organic aerosols in Pittsburgh: insights into sources and processes of organic aerosols. Atmos. Chem. Phys. 5, 3289–3311.

2 Secondary Organic Aerosol Formation Potential of 17 Aromatic Hydrocarbons

2.1 Introduction

Secondary organic aerosol (SOA) formed from the oxidation of biogenic and anthropogenic VOC precursors have garnered wide attention because of their direct and indirect negative impacts on human health and the environment. Aromatic hydrocarbons are an important class of anthropogenic SOA in the urban area contributing. It is estimated that aromatic compounds contribute up to 50-70% of total SOA formation in the urban atmosphere (Na *et al.*, 2004).

Environmental simulation chambers are usually employed to investigate gas-phase partitioning of the oxidation products of photochemical reactions involving anthropogenic and biogenic precursors. Over the last two decades, significant efforts have been made to quantify and empirically predict the aerosol formation from aromatics precursors (Borrás and Tortajada-Genaro, 2012; Chhabra *et al.*, 2011; Cocker III *et al.*, 2001; Edney *et al.*, 2000; Healy *et al.*, 2009, 2008; Izumi and Fukuyama, 1990; Kleindienst *et al.*, 1999; Martín-Reviejo and Wirtz, 2005; Ng *et al.*, 2007; Odum *et al.*, 1997; Sato *et al.*, 2012, 2010, 2007; Song *et al.*, 2007; Takekawa *et al.*, 2003; Wyche *et al.*, 2009). Izumi and Fukuyama (1990) first investigated the aerosol yields of different aromatic species and observed higher aerosol formation for toluene and ethylbenzene than for p-ethyltoluene and trimethylbenzene. Odum *et al.* (1996) performed an extensive study on aromatic SOA formation, first developing the two-product absorptive partitioning model based on the gas/particle partitioning absorption model outlined by Pankow (1994) to describe aerosol formation as a function of organic aerosol mass loading. SOA yield curves obtained for 17 individual aromatic precursors obtained under high NO_X loadings (Odum *et al.*, 1997) were observed two fall into two distinct classes: low-yield (one or less ring substituents) and high-yield (two-or more ring substituents) aromatics. Forstner *et al.* (1997) further reported that many individual aromatic compounds generate similar oxidation products.

The chemistry and partitioning process involved in SOA formation is observed to have varying sensitivities to a number of atmospherically relevant conditions such as temperature (e.g., Hildebrandt *et al.*, 2009; Takekawa *et al.*, 2003; Warren *et al.*, 2009), humidity (e.g., Cocker III *et al.*, 2001; Edney *et al.*, 2000), photolysis constant *(Presto et al.*, 2005a; Warren *et al.,* 2008) and NO_X levels (e.g., Hurley *et al.*, 2001; Ng *et al.*, 2007; Presto *et al.*, 2005b; Song *et al.*, 2005; Wyche *et al.*, 2009).

Many studies have focused on the role of particle seed characteristics on SOA formation. It is found that $(NH_4)_2SO_4$ seed had no significant effect on SOA formation for aromatic photooxidation experiments (Cocker III *et al.*, 2001; Edney *et al.*, 2000; Kleinman *et al.*, 2008). However, Kroll *et al.*, (2007) found that SOA yields are enhanced by inorganic seed particles because even a small amount of existing particles enabled the uptake of organics. Lu *et al.* (2009) suggested that high concentration of dry acidic $(NH_4)_2SO_4$ seed particles facilitated the formation of oligomers through heterogeneous reactions thus enhanced SOA yield. Jang *et al.* (2002) suggested that inorganic acids (e.g. H_2SO_4) catalyzed carbonyl heterogeneous reactions and led to a larger SOA yield.

For many of the experiments that have been reported, only a small fraction of aromatic compounds in the atmosphere have been examined and most of these experiments have been conducted at NO_X levels much higher than ambient air. Thus, studies conducted under conditions much closer to ambient levels could provide information that cannot easily be extrapolated from previous studies. In this study, a series of chamber experiments were performed to evaluate the aerosol formation potential of a wide variety of aromatic hydrocarbons, e.g. toluene, ethylbenzene, xylene isomers, ethyltoluene isomers, thrimethylbenzene isomers, propylbenzene, isopropylbenzene, tetramethylbenzene, pentamethylbenzene and hexamethylbenzene. Most of the experiments were conducted under low-NO_X conditions that are more representative of ambient atmospheres. SOA yield was compared among aromatic precursors with different chemical structure and also compared with previous aromatic photooxidation studies.

2.2 Experimental Methods

All the experiments in this paper were carried out in UC Riverside/CE-CERT indoor environmental chamber, which is described in detail elsewhere (Carter *et al.*, 2005). All experiments were conducted under dry conditions (RH<0.1%) and in the absence of inorganic seed aerosol for environmental chamber temperatures of 27°C. Hydrocarbon decay was measured by an Agilent6890 (Palo Alto, CA) gas chromatograph (GC) equipped with a DB-5 column and a flame ionization detector (FID). NO_X and O_3 were monitored by a Thermo Environmental Instruments model 42C chemiluminescence NO_X analyzer and Dasibi Envrionmental Corp. Model 1003-AH O_3 analyzer, respectively. Perfluorohexane is used as a tracer in this study to monitor dilution of the reactor.

Particle size distribution and number concentrations were monitored using an in-house built scanning mobility particle sizer (SMPS) located inside the chamber enclosure to ensure the SMPS sampled at 27 C to match the temperature of the chamber. Particle number and volume were corrected for wall loss following the 1st order loss correction method (Bowman *et al.*, 1997). Real-time particle density was measured using an Aerosol Particle Mass Analyzer (APM) and SMPS in series (Malloy *et al.*, 2009).

2.3 **Results and Discussion**

Key experimental details for all aromatic hydrocarbon photooxidation experiments studied are summarized in Table 2.1 including the initial concentration of the parent hydrocarbon (HC_0), the concentration of the parent hydrocarbon consumed (ΔHC), the initial concentration of NO_X, the mass concentration of SOA produced (M_o) and the SOA yield (Y). The density of aromatic photooxidation experiments are reported as 1.4 g cm^{-3} (Nakao *et al.*, 2013); therefore a density of 1.4 g $cm^{-3}$was used to convert volume concentration to mass concentration in this study.

Aerosol yield (Y), measured as the mass based ratio of organic aerosol mass (M_o) to parent hydrocarbon reacted (ΔHC) was obtained for each experiment after wall-loss corrected aerosol mass concentration plateaued. A two-products gas-particle partitioning equation (eqn (1), Odum *et al.*, 1996) was used to fit the yield data.

$$Y = M_o \sum_{i=1}^{2} \frac{\alpha_i K_{om,i}}{1+K_{om,i} M_o} \tag{1}$$

Where α_i is the mass-based stoichiometric factor for compound i, and $K_{om,i}$ ($m^3 \mu g^{-1}$) is the partitioning coefficient in terms of the organic mass concentration. For this work a two-product model was sufficient to fit measured aerosol yield data with each product representative of a lumped group of aerosol forming species.

2.3.1 SOA Yields of Aromatic Hydrocarbons under low-NO_X conditions

SOA yields of the 17 aromatic hydrocarbons investigated in this work versus M_o are shown in Figure 2.1. Most experiments were conducted under low- NO_X conditions (HC (ppbC)/ NO_X (ppb) > 7, Song *et al.*, 2005). It is noted that lower NO_X conditions are more representative of the NO_X loadings in typical urban or rural areas. Data points are grouped and labeled by the number of carbons in the parent aromatic. Yield curves are fit to each data group (C6 and C7 are combined as are C10 and higher) using the two-product model (eqn (1)) by minimizing the weighted squared residuals. Table 2.2 summarizes the best-fit parameters obtained.

It is observed that as the number of carbon atoms in the aromatic molecule increases, the aerosol yield of the aromatic compound decreases. This observation is generally consistent with observations by Odum *et al.*, (1996) who noted that aromatics with one or fewer substituents formed more aerosol than species containing two or more substituents. However, ethylbenzene and propyl benzene tend to follow the aerosol yield carbon number trends better than the single substituent trend. It is observed that aerosol formation relates more strongly to the number of carbons present in the aromatic than to its actual chemical structure. These observations are consistent with Odum's suggestion that lighter compounds tend to form more ring-retaining products with lower vapor pressures than the ring-cleavage products produced by heavier aromatics. Smith *et al.* (1999) further supports this suggestion as they observed that the total yield of ring-retaining products of trimethylbenzene isomers oxidation yielded far less ring-retaining products than xylenes and toluene. Other laboratory studies (Chhabra *et al.*, 2011; Sato *et al.*, 2010) using Aerodyne Aerosol Mass Spectrometer (AMS) found that the photooxidation of aromatics with more alkyl substituents yielded a higher m/z 43 to organic aerosol (OA) ratio and lower m/z 44 to OA ratio. Sato *et al.* (2010) suggests that more low-reactive ketones are produced rather than aldehydes with increasing number of substituents. The lower reactivity may also explain the decreases in aromatic SOA yields with increase of the number of substituents.

2.3.2 SOA Yields of Benzene and Toluene

Benzene and toluene are two of the most abundant aromatic hydrocarbons in the urban atmosphere. Figure 2.2 combines SOA yields observed from benzene and toluene from this work and previous studies. Curve 1 represents the best two-product fit from this work while black dashed line is Odum's high-yield curve for aromatics with 1 or less substituent. Most low-NO_X benzene and toluene photooxidation experiments reported by Ng *et al.* (2007) are consistent with curve 1. The current and Ng *et al.* experiments both used black lights as a light source. Takekawa *et al.* (2003) also performed low NO_X experiments at levels similar to this study. However, only the low temperature data (283 K) experiments lie on curve 1. Those experiments conducted at (303 K) are consistently lower than this work. The differences may be attributable to enhanced semi-volatile wall losses for their 2 m^3 chamber due to the noticeably higher surface area-to-volume ratio in their system.

Aromatic aerosol yield data reported by Izumi and Fukuyama (1990), Kleindienst *et al.* (1999) and Edney *et al.* (2000) agree well with the high yield curve of Odum *et al.* (1996). Unlike recent studies, each of these works assumes a unit density to convert particle volume to mass concentration. However, even applying a density correction of 1.4 g/cm^3 to these datasets, SOA yield is still lower than our work. This difference is attributed to the higher NO_X conditions in their experiments compared to the present experiments (5~10 times higher). A number of researchers have noted that higher NO_X levels lead to lower SOA formation for aromatic precursors due to suppression of HO_2 and RO_2 radicals (Hurley *et al.*, 2001; Ng *et al.*, 2007; Presto *et al.*, 2005b; Song *et al.*, 2005; Wyche *et al.*, 2009).

It is also observed (Figure 2.2) that aerosol yield data from Sato *et al.* (2010, 2007) is lower than the rest of the reported works. For these experiments the NO_X levels were high (0.2~1 ppmv) and the duration of the experiments were considerably shorter than other experiments reported. It is likely that the combination of elevated NO_X, insufficient time for secondary reactions to occur, and perhaps small reactor volume led to these lower values.

A summary of experimental conditions including light intensity, reactor size, and reaction times are provided in Table 2.3.

2.3.3 SOA Yields of Ethylbenzene and Propylbenzenes

There are only two studies reporting SOA formation from ethylbenzene and propylbenzenes (Izumi and Fukuyama, 1990; Odum *et al.*, 1997). Both ethylbenzene and propylbenzenes are single substituent aromatics and therefore are expected to fall on the

Odum high yield curve (1996). Both of these studies, as discussed in the previous section, were conducted under high than ambient NO_X conditions leading to suppression of RO_2 and HO_2 radicals.

The aerosol formation potential of these two compounds obtained from this study are best described by curve 2 (Figure 2.1 and Figure 2.3). It is noted that for these lower NO_X conditions (more typical atmospheric conditions), the aerosol formation for the single substituent aromatics are lower than that of benzene and toluene. It is hypothesized that the increased reactivity toward the longer side chains might have led to the production of higher volatility products than obtained for benzene and toluene.

2.3.4 SOA Yields of Xylene Isomers

m-Xylene and its isomers have been widely studied. Figure 2.4 includes the yield data obtained from all three xylene isomers (m, o, and p) studied in this work. Curve 2 is the most representative fit to these isomers. A closer look at this data (Figure 2.5) reveals that p-xylene has a slightly lower yield than m-xylene and o-xylene for experiments conducted with similar initial conditions. The "para" effect is consistent with earlier studies (Izumi and Fukuyama, 1990; Johnson *et al.*, 2005; Song *et al.*, 2007) and is attributed to the production of more unsaturated diketones and less aldehydes during p-xylene photooxidation; unsaturated diketones are known to be less photoreactive. Song *et al.* (2007) further points out that the yield difference is larger in the low HC_0/NO_X due to differences increasing between p-xylene and m-, p-xylene organic peroxide yields with decreasing NO levels.

Studies by Ng *et al.* (2007), Song *et al.* (2007) and Chhabra *et al.* (2011) are consistent with “Curve 3” reported in this work (Figure 2.1 and Figure 2.4). Odum *et al.* (1997, 1996) and Izumi and Fukuyama (1990) data fall on the low-yield curve reported by Odum (all data reported assuming unit density) along with Healy *et al.* (2009) (assumed density of 1.4 g/cm^3). Each of these studies was performed with very high NO_X levels leading to the suppression of SOA formation from the aromatic compounds (see above). The work reported by Cocker *et al.* (2001) was also conducted at elevated NO_X levels; however, for that work the light intensity is considerably higher (Table 2.3) than for the other studies. The increase in SOA formation relative to other high NO_X experiments is attributed to the raised light intensity, consistent with observations by Warren *et al.* (2008) who demonstrated that higher NO_2 photolysis rates significantly increases SOA formation for aromatic compounds.

2.3.5 SOA Yields of Ethyltoluene Isomers

Previously reported SOA studies for ethyltoluenes are limited to high-NOx condition (Izumi and Fukuyama, 1990; Odum *et al.*, 1997). The ethyltoluene yield data for this study along with the two previous studies are displayed in Figure 2.6. Generally, the SOA yield for the ethyltoluene isomers is lower than for the xylene isomers (Curve 3 vs. Curve 2,). This follows the same trend as with the longer chain monosubstituted aromatics, which had smaller yields than the methyl monosubstituted aromatic observed above.

The relatively large scatter in data points for the ethyltoluene isomers is attributed to differences in NOx loadings for each experiment. Figure 2.7 provides yield data scaled by initial NO concentration (shading) in each experiment. Lower yields are observed for experiments conducted with relatively higher initial NO concentrations; consistent with other observations of decreasing SOA yields for systems with higher NO_x levels. It is observed that p-ethyltoluene, like p-xylene, has lower yields than the m- and o- isomers. Izumi *et al.* (1990) also observed a smaller yields for *p*-ethyltoluene (<1.5 %) than for *m*- and *o*-ethyltoluene (3.3 and 3.7%).

Izumi and Fukuyama (1990) and Odum *et al.* (1997) are observed to be more consistent with the Odum high yield curve despite the presence of two substituents on the aromatic ring. The lower aerosol formation observed by both of these works are again attributed to the high NO_x loadings used for their work.

2.3.6 SOA Yields of Trimethylbenzene Isomers

SOA formation from the trimethylbenzene isomers is similar to that observed in this study for the other 9 carbon aromatic compounds (ethyltoluene isomers) reported above (Curve 3, Figure 2.8) and is much higher than earlier studies of trimethylbenzene isomers. It is further observed that 1,2,3-trimethylbenzene forms more aerosol than 1,2,4- and 1,3,5-trimethylbenzene for experiments commencing with similar conditions. While 1,2,4-trimethylbenzene has 2 methyl groups in the para-position to one another, its yield was not observed to be lower than for 1,3,5-trimethylbenzene.

Yield data previously reported (Figure 2.8) are consistent with Odum's low-yield curve for aromatics with 2 or more substituents. The studies of Izumi and Fukuyama (1990), Odum *et al.* (1997), Healy *et al.* (2008), Kleindienst *et al.* (1999), and Cocker *et al.* (2001) were all conducted at higher NO_X leading to lower aerosol yields as noted previously. As noted above, Sato *et al.* (2012) experiments also contained considerable amounts NO_X levels (from methylnitrate photolysis) and were conducted for shorter photooxidation times (Table 2.3) thereby minimizing the extent of oxidation of secondary products leading to his work having the lowest SOA yield. Takekawa *et al.* (2003) study may have had suppressed aerosol formation due to wall losses of semi-volatile components in the smaller chamber (Table 2.3).

2.3.7 SOA Yields from Aromatic with 10 or More Carbon Numbers

Photooxidation of aromatic compounds with 10 or more carbon numbers (1,2,4,5-tetramethylbenzene, pentamethylbenzene and hexamethylbenzene) have the lowest SOA yields of all aromatics studied in this work (Figure 2.9, curve 4). The yields of these species are similar, but slightly higher, than the Odum *et al.* low yield curve. The work of Odum *et al.* (1997) appears to be the only previously reported study on 1,2,4,5-tetramethylbenzene aerosol formation; to the best of our knowledge this is the first aerosol formation data for pentamethyl and hexamethyl benzene. The trends observed for the less substituted compounds hold for these compounds as well; the greater the number of substituents, the lower the aerosol yields. Further, observed aerosol production for this study conducted at lower NO_X is higher than that reported for the high-NO_X regime from Odum *et al.* (1996).

2.4 **Summary**

In this study, SOA formation of 17 aromatic hydrocarbons was investigated in the environmental chamber under low-NO_X conditions. It is observed that aerosol formation from the compounds can be best described by four separate aerosol yield curves based on carbon number. Generally, aerosol formation was observed to be higher for all aromatics studied at the lower NO_X conditions used in this work compared to previous high NO_X studies; yields for selected aromatics agreed well with earlier studies under similar low NO_X conditions. A “para”-effect was observed for the xylenes and ethyltoluenes with para isomers forming less quantities of SOA than the meta or ortho isomers of the same compound. Compared to previous yield studies by other groups, studies by Ng *et al.* (2007), Song *et al.* (2007) and Chhabra *et al.* (2011) agree well with our work, even if inorganic seeds were used in some of their experiments or the relative humidity was different. Other groups (Cocker *et al.*, 2001; Healy *et al.*, 2009, 2008; Izumi and Fukuyama, 1990; Kleindienst *et al.*, 1999; Odum *et al.*, 1997; Takekawa *et al.*, 2003) all have much lower yield than our work, consistent with the higher initial NO concentrations used in their studies and in agreement with NO_X effects reported by others (Hurley *et al.*, 2001; Ng *et al.*, 2007; Presto *et al.*, 2005b; Song *et al.*, 2005; Wyche *et al.*, 2009). Despite the difference in NO_X level, yield data by Sato *et al.* (2012, 2007) is the lowest due to the short photooxidation time and possibly due to their smaller environmental chamber.

2.5 **References**

Borrás, E., Tortajada-Genaro, L.A., 2012. Secondary organic aerosol formation from the photo-oxidation of benzene. Atmospheric Environment 47, 154–163.

Bowman, F.M., Odum, J.R., Seinfeld, J.H., Pandis, S.N., 1997. Mathematical model for gas-particle partitioning of secondary organic aerosols. Atmospheric Environment 31, 3921–3931.

Chhabra, P.S., Ng, N.L., Canagaratna, M.R., Corrigan, A.L., Russell, L.M., Worsnop, D.R., Flagan, R.C., Seinfeld, J.H., 2011. Elemental composition and oxidation of chamber organic aerosol. Atmos. Chem. Phys. 11, 8827–8845.

Edney, E.O., Driscoll, D.J., Speer, R.E., Weathers, W.S., Kleindienst, T.E., Li, W., Smith, D.F., 2000. Impact of aerosol liquid water on secondary organic aerosol yields of irradiated toluene/propylene/NO_X/$(NH_4)_2SO_4$/air mixtures. Atmospheric Environment 34, 3907–3919.

Forstner, H.J.L., Flagan, R.C., Seinfeld, J.H., 1997. Secondary Organic Aerosol from the Photooxidation of Aromatic Hydrocarbons: Molecular Composition. Environ. Sci. Technol. 31, 1345–1358.

Healy, R.M., Temime, B., Kuprovskyte, K., Wenger, J.C., 2009. Effect of Relative Humidity on Gas/Particle Partitioning and Aerosol Mass Yield in the Photooxidation of p-Xylene. Environ. Sci. Technol. 43, 1884–1889.

Healy, R.M., Wenger, J.C., Metzger, A., Duplissy, J., Kalberer, M., Dommen, J., 2008. Gas/particle partitioning of carbonyls in the photooxidation of isoprene and 1,3,5-trimethylbenzene. Atmos. Chem. Phys. 8, 3215–3230.

Hildebrandt, L., Donahue, N.M., Pandis, S.N., 2009. High formation of secondary organic aerosol from the photo-oxidation of toluene. Atmos. Chem. Phys. 9, 2973–2986.

Hurley, M.D., Sokolov, O., Wallington, T.J., Takekawa, H., Karasawa, M., Klotz, B., Barnes, I., Becker, K.H., 2001. Organic Aerosol Formation during the Atmospheric Degradation of Toluene. Environ. Sci. Technol. 35, 1358–1366.

Izumi, K., Fukuyama, T., 1990. Photochemical aerosol formation from aromatic hydrocarbons in the presence of NO_X. Atmospheric Environment 24A, 1433–1441.

Jang, M., Czoschke, N.M., Lee, S., Kamens, R.M., 2002. Heterogeneous Atmospheric Aerosol Production by Acid-Catalyzed Particle-Phase Reactions. Science 298, 814–817.

Johnson, D., Jenkin, M.E., Wirtz, K., Martin-Reviejo, M., 2005. Simulating the Formation of Secondary Organic Aerosol from the Photooxidation of Aromatic Hydrocarbons. Environ. Chem. 2, 35–48.

Kleindienst, T.E., Smith, D.F., Li, W., Edney, E.O., Driscoll, D.J., Speer, R.E., Weathers, W.S., 1999. Secondary organic aerosol formation from the oxidation of aromatic hydrocarbons in the presence of dry submicron ammonium sulfate aerosol. Atmospheric Environment 33, 3669–3681.

Kroll, J.H., Chan, A.W.H., Ng, N.L., Flagan, R.C., Seinfeld, J.H., 2007. Reactions of Semivolatile Organics and Their Effects on Secondary Organic Aerosol Formation. Environ. Sci. Technol. 41, 3545–3550.

Lu, Z., Hao, J., Takekawa, H., Hu, L., Li, J., 2009. Effect of high concentrations of inorganic seed aerosols on secondary organic aerosol formation in the m-xylene/NO_X photooxidation system. Atmospheric Environment 43, 897–904.

Malloy, Q.G.J., Nakao, S., Qi, L., Austin, R., Stothers, C., Hagino, H., Cocker, D.R., 2009. Real-Time Aerosol Density Determination Utilizing a Modified Scanning Mobility Particle Sizer - Aerosol Particle Mass Analyzer System. Aerosol Science and Technology 43, 673–678.

Martín-Reviejo, M., Wirtz, K., 2005. Is Benzene a Precursor for Secondary Organic Aerosol? Environ. Sci. Technol. 39, 1045–1054.

Na, K., Sawant, A.A., Song, C., Cocker, D.R., 2004. Primary and secondary carbonaceous species in the atmosphere of Western Riverside County, California. Atmospheric Environment 38, 1345–1355.

Nakao, S., Tang, P., Tang, X., Clark, C.H., Qi, L., Seo, E., Asa-Awuku, A., Cocker III, D., 2013. Density and elemental ratios of secondary organic aerosol: Application of a density prediction method. Atmospheric Environment 68, 273–277.

Ng, N.L., Kroll, J.H., Chan, A.W.H., Chhabra, P.S., Flagan, R.C., Seinfeld, J.H., 2007. Secondary organic aerosol formation from m-xylene, toluene and benzene. Atmospheric Chemistry and Physics 7, 3909–3922.

Odum, J.R., Hoffmann, T., Bowman, F., Collins, D., Flagan, R.C., Seinfeld, J.H., 1996. Gas/Particle Partitioning and Secondary Organic Aerosol Yields. Environ. Sci. Technol. 30, 2580–2585.

Odum, J.R., Jungkamp, T.P.W., Griffin, R.J., Flagan, R.C., Seinfeld, J.H., 1997. The Atmospheric Aerosol-Forming Potential of Whole Gasoline Vapor. Science 276, 96–99.

Pankow, J.F., 1994. An absorption model of the gas/aerosol partitioning involved in the formation of secondary organic aerosol. Atmospheric Environment 41, Supplement, 75–79.

Presto, A.A., Huff Hartz, K.E., Donahue, N.M., 2005a. Secondary Organic Aerosol Production from Terpene Ozonolysis. 2. Effect of NO_X Concentration. Environ. Sci. Technol. 39, 7046–7054.

Presto, A.A., Huff Hartz, K.E., Donahue, N.M., 2005b. Secondary Organic Aerosol Production from Terpene Ozonolysis. 1. Effect of UV Radiation. Environ. Sci. Technol. 39, 7036–7045.

Sato, K., Hatakeyama, S., Imamura, T., 2007. Secondary organic aerosol formation during the photooxidation of toluene: NOx dependence of chemical composition. J Phys Chem A 111, 9796–9808.

Sato, K., Takami, A., Isozaki, T., Hikida, T., Shimono, A., Imamura, T., 2010. Mass spectrometric study of secondary organic aerosol formed from the photo-oxidation of aromatic hydrocarbons. Atmospheric Environment 44, 1080–1087.

Sato, K., Takami, A., Kato, Y., Seta, T., Fujitani, Y., Hikida, T., Shimono, A., Imamura, T., 2012. AMS and LC/MS analyses of SOA from the photooxidation of benzene and 1,3,5-trimethylbenzene in the presence of NO_X: effects of chemical structure on SOA aging. Atmos. Chem. Phys. 12, 4667–4682.

Smith, D.F., Kleindienst, T.E., McIver, C.D., 1999. Primary Product Distributions from the Reaction of OH with m-, p-Xylene, 1,2,4- and 1,3,5-Trimethylbenzene. Journal of Atmospheric Chemistry 34, 339–364.

Song, C., Na, K., Cocker, D.R., 2005. Impact of the Hydrocarbon to NO_X Ratio on Secondary Organic Aerosol Formation. Environ. Sci. Technol. 39, 3143–3149.

Song, C., Zaveri, R.A., Alexander, M.L., Thornton, J.A., Madronich, S., Ortega, J.V., Zelenyuk, A., Yu, X.Y., Laskin, A., Maughan, D.A., 2007. Effect of hydrophobic primary organic aerosols on secondary organic aerosol formation from ozonolysis of α-pinene. Geophysical Research Letters 34.

Takekawa, H., Minoura, H., Yamazaki, S., 2003. Temperature dependence of secondary organic aerosol formation by photo-oxidation of hydrocarbons. Atmospheric Environment 37, 3413–3424.

Warren, B., Austin, R.L., Cocker III, D.R., 2009. Temperature dependence of secondary organic aerosol. Atmospheric Environment 43, 3548–3555.

Warren, B., Song, C., Cocker, D.R., 3rd, 2008. Light intensity and light source influence on secondary organic aerosol formation for the m-xylene/NO(x) photooxidation system. Environ. Sci. Technol. 42, 5461–5466.

Wyche, K.P., Monks, P.S., Ellis, A.M., Cordell, R.L., Parker, A.E., Whyte, C., Metzger, A., Dommen, J., Duplissy, J., Prevot, A.S.H., Baltensperger, U., Rickard, A.R., Wulfert, F., 2009. Gas phase precursors to anthropogenic secondary organic aerosol: detailed observations of 1,3,5-trimethylbenzene photooxidation. Atmos. Chem. Phys. 9, 635–665.

2.6 Tables

Table 2.1 Summary of aromatic hydrocarbon photooxidation experiments under low-NO_X conditions.

Compound	Run ID	NO ppb	HC_0 ppb	ΔHC $\mu g.m^{-3}$	Mo $\mu g.m^{-3}$	Yield
Benzene	EPA1236A	53.58	928.5	406.79	106.44	0.262
	EPA1236B	154.7	938.2	449.68	34.85	0.078
	EPA1237A	41.64	435.1	265.78	45.93	0.173
	EPA1237B	21.12	453.4	252.78	51.39	0.203
	EPA1223A	59.47	972.4	397.7	138.73	0.349
	EPA1223B	119.26	603	453.26	104.69	0.231
Toluene	EPA1101A	19.24	79.7	206.2	30.13	0.146
	EPA1101B	9.38	78.8	175.54	25.14	0.143
	EPA1102A	43.33	75.7	222.68	21.76	0.098
	EPA1102B	32.96	82.5	238.39	22.19	0.093
	EPA1106A	20.14	38	126.1	9.8	0.078
	EPA1106B	10.6	36.9	111.15	12.42	0.112
	EPA1107A	40.11	36.9	121.5	2.8	0.023
	EPA1107B	30.03	36.6	118.05	5.89	0.05
	EPA1468A	64.07	239.2	666.9	130.21	0.196
	EPA1468B	63.03	238.4	671.12	126.66	0.189
Ethylbenzene	EPA1142A	47.37	100.6	331.22	21.99	0.066
	EPA1142B	66.56	99.9	341.12	4.35	0.013
	EPA1146A	22.22	99	256.58	35.99	0.14
	EPA1146B	34.78	100	330.78	23.62	0.071
	EPA1147A	66.91	347.9	845.71	87.49	0.103
	EPA1147B	36.51	341.7	625.78	88.13	0.141
Propylbenzene	EPA1245A	22.12	100.7	230.98	11.84	0.051
	EPA1246A	68.46	203.6	420.46	22.93	0.054
Isopropylbenzene	EPA1247A	22.36	100.2	300.97	33.24	0.11
	EPA1247B	48.12	99.3	299.98	16.55	0.055
	EPA1253A	56.36	200	537.95	53.09	0.099
	EPA1253B	100.07	195.9	526.46	16.52	0.031
m-Xylene	EPA1193A	36.78	71.1	238.9	13.59	0.057
	EPA1193B	36.52	69.5	236.25	11.23	0.047
	EPA1516A	26.69	92.9	357.25	48.71	0.136
o-Xylene	EPA1315A	49.8	82.2	324.13	26.32	0.081
	EPA1315B	22.24	80	278.21	25.37	0.091
	EPA1321A	20.47	79.2	263.19	16.16	0.061

	EPA1321B	10.44	80	225.66	9.84	0.044
p-Xylene	EPA1308A	55.55	78.4	278.65	6.8	0.024
	EPA1308B	22.93	78.8	273.79	11.28	0.041
m-Ethyltoluene	EPA1151A	62.48	84.8	408.97	8.26	0.02
	EPA1151B	32.27	86.4	414.96	28.69	0.069
	EPA1199A	45.43	100.2	447.46	72.03	0.161
	EPA1199B	91.08	100	482.46	54.63	0.113
	EPA1222A	107.83	99.2	493.46	68.91	0.14
	EPA1222B	69.44	100	483.96	70.88	0.146
	EPA1226A	251.13	200	982.42	132.82	0.135
	EPA1226B	137.64	201.1	895.43	137.91	0.154
	EPA1232A	121.95	200	900.92	150.09	0.167
	EPA1232B	67.52	194.8	751.44	116.62	0.155
	EPA1421A	22.08	97.9	409.46	46.2	0.112
	EPA1421B	44.88	98.7	477.46	54.6	0.114
o-Ethyltoluene	EPA1179A	52.85	91.7	399.47	86.49	0.216
	EPA1179B	52.92	93	415.46	75.33	0.181
	EPA1202A	60.31	99.7	421.96	69.89	0.166
	EPA1202B	107.86	100	453.46	34.1	0.075
	EPA1215A	107.85	180.3	637.45	150.91	0.237
	EPA1215B	56.47	200	581.45	97.71	0.168
	EPA1233A	197.48	204.3	925.92	157.98	0.171
	EPA1233B	259.1	198.9	896.92	120.69	0.134
	EPA1413A	21.33	100.4	370.97	64.47	0.174
	EPA1413B	45.83	98.4	455.46	64.37	0.141
p-Ethyltoluene	EPA1194A	90.69	196.4	741.44	90.43	0.122
	EPA1194B	88.4	200	760.94	72.99	0.096
	EPA1197A	56.36	191.7	653.44	66.43	0.102
	EPA1197B	98.54	192.1	710.44	58.35	0.0821
	EPA1214A	103.9	100	455.96	19.17	0.042
	EPA1214B	53.41	101.7	417.96	29.06	0.069
	EPA1229A	192.1	200	888.43	87.56	0.098
	EPA1229B	258.21	197.1	819.93	37.41	0.046
1,2,3-Trimethylbenzene	EPA1158A	10.27	79.9	295.97	22.18	0.075
	EPA1158B	22.37	79.9	378.97	32.28	0.085
	EPA1162A	33.39	80.1	390.97	46.52	0.119
	EPA1162B	N/A	N/A	398.46	46.59	0.117
	EPA1330A	150	83.6	416.96	14.13	0.034
	EPA1330B	100	79.3	394.97	17.37	0.044
1,2,4-Trimethylbenzene	EPA1117A	10.31	80	334.97	16.8	0.05
	EPA1117B	20.71	80	367.97	18.2	0.049
	EPA1119A	49.78	78	384.97	19.6	0.051

	EPA1119B	41.57	79	389.97	25.48	0.065
	EPA1123A	10.14	80	299.98	11.2	0.037
	EPA1123B	22.09	80	344.97	15.4	0.045
	EPA1126A	10.07	77.5	286.48	12.6	0.044
	EPA1126B	24.3	75.9	332.97	15.4	0.046
	EPA1129A	41.64	40.8	200.48	4.2	0.021
	EPA1129B	15.63	42	200.98	5.6	0.028
	EPA1352A	186.06	80	394.97	5.71	0.014
	EPA1352B	132.44	79	394.96	8.9	0.022
	EPA1354A	200.17	78	387.47	5.77	0.015
	EPA1354B	152.7	78	385.97	9.25	0.024
	EPA1356A	120.61	80	389.97	14.66	0.037
	EPA1356B	100.2	79.3	388.97	11	0.028
1,3,5-Trimethylbenzene	EPA1153A	10.98	79.5	309.47	12.36	0.04
	EPA1153B	20.38	80	381.47	19.63	0.051
	EPA1156A	32.31	80.2	379.47	24.77	0.065
	EPA1156B	46.11	79.6	390.47	19	0.049
	EPA1329A	86.18	80	388.97	0.6	0.001
	EPA1329B	64.78	80	296.47	3.01	0.007
1,2,4,5-Tetramethylbenzene	EPA1529A	70	49.3	274.69	3.17	0.012
	EPA1531A	25	180	751.5	17.94	0.024
Pentamethylbenzene	EPA1488A	25.14	150.9	834.93	165.07	0.198
	EPA1521A	23.54	147.2	892.89	32.69	0.037
Hexamethylbenzene	EPA1557A	28	168	999	15.28	0.015

a) yields calculated using SOA density 1.4 g/cm^3

Table 2.2 SOA yield parameters

Yield Curve	α_1	$K_{om,1}$ (m^3/ μg)	α_2	$K_{om,2}$ (m^3/ μg)
Curve 1	0.085	0.251	2.420	0.00064
Curve 2	0.101	0.042	1.840	0.00064
Curve 3	0.106	0.025	1.42	0.00064
Curve 4	0.038	0.050	0.167	0.00190

Table 2.3 Summary of experimental conditions

Groups	Light Source	NO_2 Photolysis Rate/s^{-1}	Reactor Volume/m^3	Reaction Time/h
This work	Blacklights	6.68×10^{-3}	90	6~10
Odum J.R.	Solar irradiation	N/A	60	N/A
Kleidienst T.E.	244 cm fluorescent bulbs	8.3×10^{-3}	11.3	12 ~ 15
Edney E.O.	244 cm fluorescent bulbs	8.3×10^{-3}	11.3	12 ~ 15
Izumi K.	1.6 kW Xe lamps	4.5×10^{-3}	4	1 ~ 5
Sato K.	19 kW xenon arc lamps	$(4.7 \pm 0.2) \times 10^{-3}$	6	3 ~ 4.5
Takekawa H.	Blacklights	4×10^{-3}	2	~6
Ng N.L	Blacklights	N/A	28	4 ~ 20
Chhabra P.S.	Blacklights	N/A	28	N/A
Borras E.	Solar irradiation	7×10^{-3}	200	~6
Cocker D.	Blacklights	18.3×10^{-3}	28	~12
Song C.	Blacklights	6.68×10^{-3}	90	~6
Healy R./UCC	12 Philips TL05 and TL12 lamps	N/A	6.5	6~8
Healy R./PSI	4 kW xenon arc lamps	N/A	27	6~8
Wyche K.P./PSI	4 kW xenon arc lamps	N/A	27	N/A
Martin-Reviejo M.	Solar irradiation	8.67×10^{-3}	N/A	N/A

N/A: not applicable

2.7 Figures

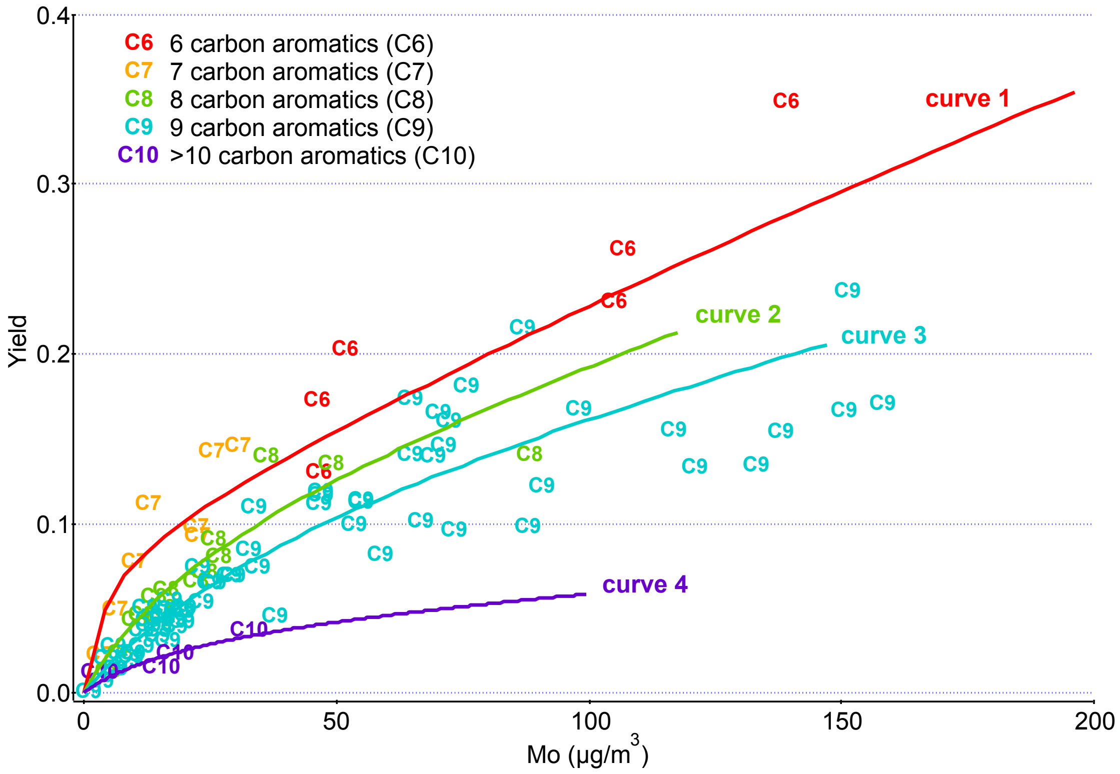

Figure 2.1 Secondary organic aerosol yields for 17 individual aromatic hydrocarbons under low-NO_X conditions. Yield curves are fit to each data group (C6 and C7 are combined as are C10 and higher) using the two-product model by minimizing the weighted squared residuals.

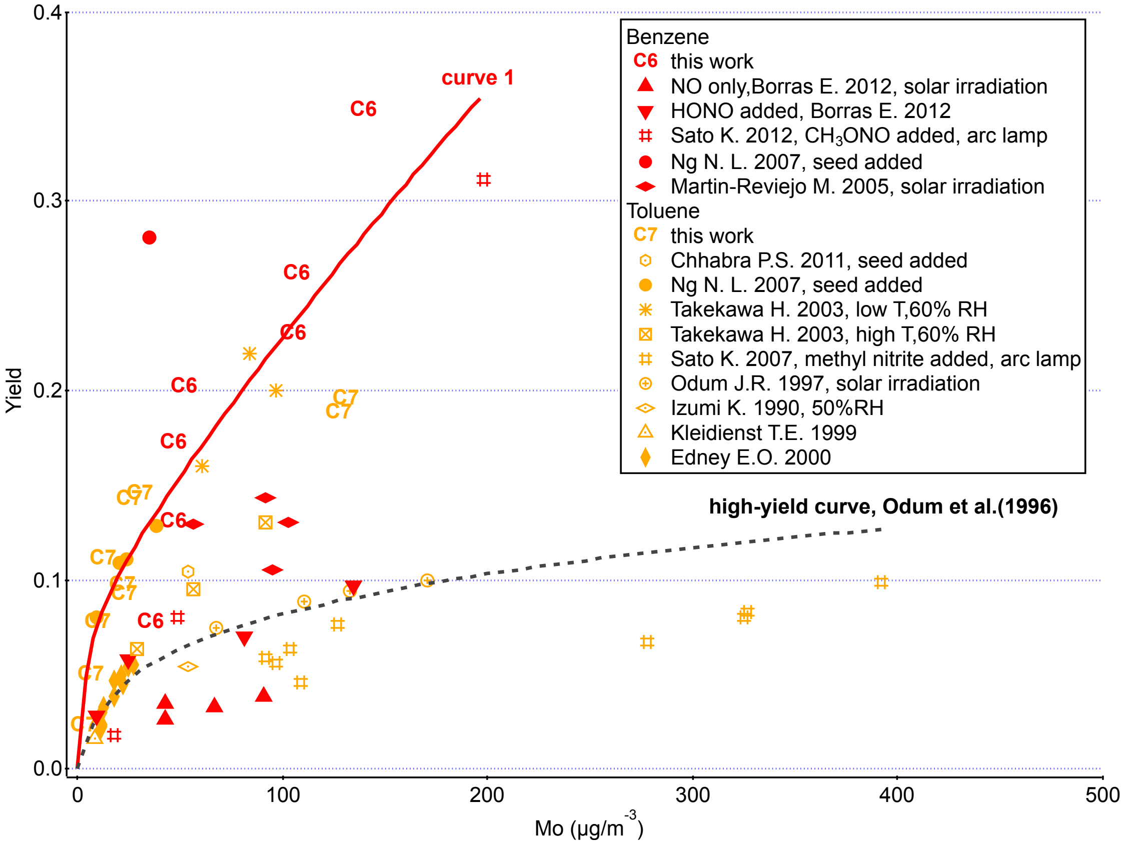

Figure 2.2 Secondary organic aerosol yields for benzene and toluene.

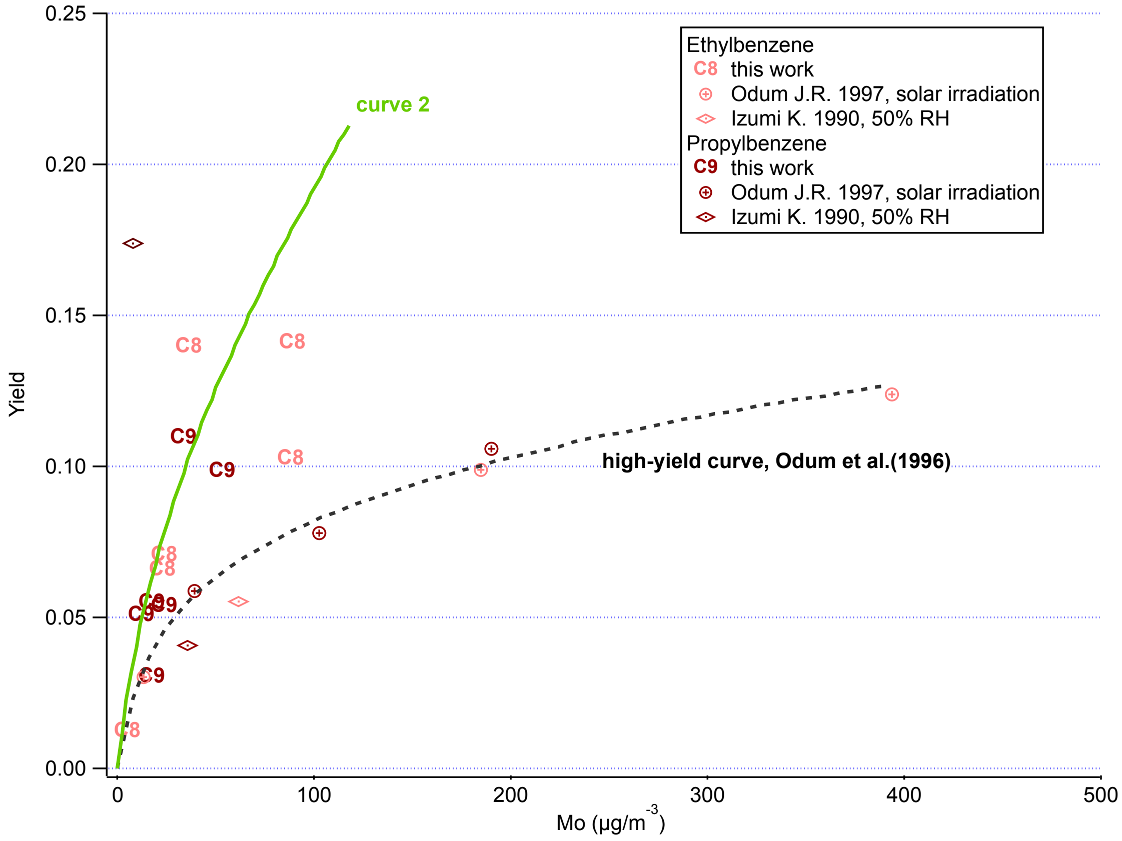

Figure 2.3 Secondary organic aerosol yields for ethylbenzene and propylbenzenes.

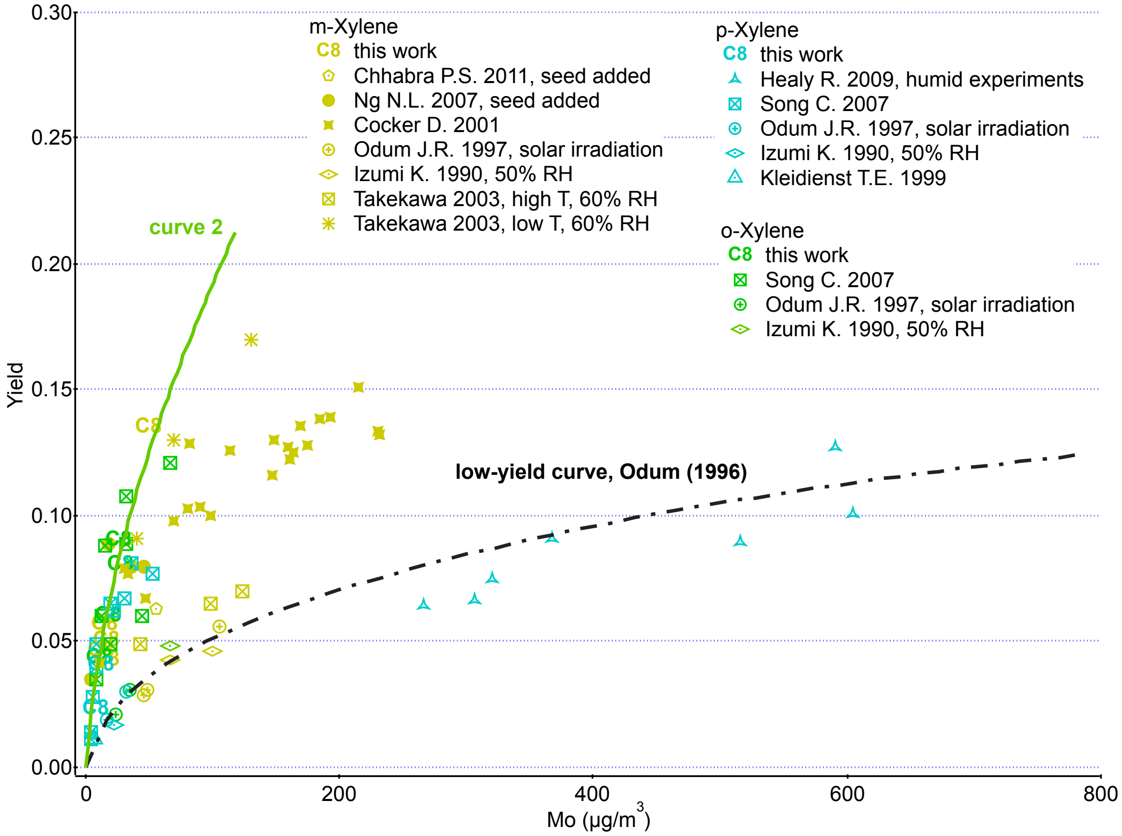

Figure 2.4 Secondary organic aerosol yields for xylene isomers.

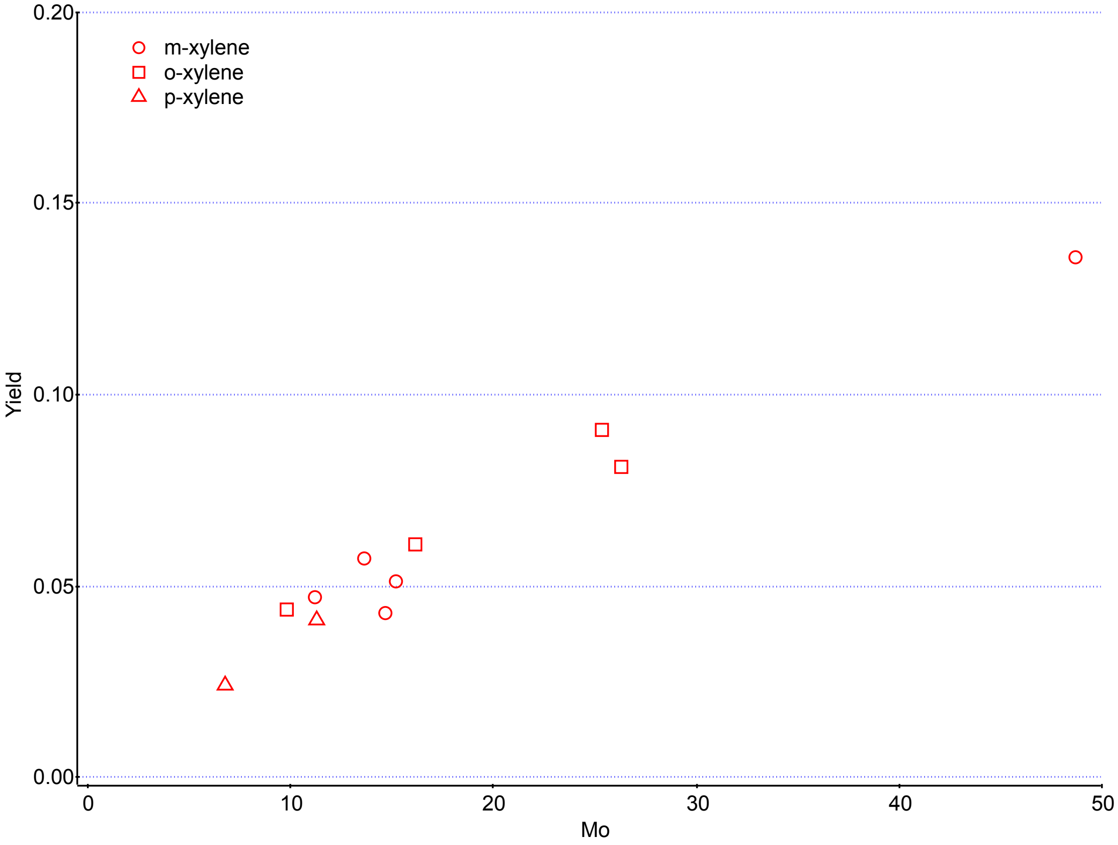

Figure 2.5 Comparison of secondary organic aerosol formation from xylene isomers.

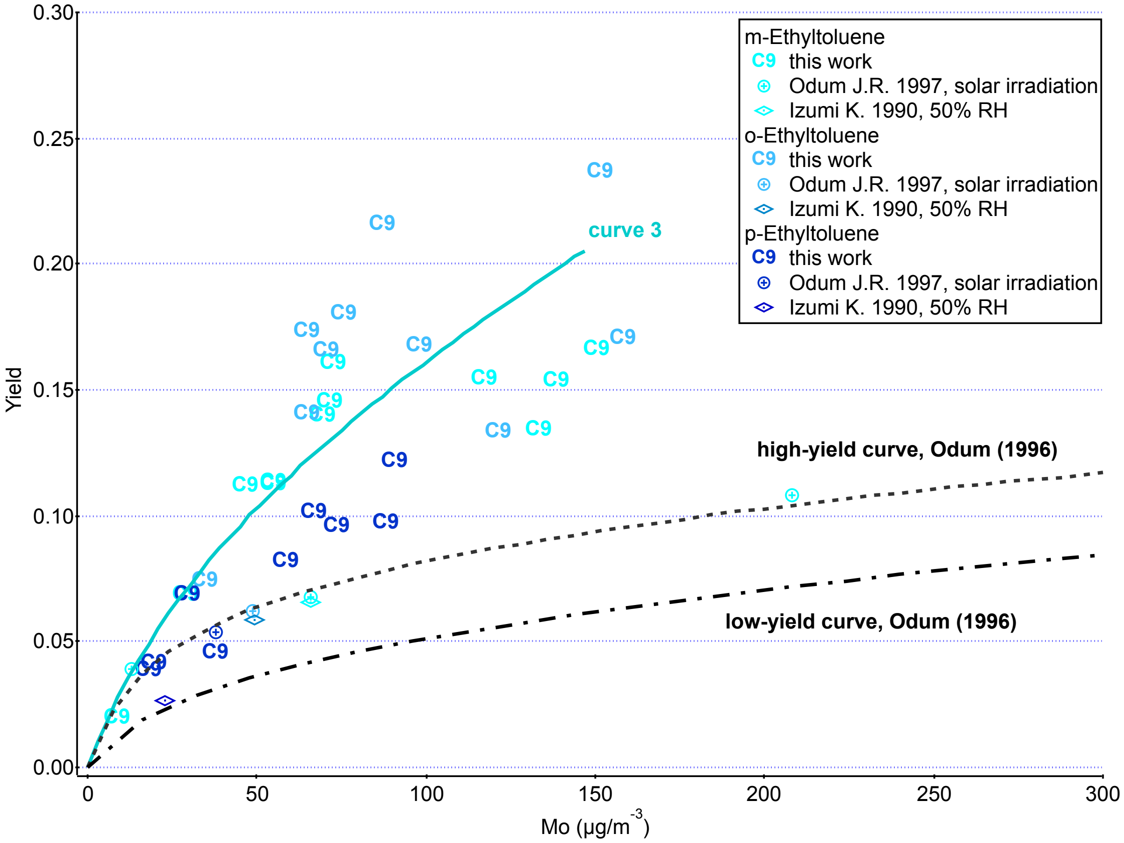

Figure 2.6 Secondary organic aerosol yields for ethyltoluene isomers.

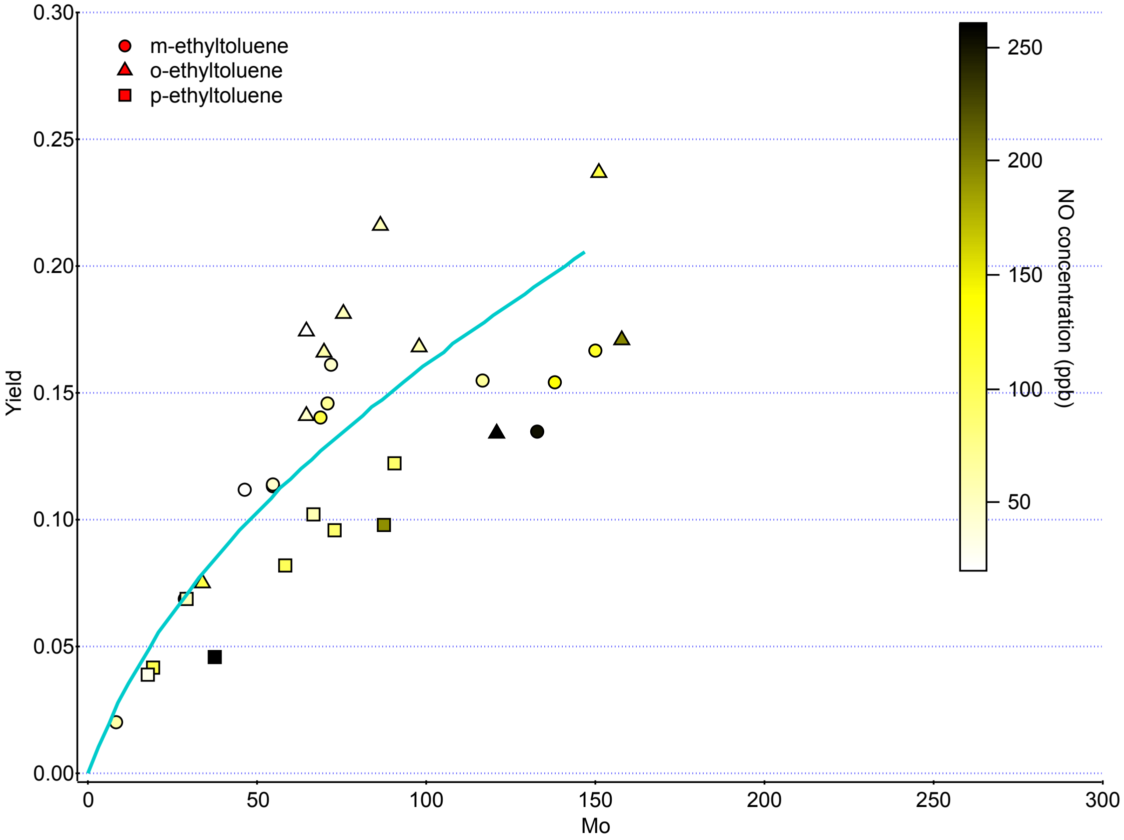

Figure 2.7 Secondary organic aerosol yields for ethyltoluene isomers in this study as a function of NO_X loading. Data points are colored with NO concentration in each experiment.

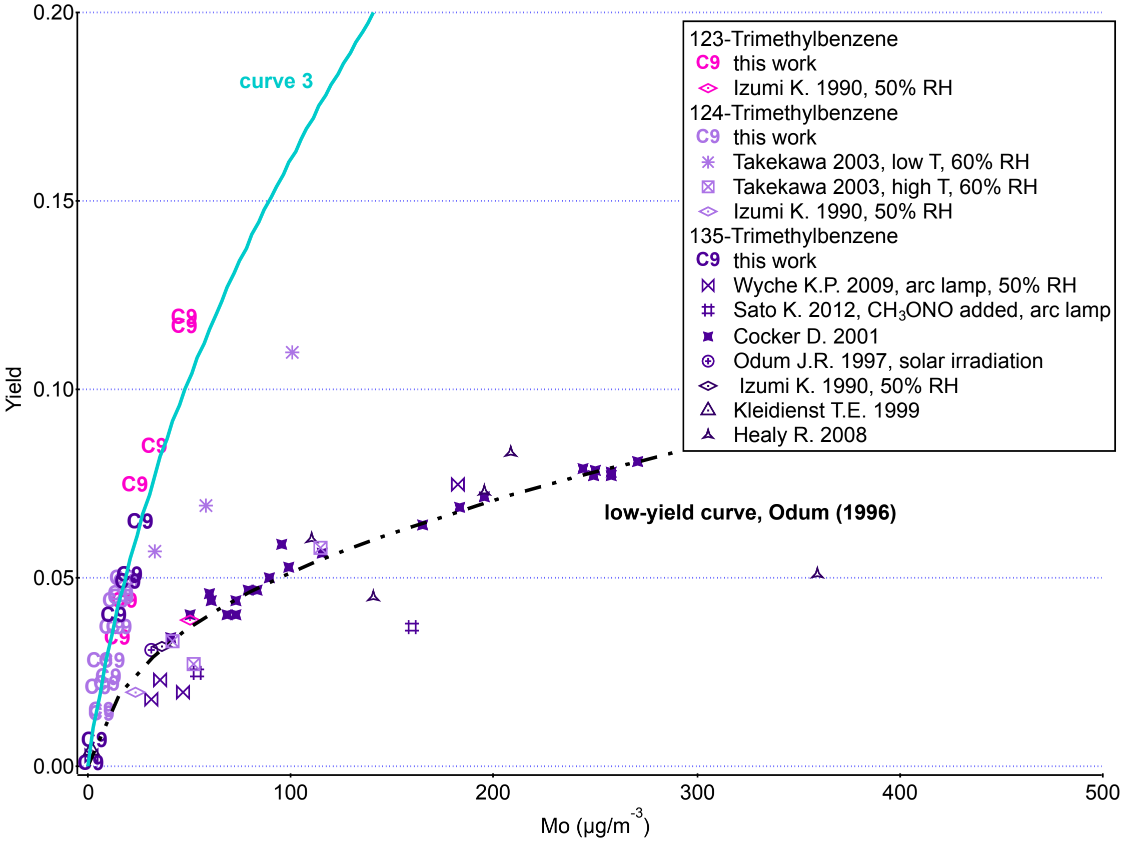

Figure 2.8 Secondary organic aerosol yields for trimethylbenzene isomers.

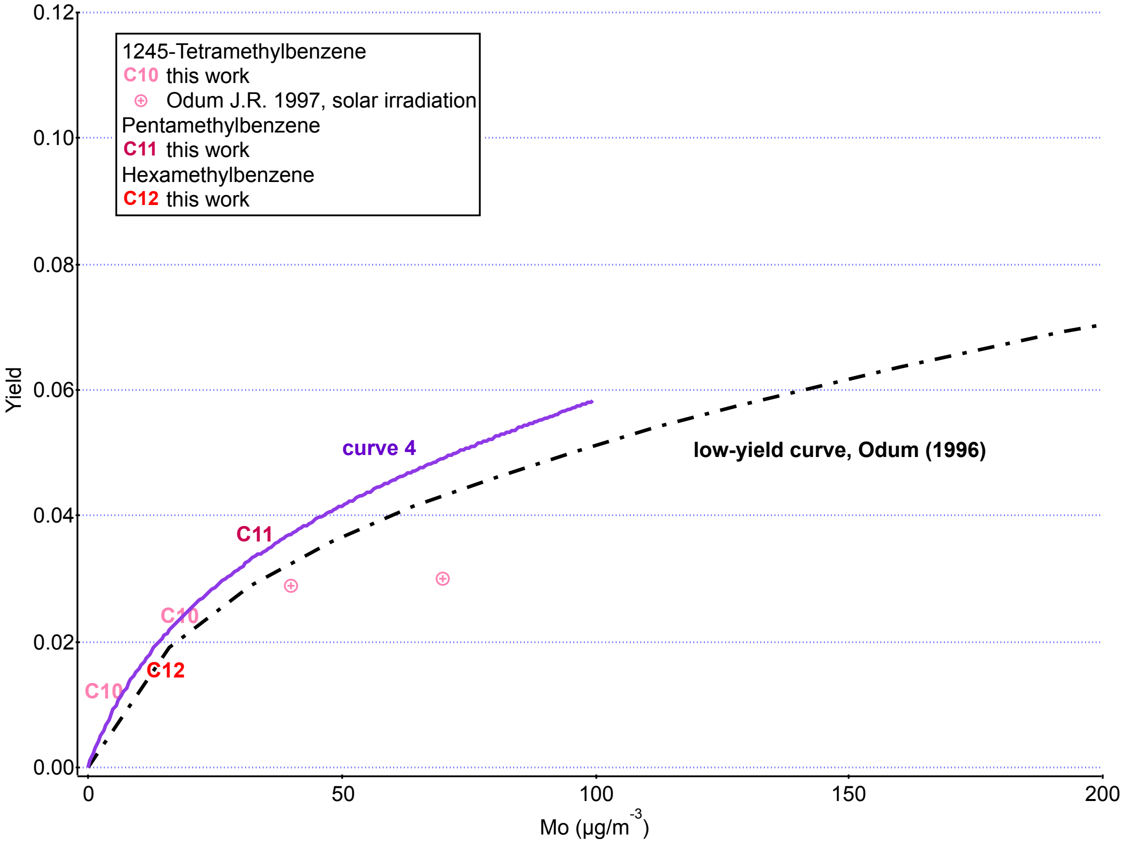

Figure 2.9 SOA formation for 1,2,4,5-tetramethylbenzene, pentamethylbenzene, and hexamethylbenzene.

3 Chemical Composition of Secondary Organic Aerosol Formed from Different Aromatic Hydrocarbon

3.1 Introduction

Atmospheric aerosols have profound impacts on both global climate and human health through processes such as light absorption and scattering, lung deposition. A key aspect to understand these impacts is comprehensive characterization of the physical and chemical properties of particles. Among a family of online techniques (AMS, FTIR and NMR spectroscopy) that attempt to analyze organic aerosol (OA) chemical composition, the aerodyne aerosol mass spectrometer (AMS) has much higher time and size resolution (DeCarlo *et al.*, 2006a). Further, the elemental analysis (EA) technique (Aiken *et al.*, 2008, 2007) is demonstrated to provide elemental composition of organic aerosol and is widely used to investigate the chemical composition of OA.

A number of field studies have used AMS to quantify organic mass (OM). Zhang *et al.* (2005a) used mass-to-charge ratios m/z 57 and m/z 44 obtained using the AMS from ambient Pittsburgh aerosol as tracers to quantify the mass concentration of hydrocarbon-like and oxygenated organic aerosol (HOA and OOA). Zhang *et al.* (2005b) also indicated a direct correspondence of HOA to primary OA from local emissions; and found the mass spectrum of OOA highly resembled aged and oxidized OA, which indicated a direct correspondence of OOA to SOA. Subsequent field studies (DeCarlo *et al.*, 2008; Lanz *et al.*, 2008, 2007b; Ulbrich *et al.*, 2009) confirmed the results of Zhang *et al.* (2005a,2005b). Recently, Ng *et al.* (2010) compiled results from the factor analysis of 43 Northern Hemisphere AMS datasets, and found that OOA can be furthered deconvolved into low-volatility OOA (LV-OOA) and semi-volatile OOA (SV-OOA) characterized by AMS signal at m/z 43 (mostly $C_2H_3O^+$) and m/z 44 (CO_2^+). Ng *et al.* (2010) also examined the OOA components by plotting f44 vs. f43 from different studies, where f44 and f43 are the ratios of m/z 44 and m/z 43 to the total OA in the spectrum. Ng *et al.* (2010) found that ambient OOA was located in a triangular area in the f44 vs. f43 plot and indicated that ambient OA converged towards highly aged LV-OOA with increasing atmospheric oxidation.

Many laboratory studies have been conducted to investigate SOA chemical composition and formation mechanisms using simulation chambers. Aiken *et al.* (2008) first applied EA analysis of AMS to both field and chamber studies and found O/C ratios ranging from 0.27-0.42, which indicated a less oxidized OA was formed in environmental chambers than is observed in ambient air. Recent studies by Ng *et al.* (2010) and Chhabra *et al.* (2010) observed that chamber SOA were more similar to SV-OOA on triangle-plot. Chhabra *et al.* (2010) observed that the O/C ratio of SOA formed from single-ring aromatic and naphthalene SOA can reach up to 0.7, which is within the range of ambient OOA as suggested by Ng *et al.* (2010). Sato *et al.* (2010) investigated the photo oxidation of seven aromatic hydrocarbons using an AMS with continuous aging of SOA observed during the course of experiments. Sato *et al.* (2010) also observed an increase of f43 and decrease of f44 with increasing number of alkyl substituents of parent aromatics, which indicated more low-reactive ketones are formed with increasing number of alkyl substituents.

Heald *et al.* (2010) employed a new AMS method, Van-Krevelen graph, to interpret the high-resolution mass spectrometric data and the evolution of OA composition. On Van-Krevelen Diagram (Van Krevelen et al., 1950), a straight line with a slope of 0 indicates the addition of alcohols or peroxides; a slope of -1 represents addition of carboxylic acids, a slope of -2, addition of ketones or aldehydes. Heald *et al.* (2010) found that a variety of lab and field data clustered around the line with a slope of -1 on Van-Krevelen Graph. Movement along this line reflects atmospheric aging processes such as volatilization, oxidation and mixing.

In this study, SOA chemical composition formed from the photooxidation of 17 different aromatic hydrocarbons are evaluated using the Van Krevelen and triangle plot analyses. The impact of precursor structure on SOA composition is investigated by exploring the high-resolution time-of-flight AMS (HR-ToF-AMS) spectra and elemental composition. Finally, volatility of the SOA produced in the chamber is explored as a function of precursor chemical structure.

3.2 **Experimental Methods**

All experiments within this paper were conducted in the UC Riverside/CE-CERT indoor environmental chamber, which has been described in detail elsewhere (Carter *et al.*, 2005). All experiments were performed under dry conditions (RH<0.1%), in the absence of inorganic seed aerosol, and at chamber temperatures of 27°C. The UV-radiation is generated by 272 115 W Sylvania 350 Black lights, with a NO_X photolysis rate measured at 0.4 min^{-1}.

The Aerodyne High Resolution Time-of-Flight Aerosol Mass Spectrometer (HR-ToF-AMS) (Canagaratna *et al.*, 2007; DeCarlo *et al.*, 2006) is used to provide on-line quantitative measurements of bulk chemical composition. The AMS was switched between a high resolution "W-mode" and a high sensitivity "V-mode". The higher resolution "W-mode" allowed for identification of different elemental compositions from each unit mass using the PIKA toolbox (DeCarlo *et al.*, 2006). Elemental ratios for total organic mass, oxygen to carbon (O/C), and hydrogen to carbon (H/C) were determined using the elemental analysis (EA) technique (Aiken *et al.*, 2007). "V-mode" data were used to produce "triangle plots" and "W-mode" data were used in Van-Krevelen diagrams reported within this paper.

SOA volatility was continuously measured using a custom built Volatility Tandem Differential Mobility Analyzer (VTDMA) based on the original TDMA design of (Rader and McMurry, 1986). Volatility was measured as the volume fraction remaining (VFR) of the aerosol after transport through a Dekati® Thermodenuder TD3 operated at 100 °C (particle residence time of 16 sec).

For each experiment, one of seventeen individual aromatic compounds were introduced into the environmental reactor along with either NO (~10:1 HC (ppbC) / NO (ppb) ratio) or H_2O_2 (OH radical source). Table 3.1 and Table 3.2 summarize the 45 experiments performed including hydrocarbon reacted and quantity of NO or H_2O_2 injected.

3.3 Results and Discussion

m/z 43 ($C_2H_3O^+$) and m/z 44 (CO_2^+) are the two major AMS fragmentation ions from aromatic secondary organic aerosol. The $C_2H_3O^+$ fragment ion at m/z 43 is commonly associated with oxidized organic molecules containing carbonyl groups, while the m/z 44 fragment ion is typically associated with carboxylic acids and is often used as a marker of oxygenated organic aerosol (OOA). It is observed that the fraction of m/z 44 formed ((m/z 44)/organic mass) decreases with increasing number of alkyl substituents of aromatic hydrocarbons in agreement with previous observations by Sato *et al.* (2010). Further, SOA produced from Aerosol formed from aromatics with ethyl or propyl substituents is observed to have relatively strong intensities at m/z 57 ($C_3H_5O^+$) and m/z 71 ($C_4H_7O^+$) along with m/z 43 ($C_2H_3O^+$), presumably as oxidized fragments of the longer alkyl chains. Sato *et al.* (2010) also observed that the $C_3H_5O^+$ (m/z 57) was found together with $C_2H_3O^+$ in the oxidation of ethylbenzene.

A linear increasing trend (slope = 0.8853, $R^2 = 0.8857$) of (m/z 43 + m/z 57 + m/z 71) to m/z 44 ratio is observed with increasing numbers of alkyl substitutents on the aromatic ring (Figure 3.1). This trend is observed for both HC/NO_X photooxidation experiments as well as H_2O_2 photooxidation experiments; with slightly higher (m/z 43 + m/z 57 + m/z 71) to m/z 44 observed for H_2O_2 experiments compared to the HC/NO_X experiments.

3.3.1 Benzene SOA Fragmentation Patterns

Figure 3.2 shows the triangle plot (f44 vs. f43) and Van Krevelen diagram (H/C vs. O/C) for SOA produced from benzene photooxidation for both the no-NO_X and low-

NO_X conditions. The time progression of each system is illustrated using a color scale from red to purple representing the beginning to the end of each experiment. For both the benzene/NO_X and benzene/H_2O_2 systems the f44 and the O/C ratio increases with aerosol production as a result of aerosol aging. According to previous studies (Aiken *et al.*, 2007; Alfarra, 2004; Takegawa *et al.*, 2007), the AMS signal CO_2^+ at m/z 44 originates from the decarboxylation of organic acid groups and acyl peroxides. Photooxidation of benzene can form ring-opening products (e.g. dialdehydes, Calvert *et al.*, 2002; Sato *et al.*, 2010) while gas-phase oxidation of aldehydes can produce carboxylic acids (Keywood *et al.*, 2004). Jang and Kamens (2001) suggest that high vapor pressure oxocarboxylic acids could form from low-volatility acetals through heterogeneous reactions. Sato *et al.* (2010) further suggests that acetals could be dissociated reversibly to form oxocarboxylic acids during heating at the vaporization plate in the AMS.

Ng *et al.* (2010) observed that the ambient OOA components cluster within a triangle region of the f44 vs. f43 plot (dashed lines, Figure 3.2 a). Benzene SOA data obtained from this study is located at the top of the triangle; the O/C ratio (Figure 3.2 b) and f44 are close to LV-OOA, which suggests that the benzene SOA is well-oxidized (OSc ranges from ~ -0.1 to 0.5).

3.3.2 Toluene SOA

The triangle and Van Krevelen plots for toluene photooxidation SOA is shown in Figure 3.3. Toluene SOA sits to the right side of the triangle from Ng *et al.* (2010). Compared to benzene SOA, toluene SOA has a higher m/z 43 ratio and relatively lower m/z 44 ratio, and also shows a lower O/C ratio and higher H/C ratio on Van Krevelen graph. This indicates that the SOA produced from toluene is less oxidized than SOA produced from benzene (OSc ranges from ~ -0.5 to 0.1). No obvious increase in O/C ratio was observed in the Van Krevelen diagram as the experiment progressed (Figure 3.3 b), which also indicates a less oxygenated aerosol was formed during the course of the toluene experiments than in the benzene experiments.

It is estimated that 90% of the OH-toluene reaction starts from OH addition to the aromatic ring (Atkinson and Arey, 2003; Atkinson, 2000; Forstner *et al.*, 1997), and both ring-retaining (e.g., benzaldehyde and 2-methyl-4-nirophenol) and ring-fragmentation products (e.g., furans and furanones) are formed mainly from the reaction of methylhydroxycyclohexadienyl radical. Jang and Kamens (2001) identified a wide range of ring opening oxycarboxylic acids and ring retaining products from toluene photooxidation. Moreover, quite volatile compounds like glyoxal and methyl glyoxal were also found in particle phase, which suggest that early generation products condensed into particle phase before secondary reaction could occur. Kleindienst *et al.* (2004) also detected glyoxal and methyl glyoxal in particle phase while studies by Sato *et al.* (2007) suggested that the major products in the toluene aerosols were second generation products, such as hemiacetal and low-molecular-weight dicarboxylic acids. However, products quantified in these studies comprised only a small portion of the aerosol.

Recent study by Chhabra *et al.* (2011) investigated toluene SOA using triangle and Van Krevelen graph. Their toluene SOA was located on the right side of the triangle and migrated upwards suggested an increase of organic acid content. In this study, toluene SOA has a higher fraction of m/z 43, which indicates more first generation aldehydes/ketones were formed than second generation acids in the current study.

3.3.3 Ethylbenzene SOA

The triangle and Van Krevelen plots for ethylbenzene photooxidation SOA appear in Figure 3.4. The chemical structure of ethylbenzene is similar to toluene; both of them have one alkyl group attached to the ring. On triangle plot, we found that the m/z 44 fraction of ethylbenzene SOA is at the same range as toluene SOA, but ethylbenzene SOA has a lower fraction of m/z 43; however, when m/z 57 is included in the analysis, the fraction of m/z 43 + m/z 57 is similar to that of toluene. More $C_3H_5O^+$ was produced than $C_2H_3O^+$ during electron ionization in the AMS because of the ethyl group on the ring. Sato *et al.* (2010) also found that ketones with a propionyl ($-COC_2H_5$) group were produced in the oxidation of ethylbenzene, and $C_3H_5O^+$ ions were detected together with $C_2H_3O^+$. Forstner *et al.* (1997) identified acetophenone and 3-methyl-2,5-furandione to be the predominant components of ethylbenzene aerosols; as a secondary alkyl radical is more stable than a primary alkyl radical, the abstraction mechanism results in more acetophenone.

Ethylbenzene SOA is located in the same region of the Van Krevelen diagram as toluene SOA; like toluene photooxidation, no obvious aging process was observed for ethyltoluene.

3.3.4 Propylbenzene and Isopropylbenzene SOA

The triangle plot and Van Krevelen diagram for SOA formed from photooxidation of propylbenzene and isopropylbenzene is plotted in Figure 3.5. On the triangle plot (Figure 3.5 a), isopropylbenzene SOA has a higher m/z 43 fraction than propylbenzene, because the propyl substituents on aromatic ring produced $C_3H_5O^+$ and $C_4H_7O^+$ besides $C_2H_3O^+$ from aldehydes/ketones in the AMS. Similar to observations made for ethylbenzene and toluene SOA, propylbenzene and isopropylbenzene SOA cluster at the same region of the triangle plot and Van Krevelen diagram, no aging of the SOA was observed during the experiments.

3.3.5 Xylene Isomer SOA Composition Data

The three isomers of xylene isomers were investigated in this study and the triangle and Van Krevelen plots are shown in Figure 3.6 and Figure 3.7. Data points of xylene/NO photooxidation are relatively more scattered than for the H_2O_2 experiments, possibly due to shorter reaction times (~5 hours) and lower mass concentration of aerosol produced for the NO_X experiments. SOA is observed to beat the right side of the triangle. The fraction of m/z 43 is 0.2~0.3 which is much higher than SOA from one substituent aromatics. Among three xylene isomers, m-xylene SOA is observed to have a relatively lower fraction of m/z 44, and also a lower O/C ratio on Van-Krevelen plot.

Aerosol formed from xylenes/H_2O_2 photooxidation (Figure 3.7) has a lower O/C ratio compared to toluene (Figure 3.3 b) and ethylbenzene (Figure 3.4 b) and propylbenzene (Figure 3.5 b). The lower O/C ratio is attributed to the presence of the second xylene methyl group. The time elapse for O/C and H/C evolution during the xylene/H_2O_2 experiments are also displayed in Figure 3.7. No obvious aging is observed for p-xylene and o-xylene SOA. However, an increase of O/C ratio (slope of -1) is observed for the m-xylene SOA indicating ongoing oxidation of m-xylene SOA, perhaps due to oxidation of unsaturated compounds in particle phase to form organic acids. Similar trends were also observed by Chhabra *et al.* (2010). Further, in a recent study by Loza *et al.* (2012) for m-xylene/low-NO_X photooxidation experiments over extended reaction times (up to 12~36 hours), observed continuous aging of the *m*-xylene SOA. Loza *et al.* (2012) suggests that during SOA aging, multi-generation products are formed through molecular functionalization. Loza *et al.* (2012) also suggests that gas-phase OH reaction of low volatility SOA precursors is the dominant pathway of aging in m-xylene systems. The difference between o-xylene, p-xylene SOA and m-xylene SOA might be attributed to the different rate constants for the reactions of OH radical with xylenes. For o-xylene and p-xylene, k_{OH} are 1.36e-11 cm^3/ molec·s and 1.43e-11 cm^3/ molec·s, respectively, while k_{OH} for m-xylene is 2.31e-11 cm^3/ molec·s.

3.3.6 Ethyltoluene SOA

Figure 3.8 and Figure 3.9 shows the triangle plot and Van Krevelen diagram of SOA formed from ethyltoluene photooxidation. Under low-NO_X condition, SOA of all three ethyltoluene isomers cluster in the area on the right side of the triangle, f44 and f43 are 0.12~0.21 and 0.11~0.17, respectively. A lower f43 value of ethyltoluene SOA than xylene SOA is mainly due to the ethyl group on the aromatic ring (the $C_3H_5O^+$ ion was detected instead of $C_2H_3O^+$ ion). If f57 is added to the f43, the values become similar to that of the xylene isomers. An obvious increasing of O/C ratio is observed during the course of each experiment (Figure 3.9). Ethyltoluene/H_2O_2 photooxidation produced aerosol with a slightly higher f44 value, and also a slightly higher O/C ratio, indicating more oxidized SOA (OSc = ~ -1- -0.4). SOA aging is also observed on Van Krevelen diagram for all ethyltoluene isomers.

Forstner *et al.* (1997) suggested products like m-tolualdehyde/p-tolualdehyde (O:C = 0.125, H:C=1), 1,3-ethylbenzoic acid (O:C = 0.222, H:C = 1.11) were formed through H-abstraction pathway for m-ethyltoluene and p-ethyltoluene. Andino *et al.* (1996) proposed ring-fragmentation products from the m-ethyltoluene/p-ethyltoluene-OH adducts, such as 4-oxo-2-hexenal, 4-oxo-2-pentanal (O:C = 0.33, H:C = 1.33), 2-methyl-2-butenedial (O:C = 0.4, H:C = 1.2), etc. On the Van Krevelen diagram, O:C and H:C ratio of ethyltoluene SOA are 0.33 ~ 0.51 and 1.25 ~ 1.51, suggesting that more ring-fragmentation products were formed in ethyltoluene photooxidation than ring-retaining products.

3.3.7 Trimethylbenzene SOA

Photooxidation of three trimethylbenzene isomers was also investigated in this study (Figure 3.10 and Figure 3.11). Trimethylbenzene SOA is located far to the right side of the triangle plot, with f43 and f44 values ranging from 0.21~0.38 and 0.11 ~ 0.21, respectively. The location of trimethylbenzene SOA on triangle plot is similar to that obtained by Sato *et al.* (2012, 2010). Studies by Sato *et al.* (2010, 2012) and Chhabra *et al.* (2011) found that SOA formed from aromatic phootooxidation were clustered close to the straight line with a slope of -1 on the Van Krevelen diagram. They also observe migration of data points along this straight line as the experiment progressed and the SOA aged, which suggests an aging process resulted in the formation of carboxylic acid through the oxidation of carbonyls. Sato *et al.* (2012) further identified ketocarboxylic acid in 1,3,5-trimethylbenzene SOA and noted that the SOA aging was rate-limited by the oxidation of ketone groups.

In this study, trimethylbenzene SOA is observed to cluster between the slope of -1 and slope -2 straight lines on the Van Krevelen plot; migration of SOA along the slope of -1 line observed by Sato *et al.* (2012) was not observed. It is noted that Sato *et al.* (2012) used CH_3ONO to increase the OH concentration in the system. It is possible that the OH concentration in our system was lower and limited the oxidation of ketone groups, thus SOA from trimethylbenzene photooxidation has a greater contribution from 1st generation aldehydes and ketones than the carboxylic acids further oxidized in their study.

3.3.8 SOA from Aromatic Hydrocarbon with 4 or More Methyl Groups

SOA formation from the photooxidation of 1,2,4,5-tetramethylbenzene, pentamethylbenzene and hexamethylbenzene were also investigated. SOA from aromatic hydrocarbon with 4 or more methyl groups have a fraction of m/z 43 larger than 0.3, and a fraction of m/z 44 around 0.1 (except pentamentylbenzene/NO SOA which has m/z43 around 0.2) on the triangle plot (Figure 3.12). 1,2,4,5-tetramethylbenzene SOA is located between the line with a slope of -1 and line with a slope of -2 on the Van Krevelen diagram; SOA from pentamethylbenzene and hexamethylbenzene photooxidation are more close to the line with a slope of -2, indicating more aldehydes and ketones in the aerosol. Compared to SOA formed from aromatic hydrocarbons with less alkyl groups attached, SOA from these three compounds have a higher value of f43 and a lower value of f44 and O/C ratio, indicating less oxidized aerosol were formed.

3.3.9 SOA Chemical Composition and Volatility Evolution

Measurement of SOA volatility can provide indirect information about its chemical composition. Kalberer *et al.* (2004) reported the volume fraction remaining (VFR) from SOA produced from trimethylbenzene photooxidation increased from 30% to more than 85% at 100 °C. Kalberer *et al.* (2004) attributes this increase to polymer formation. Previous studies (Carlton *et al.*, 2010; Ng *et al.*, 2007) observe SOA formed from aromatic/H_2O_2 photooxidation was considered nonvolatile. Ng *et al.* (2007) observed that for aromatic/H_2O_2 systems, SOA yields remained constant throughout the experiment which implied SOA formed from RO_2 + HO_2 reaction was nonvolatile.

Figure 3.13 shows the VFR at the end of each aromatic no-NO_X and low-NO_X experiment from the current study. It should be noted that VFR increased continuously during the course of each experiment (initial VFR is shown in Table 3.1 and Table 3.2). VFR data are plotted versus the carbon number of parent aromatics with the color of the data points scaled to average m/z 43/ m/z 44 ratio observed for each experiment. VFR observed for H_2O_2 experiments are less than 1 implying that SOA formed in this study is semi-volatile. Decreasing VFR with increasing number of ring substituents was observed for both H_2O_2 and NO experiments indicating that SOA formed from heavier aromatics are more volatile than lighter, less substituted aromatics. It is hypothesized that branches on aromatic ring made the semi-volatiles formed from RO_2 + HO_2 and RO_2 + NO reactions less stable allowing them to undergo further ring opening processes to form lower molecular mass and more volatile SOA products. VFR values were observed to decrease while m/z43/m/z 44 ratio increased as the number of carbon atoms in the aromatic increased (Figure 3.13). The trend of volatility and 43/44 ratio indicates less oxidized particles were produced for aromatic compounds with greater numbers of carbon.

3.4 Conclusions

In this study, SOA formation of 17 aromatic hydrocarbons was investigated in the environmental chamber under both low-NO_X and no-NO_X conditions. SOA chemical properties were investigated using the Ng *et al.* (2010) triangle plot and Van Krevelen diagram using data acquired using the HR-ToF-AMS. Among all the aromatic precursors, benzene SOA has the highest f44 value (0.26-0.28) and the lowest f43 value (~0.03). The higher f44 indicates higher carboxylic acid content in benzene SOA. With increasing the number of alkyl substituents on the ring led to observations of decreasing of f44 and increasing of f43. According to Sato *et al.* (2010), the f43 and f44trends result from increased yields of low-reactive ketones products relative to aldehydes production as the number of aromatic substituents increases. These observations are further confirmed using Van Krevelen diagrams. Benzene SOA has a slope of -1 on the Van Krevelen plot indicating the addition of carboxylic acids. Consistent with the f44 and f43 trend, the O/C ratio and OSc decreased with the increasing number of alkyl groups. Volatility evolution measurements shows that SOA formed form heavier aromatics are more volatile. More oxidized particles were formed from the photooxidation of lighter aromatics, which is consistent with the lower volatility of benzene and toluene SOA. Aerosol formed in this study are less oxidized than average ambient OOA.

3.5 **References**

Aiken, A.C., DeCarlo, P.F., Jimenez, J.L., 2007. Elemental Analysis of Organic Species with Electron Ionization High-Resolution Mass Spectrometry. Anal. Chem. 79, 8350–8358.

Aiken, A.C., DeCarlo, P.F., Kroll, J.H., Worsnop, D.R., Huffman, J.A., Docherty, K.S., Ulbrich, I.M., Mohr, C., Kimmel, J.R., Sueper, D., Sun, Y., Zhang, Q., Trimborn, A., Northway, M., Ziemann, P.J., Canagaratna, M.R., Onasch, T.B., Alfarra, M.R., Prevot, A.S.H., Dommen, J., Duplissy, J., Metzger, A., Baltensperger, U., Jimenez, J.L., 2008. O/C and OM/OC Ratios of Primary, Secondary, and Ambient Organic Aerosols with High-Resolution Time-of-Flight Aerosol Mass Spectrometry. Environ. Sci. Technol. 42, 4478–4485.

Alfarra, M.R., 2004. Insights into the atmospheric organic aerosols using an aerosol mass spectrometer. University of Manchester, UK.

Alfarra, M.R., Coe, H., Allan, J.D., Bower, K.N., Boudries, H., Canagaratna, M.R., Jimenez, J.L., Jayne, J.T., Garforth, A.A., Li, S.-M., Worsnop, D.R., 2004. Characterization of urban and rural organic particulate in the Lower Fraser Valley using two Aerodyne Aerosol Mass Spectrometers. Atmospheric Environment 38, 5745–5758.

Andino, J.M., Smith, J.N., Flagan, R.C., Goddard, W.A., Seinfeld, J.H., 1996. Mechanism of Atmospheric Photooxidation of Aromatics: A Theoretical Study. J. Phys. Chem. 100, 10967–10980.

Atkinson, R., 2000. Atmospheric chemistry of VOCs and NO_X. Atmospheric Environment 34, 2063–2101.

Atkinson, R., Arey, J., 2003. Gas-phase tropospheric chemistry of biogenic volatile organic compounds: a review. Atmospheric Environment 37, Supplement 2, 197–219.

Calvert, J.G., Atkinson, R., Becker, K.H., Kamens, R.M., Seinfeld, J.H., 2002. The Mechanisms of Atmospheric Oxidation of the Aromatic Hydrocarbons. Oxford University Press, New York.

Canagaratna, M.R., Jayne, J.T., Jimenez, J.L., Allan, J.D., Alfarra, M.R., Zhang, Q., Onasch, T.B., Drewnick, F., Coe, H., Middlebrook, A., Delia, A., Williams, L.R., Trimborn, A.M., Northway, M.J., DeCarlo, P.F., Kolb, C.E., Davidovits, P., Worsnop, D.R., 2007. Chemical and microphysical characterization of ambient aerosols with the aerodyne aerosol mass spectrometer. Mass Spectrom. Rev 26, 185–222.

Carlton, A.G., Bhave, P.V., Napelenok, S.L., Edney, E.O., Sarwar, G., Pinder, R.W., Pouliot, G.A., Houyoux, M., 2010. Model Representation of Secondary Organic Aerosol in CMAQv4.7. Environ. Sci. Technol. 44, 8553–8560.

Carter, W., Cockeriii, D., Fitz, D., Malkina, I., Bumiller, K., Sauer, C., Pisano, J., Bufalino, C., Song, C., 2005. A new environmental chamber for evaluation of gas-phase chemical mechanisms and secondary aerosol formation. Atmospheric Environment 39, 7768–7788.

Chhabra, P.S., Flagan, R.C., Seinfeld, J.H., 2010. Elemental analysis of chamber organic aerosol using an aerodyne high-resolution aerosol mass spectrometer. Atmos. Chem. Phys. 10, 4111–4131.

Chhabra, P.S., Ng, N.L., Canagaratna, M.R., Corrigan, A.L., Russell, L.M., Worsnop, D.R., Flagan, R.C., Seinfeld, J.H., 2011. Elemental composition and oxidation of chamber organic aerosol. Atmos. Chem. Phys. 11, 8827–8845.

DeCarlo, P.F., Dunlea, E.J., Kimmel, J.R., Aiken, A.C., Sueper, D., Crounse, J., Wennberg, P.O., Emmons, L., Shinozuka, Y., Clarke, A., Zhou, J., Tomlinson, J., Collins, D.R., Knapp, D., Weinheimer, A.J., Montzka, D.D., Campos, T., Jimenez, J.L., 2008. Fast airborne aerosol size and chemistry measurements above Mexico City and Central Mexico during the MILAGRO campaign. Atmos. Chem. Phys. 8, 4027–4048.

DeCarlo, P.F., Kimmel, J.R., Trimborn, A., Northway, M.J., Jayne, J.T., Aiken, A.C., Gonin, M., Fuhrer, K., Horvath, T., Docherty, K.S., Worsnop, D.R., Jimenez, J.L., 2006. Field-Deployable, High-Resolution, Time-of-Flight Aerosol Mass Spectrometer. Anal. Chem. 78, 8281–8289.

Forstner, H.J.L., Flagan, R.C., Seinfeld, J.H., 1997. Secondary Organic Aerosol from the Photooxidation of Aromatic Hydrocarbons: Molecular Composition. Environ. Sci. Technol. 31, 1345–1358.

Heald, C.L., Kroll, J.H., Jimenez, J.L., Docherty, K.S., DeCarlo, P.F., Aiken, A.C., Chen, Q., Martin, S.T., Farmer, D.K., Artaxo, P., 2010. A simplified description of the evolution of organic aerosol composition in the atmosphere. Geophysical Research Letters 37, n/a–n/a.

Jang, M., Kamens, R.M., 2001. Characterization of Secondary Aerosol from the Photooxidation of Toluene in the Presence of NOx and 1-Propene. Environ. Sci. Technol. 35, 3626–3639.

Kalberer, M., Paulsen, D., Sax, M., Steinbacher, M., Dommen, J., Prevot, A.S.H., Fisseha, R., Weingartner, E., Frankevich, V., Zenobi, R., Baltensperger, U., 2004.

Identification of Polymers as Major Components of Atmospheric Organic Aerosols. Science 303, 1659–1662.

Keywood, M.D., Kroll, J.H., Varutbangkul, V., Bahreini, R., Flagan, R.C., Seinfeld, J.H., 2004. Secondary Organic Aerosol Formation from Cyclohexene Ozonolysis: Effect of OH Scavenger and the Role of Radical Chemistry. Environ. Sci. Technol. 38, 3343–3350.

Kleindienst, T.E., Conver, T.S., McIver, C.D., Edney, E.O., 2004. Determination of Secondary Organic Aerosol Products from the Photooxidation of Toluene and their Implications in Ambient PM2.5. Journal of Atmospheric Chemistry 47, 79–100.

Lanz, V.A., Alfarra, M.R., Baltensperger, U., Buchmann, B., Hueglin, C., Prévôt, A.S.H., 2007. Source apportionment of submicron organic aerosols at an urban site by factor analytical modeling of aerosol mass spectra. Atmos. Chem. Phys. 7, 1503–1522.

Lanz, V.A., Alfarra, M.R., Baltensperger, U., Buchmann, B., Hueglin, C., Szidat, S., Wehrli, M.N., Wacker, L., Weimer, S., Caseiro, A., Puxbaum, H., Prevot, A.S.H., 2008. Source Attribution of Submicron Organic Aerosols during Wintertime Inversions by Advanced Factor Analysis of Aerosol Mass Spectra. Environ. Sci. Technol. 42, 214–220.

Loza, C.L., Chhabra, P.S., Yee, L.D., Craven, J.S., Flagan, R.C., Seinfeld, J.H., 2012. Chemical aging of m-xylene secondary organic aerosol: laboratory chamber study. Atmos. Chem. Phys. 12, 151–167.

Ng, N.L., Canagaratna, M.R., Zhang, Q., Jimenez, J.L., Tian, J., Ulbrich, I.M., Kroll, J.H., Docherty, K.S., Chhabra, P.S., Bahreini, R., Murphy, S.M., Seinfeld, J.H., Hildebrandt, L., Donahue, N.M., DeCarlo, P.F., Lanz, V.A., Prévôt, A.S.H., Dinar, E., Rudich, Y., Worsnop, D.R., 2010. Organic aerosol components observed in Northern Hemispheric datasets from Aerosol Mass Spectrometry. Atmos. Chem. Phys. 10, 4625–4641.

Ng, N.L., Kroll, J.H., Chan, A.W.H., Chhabra, P.S., Flagan, R.C., Seinfeld, J.H., 2007. Secondary organic aerosol formation from m-xylene, toluene and benzene. Atmospheric Chemistry and Physics 7, 3909–3922.

Rader, J.D., McMurry, P.H., 1986. Application of the tandem differential mobility analyzer to studies of droplet growth or evaporation. Journal of Aerosol Science 17, 771–787.

Sato, K., Hatakeyama, S., Imamura, T., 2007. Secondary organic aerosol formation during the photooxidation of toluene: NO_X dependence of chemical composition. J Phys Chem A 111, 9796–9808.

Sato, K., Takami, A., Isozaki, T., Hikida, T., Shimono, A., Imamura, T., 2010. Mass spectrometric study of secondary organic aerosol formed from the photo-oxidation of aromatic hydrocarbons. Atmospheric Environment 44, 1080–1087.

Sato, K., Takami, A., Kato, Y., Seta, T., Fujitani, Y., Hikida, T., Shimono, A., Imamura, T., 2012. AMS and LC/MS analyses of SOA from the photooxidation of benzene and 1,3,5-trimethylbenzene in the presence of NO_X: effects of chemical structure on SOA aging. Atmos. Chem. Phys. 12, 4667–4682.

Takegawa, N., Miyakawa, T., Kawamura, K., Kondo, Y., 2007. Contribution of Selected Dicarboxylic and ω-Oxocarboxylic Acids in Ambient Aerosol to the m/z 44 Signal of an Aerodyne Aerosol Mass Spectrometer. Aerosol Science and Technology 41, 418–437.

Ulbrich, I.M., Canagaratna, M.R., Zhang, Q., Worsnop, D.R., Jimenez, J.L., 2009. Interpretation of organic components from Positive Matrix Factorization of aerosol mass spectrometric data. Atmos. Chem. Phys. 9, 2891–2918.

Van Krevelen, D.W., Sc., D., Ch.E., M.A.I., 1950. Graphical-statistical method for the study of structure and reaction processes of coal. Fuel 29, 269.

Zhang, Q., Alfarra, M.R., Worsnop, D.R., Allan, J.D., Coe, H., Canagaratna, M.R., Jimenez, J.L., 2005a. Deconvolution and Quantification of Hydrocarbon-like and Oxygenated Organic Aerosols Based on Aerosol Mass Spectrometry. Environ. Sci. Technol. 39, 4938–4952.

Zhang, Q., Alfarra, M.R., Worsnop, D.R., Allan, J.D., Coe, H., Canagaratna, M.R., Jimenez, J.L., 2005b. Deconvolution and Quantification of Hydrocarbon-like and Oxygenated Organic Aerosols Based on Aerosol Mass Spectrometry. Environ. Sci. Technol. 39, 4938–4952.

Zhang, Q., Worsnop, D.R., Canagaratna, M.R., Jimenez, J.L., 2005. Hydrocarbon-like and oxygenated organic aerosols in Pittsburgh: insights into sources and processes of organic aerosols. Atmos. Chem. Phys. 5, 3289–3311.

3.6 Table

Table 3.1 Summary of aromatic hydrocarbon photooxidation experiments under low-NO_X conditions.

Compound	Run ID	NO ppb	ΔHC $\mu g.m^{-3}$	Mo $\mu g.m^{-3}$	VFR initial	VFR end
Benzene	EPA1236A	53.58	406.79	106.44	N/A	N/A
	EPA1618A	35.40	354.16	46.25	0.285	0.804
Toluene	EPA1468A	64.07	666.9	130.21	0.240	0.750
Ethylbenzene	EPA1146A	22.22	256.58	35.99	0.350	0.575
Propylbenzene	EPA1245A	22.12	230.98	11.84	N/A	N/A
Isopropylbenzene	EPA1247A	22.36	300.97	33.24	N/A	N/A
m-Xylene	EPA1193A	36.78	238.9	13.59	N/A	N/A
	EPA1516A	26.69	357.25	48.71	0.213	0.400
o-Xylene	EPA1321A	20.47	263.19	16.16	0.300	0.500
p-Xylene	EPA1308A	55.55	278.65	6.8	0.350	0.475
m-Ethyltoluene	EPA1199A	45.43	447.46	72.03	N/A	N/A
	EPA1421A	22.08	409.46	46.2	0.212	0.512
o-Ethyltoluene	EPA1179A	52.85	399.47	86.49	0.243	0.489
	EPA1202A	60.31	421.96	69.89	N/A	N/A
p-Ethyltoluene	EPA1197A	56.36	653.44	66.43	N/A	0.102
	EPA1601A	31.19	452.38	17.62	0.248	0.475
1,2,3-Trimethylbenzene	EPA1162A	33.39	390.97	46.52	0.257	0.375
1,2,4-Trimethylbenzene	EPA1119A	49.78	384.97	19.6	0.250	0.350
1,3,5-Trimethylbenzene	EPA1153A	10.98	309.47	12.36	0.125	0.250
	EPA1156A	32.31	379.47	24.77	N/A	N/A
1,2,4,5-Tetramethylbenzene	EPA1529A	70	274.69	3.17	0.206	0.254
Pentamethylbenzene	EPA1488A	25.14	834.93	165.07	0.232	0.630
Hexamethylbenzene	EPA1557A	28	999	15.28	0.197	0.352

N/A: not applicable

Table 3.2 Summary of aromatic hydrocarbon photooxidation experiments under no-NO_X conditions.

Compound	Run ID	H_2O_2 ppm	ΔHC µg.m^{-3}	Mo µg.m^{-3}	VFR initial	VFR end
Benzene	EPA1161A	5	330.76	90.82	0.400	0.600
Toluene	EPA1477A	1	103.67	62.22	0.300	0.600
Ethylbenzene	EPA1294A	1	317.53	34.02	0.375	0.475
Propylbenzene	EPA1256A	1	189.48	42.48	N/A	N/A
	EPA1426A	1	330.47	60.95	0.289	0.533
Isopropylbenzene	EPA1265A	1	129.99	24.39	N/A	N/A
m-Xylene	EPA1209A	2	671.23	190.33	N/A	N/A
	EPA1523A	1	1488.18	279.25	0.205	0.528
p-Xylene	EPA1304A	1	328.55	59.62	0.225	0.325
o-Xylene	EPA1313A	1	264.96	67.98	0.275	0.400
m-Ethyltoluene	EPA1218A	1	330.47	151.62	N/A	N/A
	EPA1416A	1	590.95	203	0.207	0.574
o- Ethyltoluene	EPA1406A	1	257.48	53.49	0.209	0.406
p- Ethyltoluene	EPA1239A	1	137.49	86.79	N/A	N/A
	EPA1597A	1	269.98	65.41	0.162	0.276
1,2,3-Trimethylbenzene	EPA1287A	1	343.97	103.88	0.175	0.300
1,2,4-Trimethylbenzene	EPA1292A	1	277.48	59.88	0.200	0.350
1,3,5-Trimethylbenzene	EPA1298A	1	311.97	89.7	0.125	0.275
1,2,4,5-Tetramethylbenzene	EPA1494A	1	541.57	126.72	0.028	0.239
Pentamethylbenzene	EPA1492A	1	747.98	261.61	0.124	0.395
	EPA1564A	1	837.39	115.9	N/A	N/A
Hexamethylbenzene	EPA1558A	1	376	89.86	0.094	0.226

N/A: not applicable

3.7 Figures

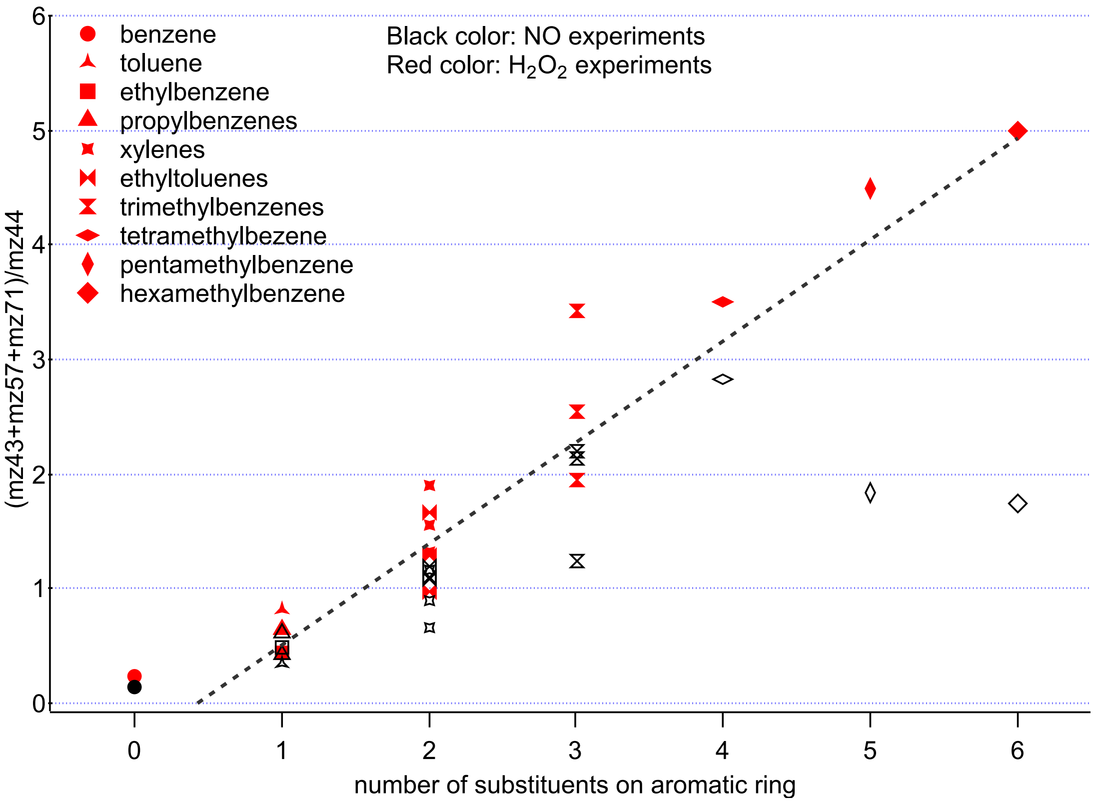

Figure 3.1 (m/z 43+m/z 57+m/z 71) to m/z 44 ratio observed by AMS versus number of alkyl substituents. Dashed line is a linear fit to both NO and H_2O_2 experimental data (except pentamethylbenzene and hexamethylbenzene NO experiments), with slope = 0.8853, $R^2 = 0.8857$.

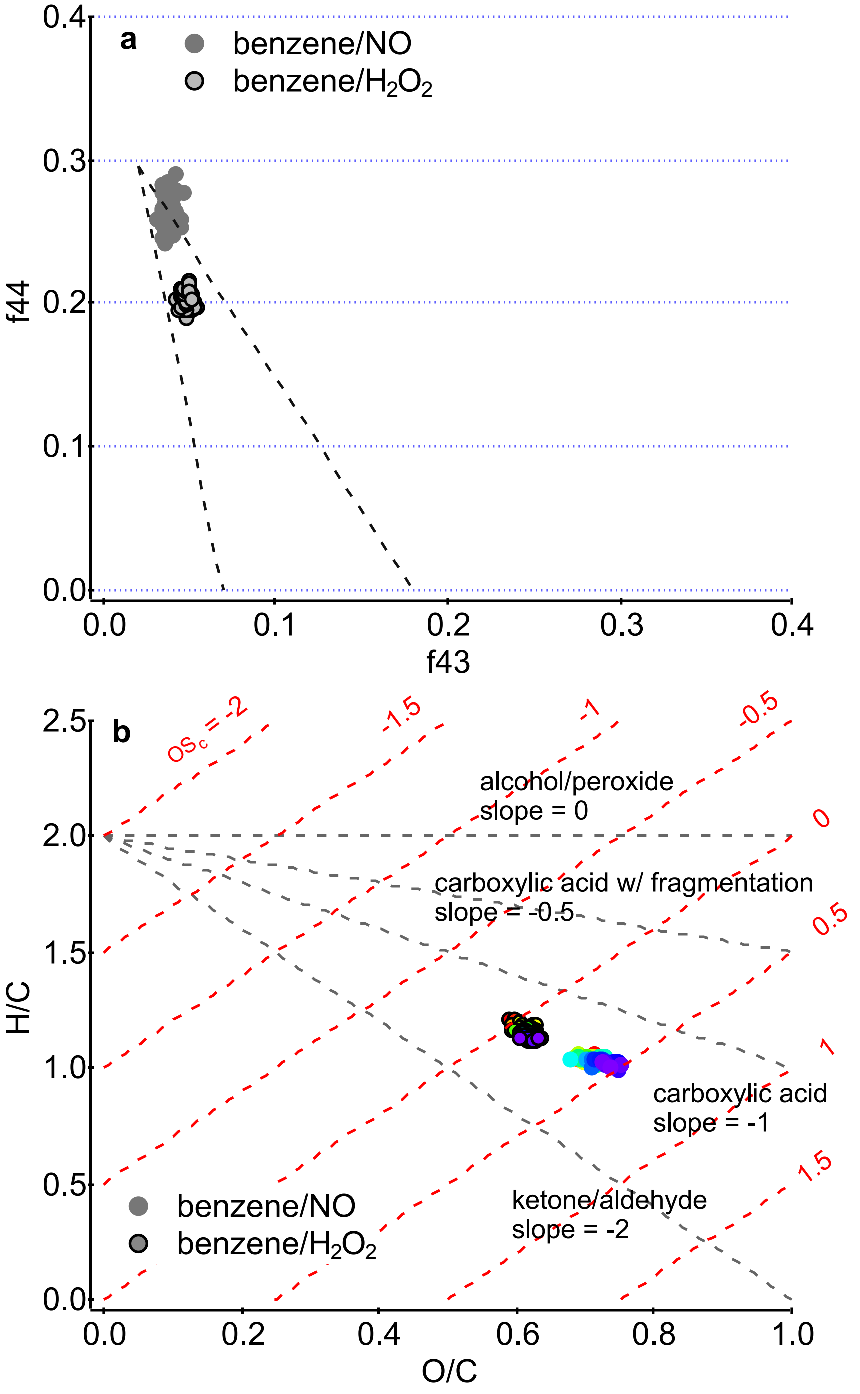

Figure 3.2 (a) Triangle plot for benzene SOA. Dashed lines represent triangle region from Ng *et al.* (2010) of ambient OA. (b) Van Krevelen diagram for benzene SOA. Color from red to purple represents the beginning to the end of each experiment.

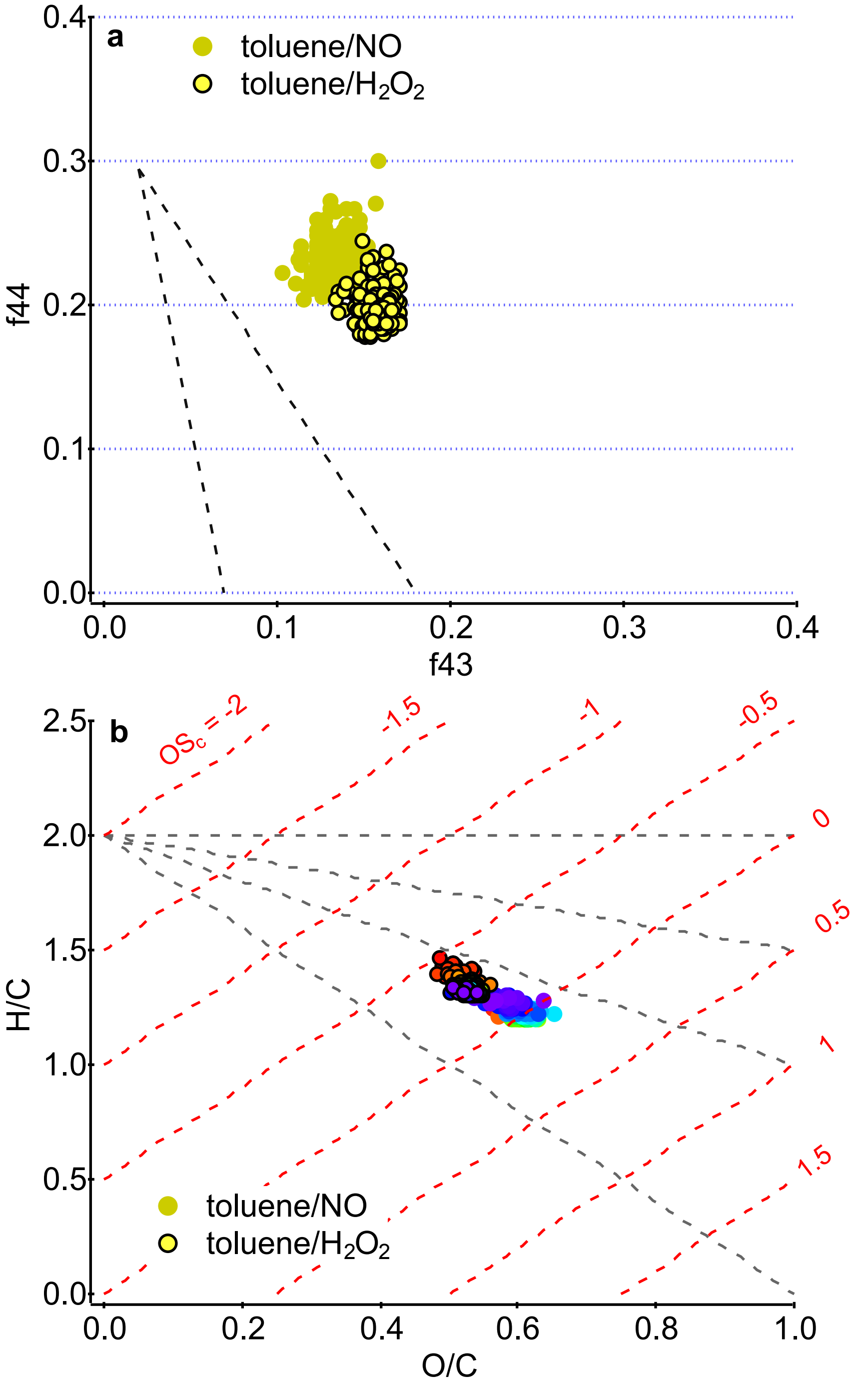

Figure 3.3 (a) Triangle plot for toluene SOA (b) Van Krevelen diagram for toluene SOA. Color from red to purple represents the beginning to the end of each experiment.

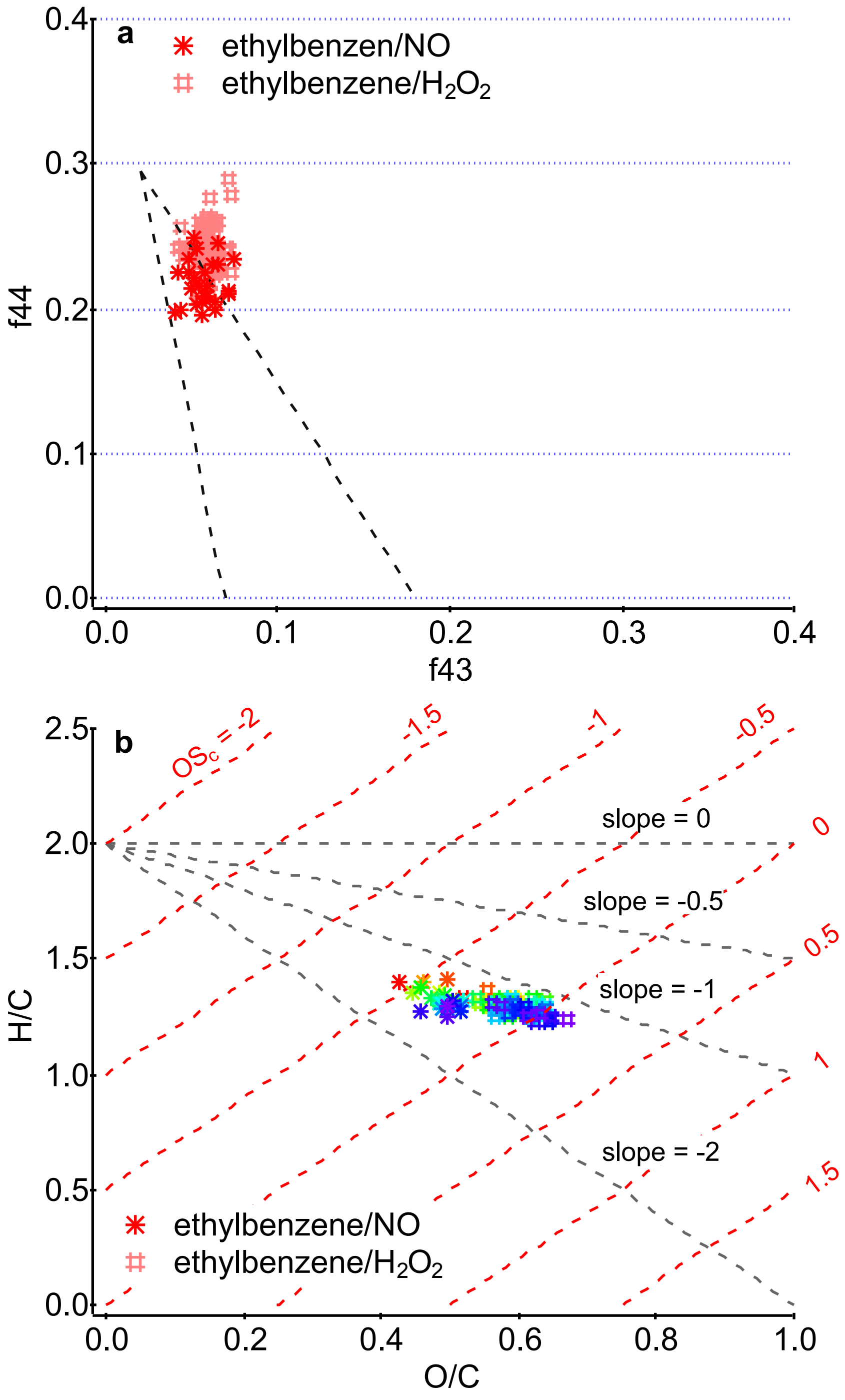

Figure 3.4 (a) Triangle plot for ethylbenzene SOA (b) Van Krevelen diagram for ethylbenzene SOA. Color from red to purple represents the beginning to the end of each experiment.

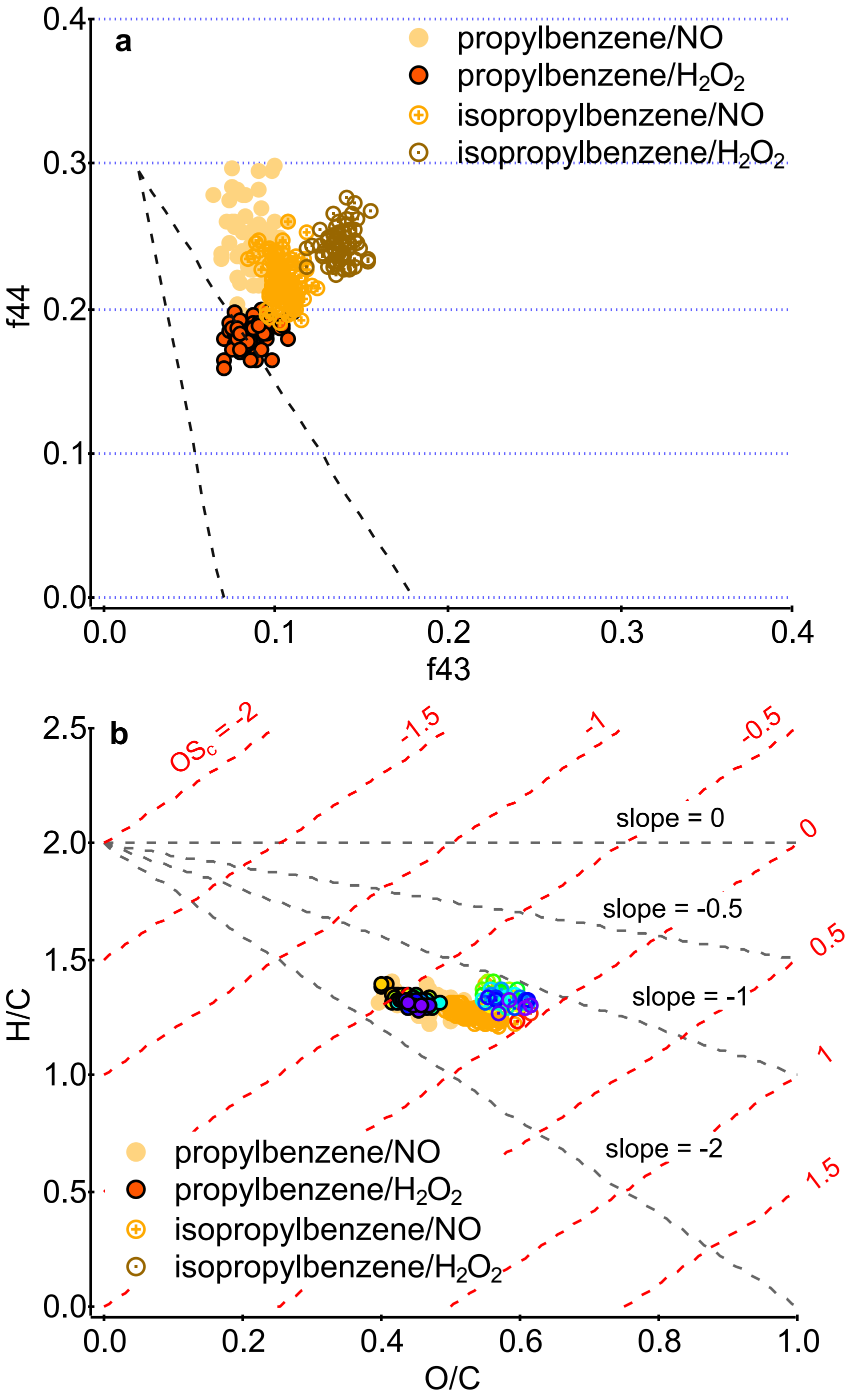

Figure 3.5 (a) Triangle plot for propylbenzene and isopropylbenzene SOA, (b) Van Krevelen diagram for propylbenzene and isopropylbenzene SOA. Color from red to purple represents the beginning to the end of each experiment.

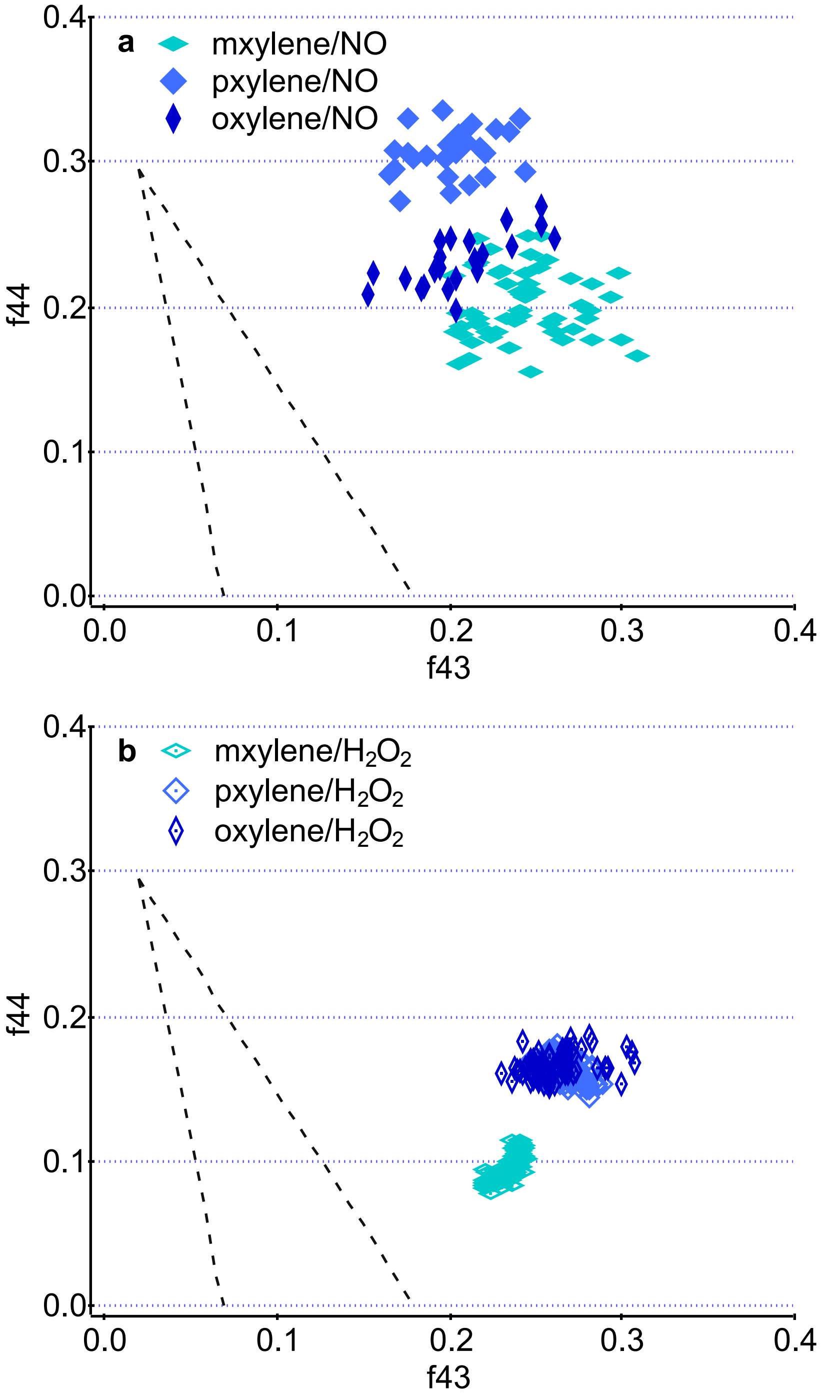

Figure 3.6 Triangle plot for xylene SOA. (a) NO experiments, (b) H_2O_2 experiments.

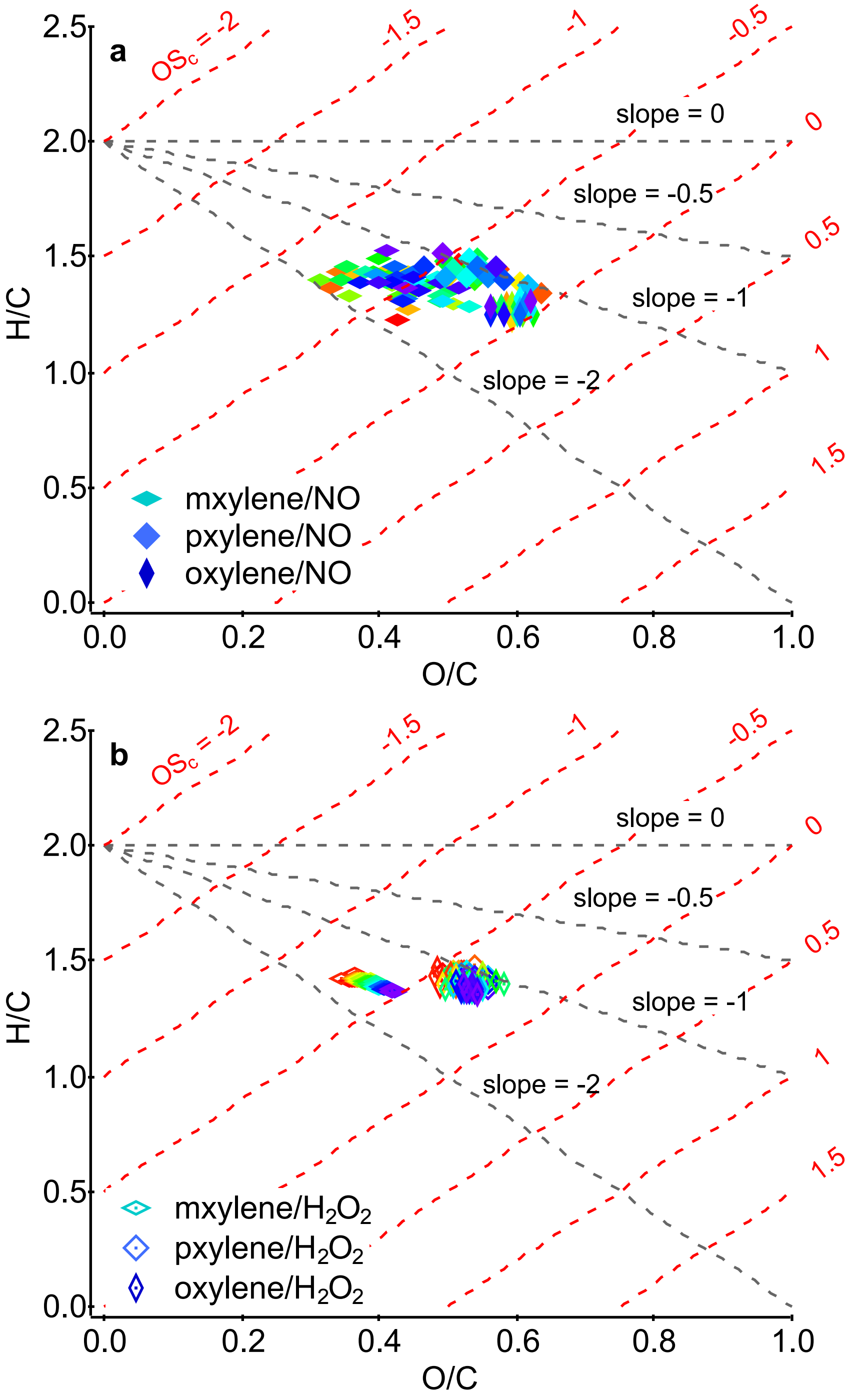

Figure 3.7 Van Krevelen diagram for xylene SOA. Color from red to purple represents the beginning to the end of each experiment. (a) NO experiments, (b) H_2O_2 experiments.

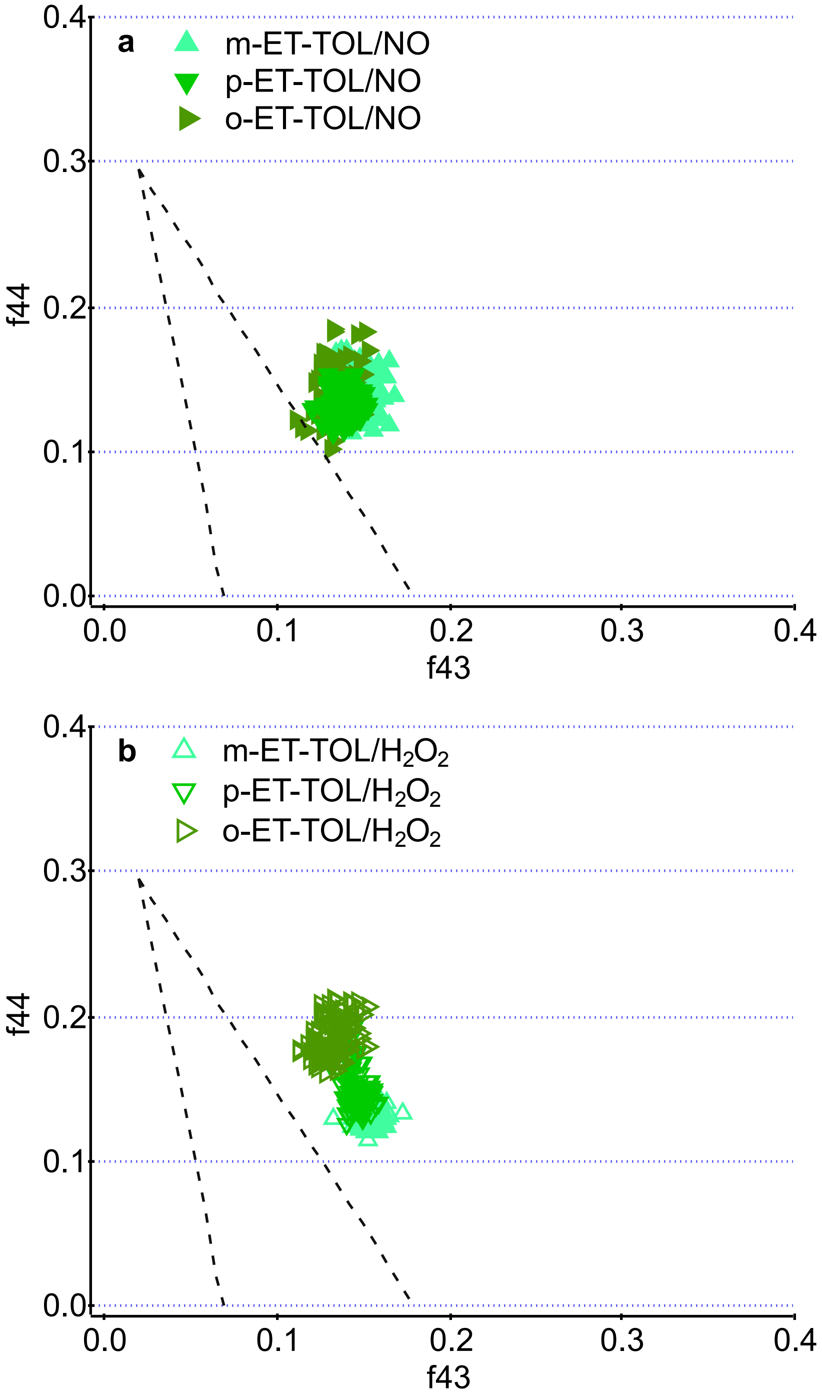

Figure 3.8 Triangle plot for ethyltoluene SOA. (a) NO experiments, (b) H_2O_2 experiments.

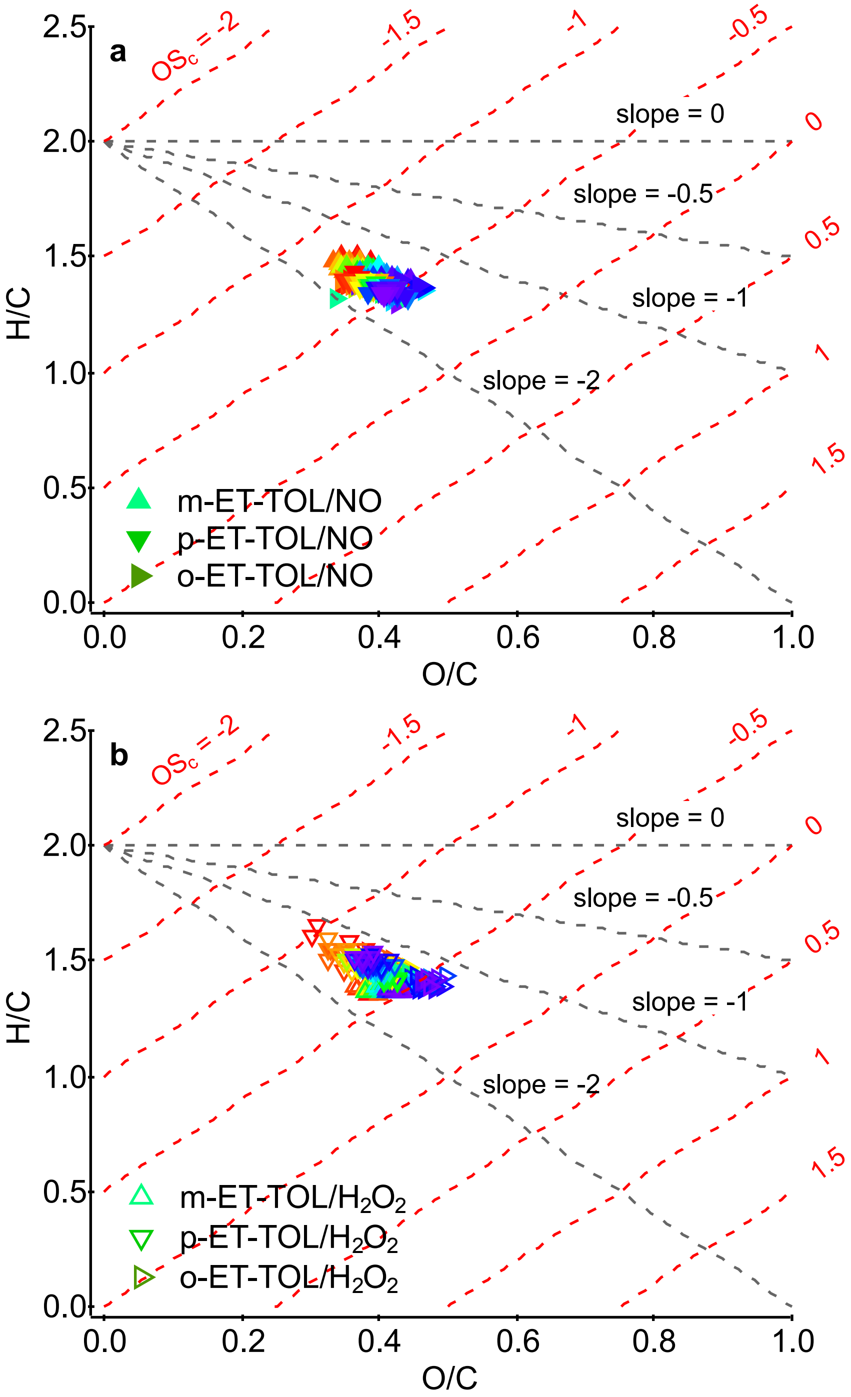

Figure 3.9 Van Krevelen diagram for ethyltoluene SOA. Color from red to purple represents the beginning to the end of each experiment. (a) NO experiments, (b) H_2O_2 experiments.

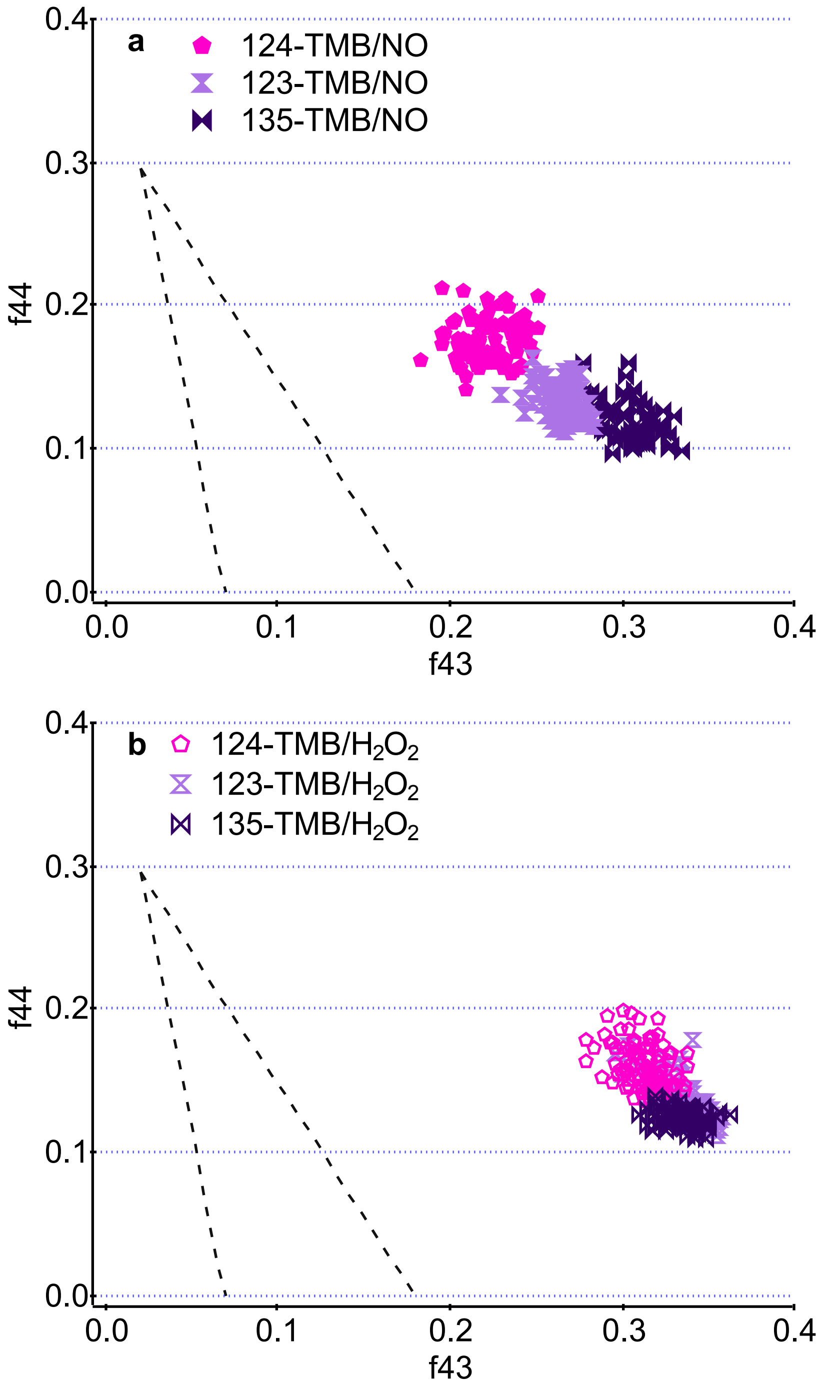

Figure 3.10 Triangle plot for trimethylbenzene SOA. (a) NO experiments, (b) H_2O_2 experiments.

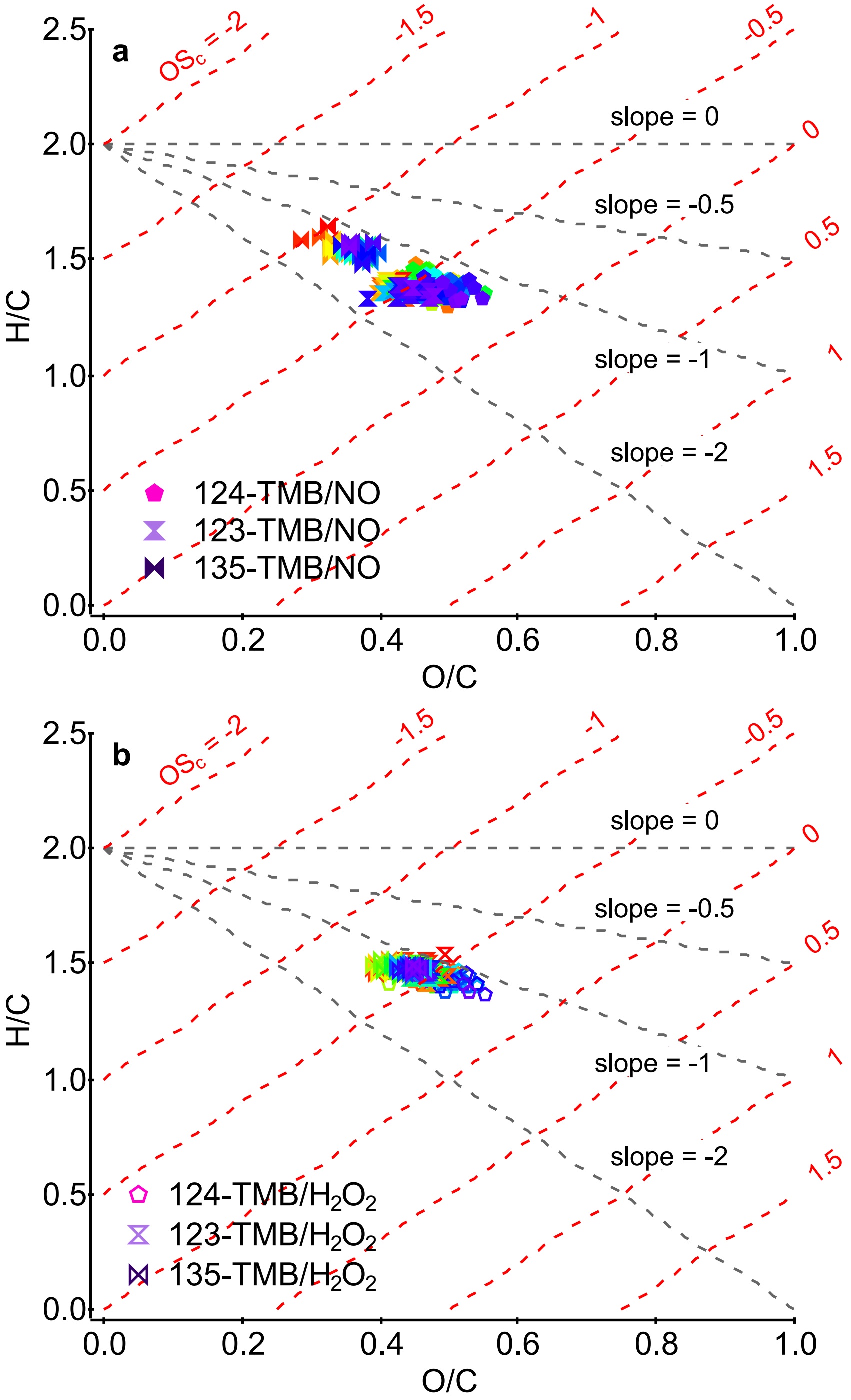

Figure 3.11 Van Krevelen diagram for trimethylbenzene SOA. Color from red to purple represents the beginning to the end of each experiment. (a) NO experiments, (b) H_2O_2 experiments.

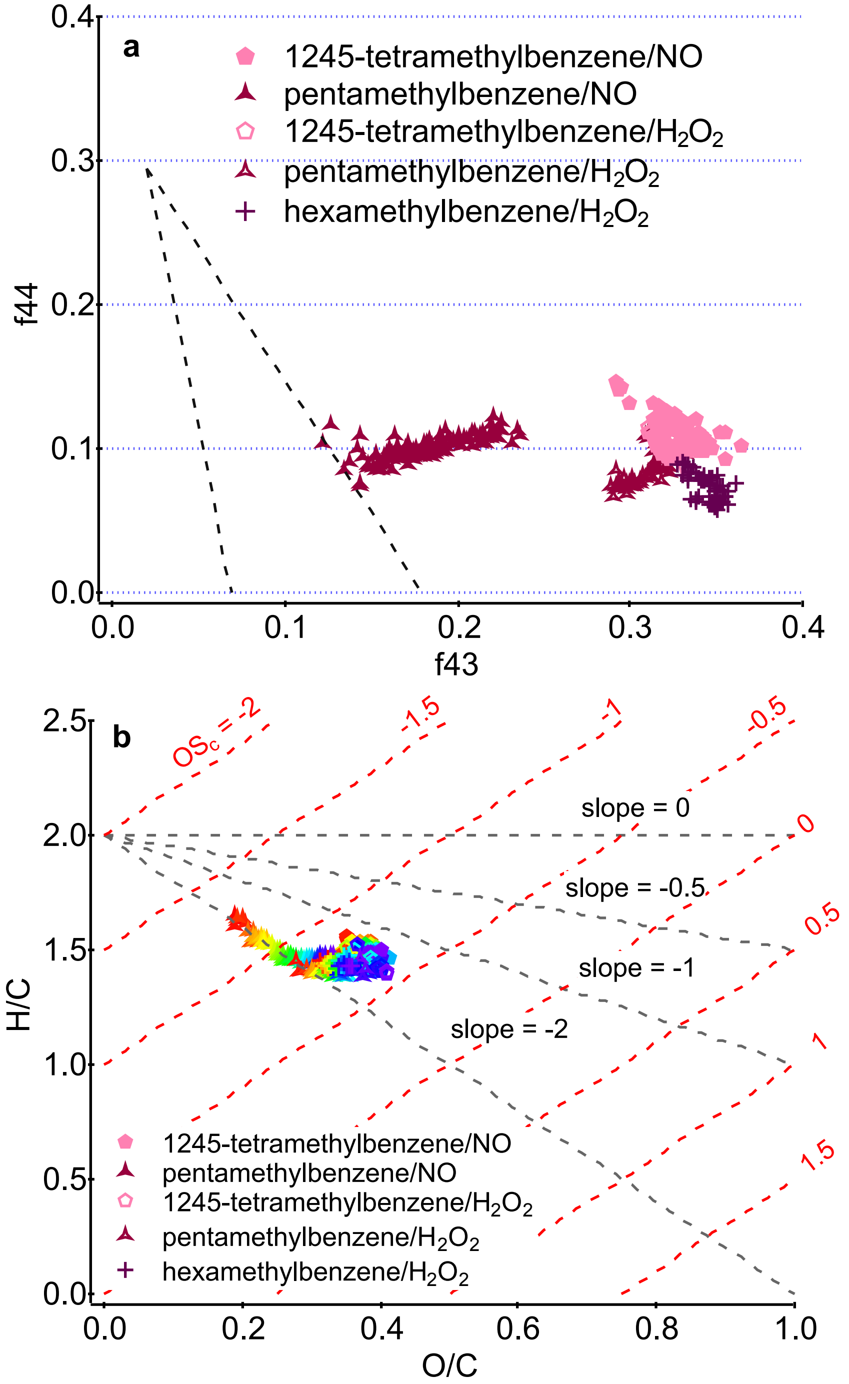

Figure 3.12 (a) Triangle plot for 1,2,4,5-tetramethylbenzene, pentamethylbenzene and hexamethylbenzene SOA (b) Van Krevelen diagram for 1245-tetramethylbenzene, pentamethylbenzene and hexamethylbenzene SOA. Color from red to purple represents the beginning to the end of each experiment.

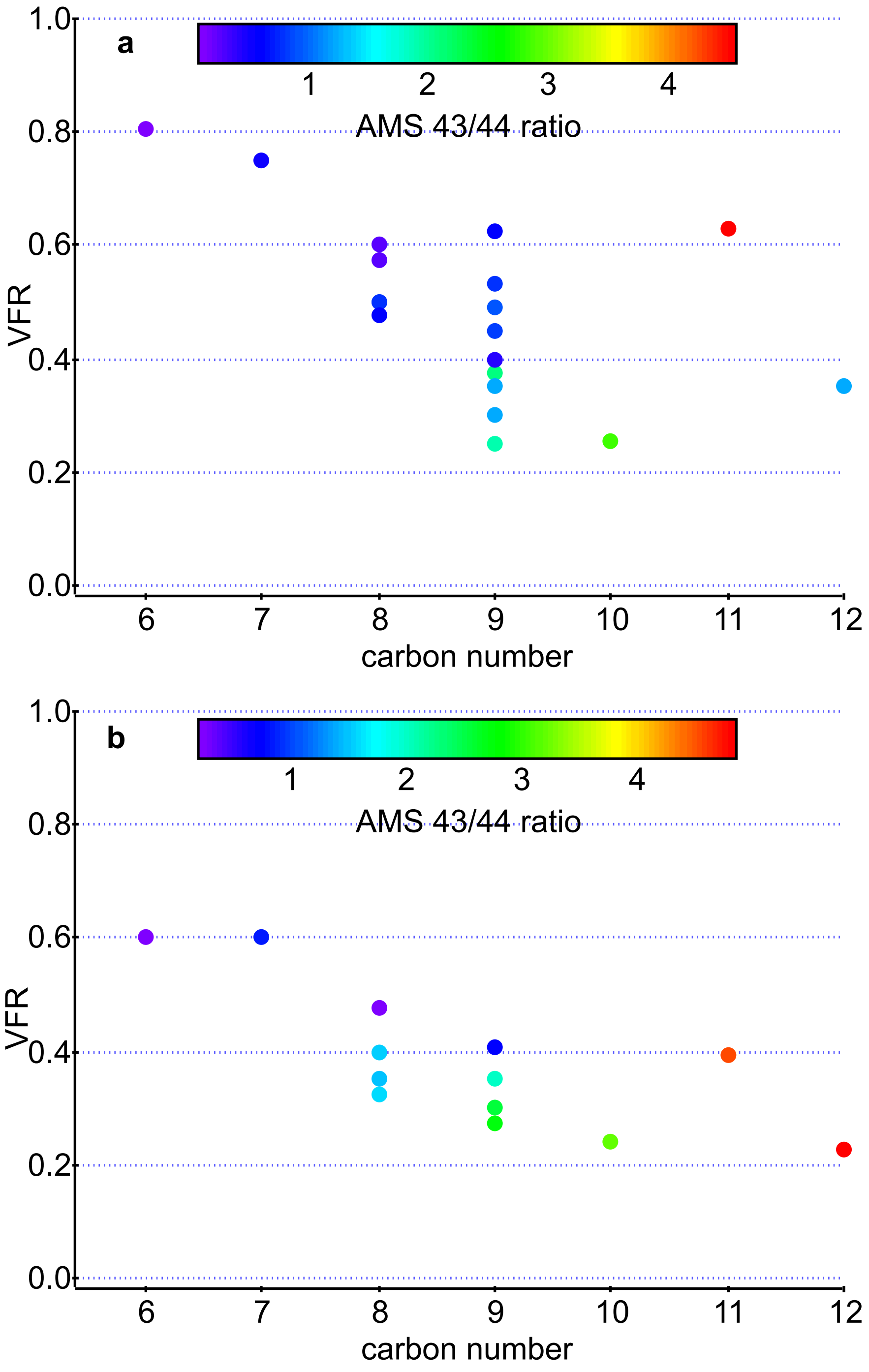

Figure 3.13 Volatility of SOA from photooxidation of aromatic hydrocarbons. (a) NO experiments, (b) H_2O_2 experiments

4 Density and elemental ratios of secondary organic aerosol: application of a density prediction method

4.1 Introduction

Aerosol contributes to climate change and adversely affects air quality (Seinfeld and Pandis, 2006). SOA volume concentration formed in environmental chambers or flow tube reactors are often quantified using a scanning mobility particle sizer (SMPS) based on particle electrical mobility diameter. Current air quality regulation for aerosol is based on mass concentrations (e.g., National Ambient Air Quality Standards for annual $PM_{2.5}$ concentration $< 15\ \mu g/m^3$), hence particle effective density is necessary to convert SOA volume concentrations to mass concentrations. Density must to be estimated when a direct measurement is not available; however, the estimation of the density of organic aerosols is highly uncertain, mostly due to lack of chemical identification (Hallquist *et al.*, 2009).

Kuwata *et al.* (2011) proposed an estimation method for density of organic material based on elemental ratios (O/C and H/C) determined by an Aerodyne High-Resolution Time-of-Flight Aerosol Mass Spectrometer (HR-ToF-AMS) (DeCarlo *et al.*, 2006). Considering the recent widespread use of the HR-ToF-AMS in the aerosol science community, the estimation method has the potential to be applied to a large number of laboratory and field studies. However the experimental verification of the semi-empirical relationship was limited to a selective few biogenic systems (isoprene, α-pinene, central Amazon Basin); therefore, further verification covering an expanded range of systems is needed. This study aims to evaluate the applicability of the Kuwata et al (2011) estimation method to 23 different SOA forming systems, including oxidation of aromatic hydrocarbons, phenolic compounds, and biogenic compounds.

4.2 **Experimental Setup**

4.2.1 Environmental chamber

All experiments were conducted in the UC Riverside/CE-CERT environmental chamber described in detail in Carter *et al.* (2005b). In short, this facility consists of dual 90 m^3 Teflon® reactors suspended by rigid frames in a temperature controlled enclosure (27 ± 1 °C) continuously flushed with dry purified air (a dew point below -40 °C) air generated by an Aadco 737 series (Cleves, Ohio) air purification system. Blacklights (272 bulbs, 115 W Sylvania 350 BL, NO_2 photolysis rate 0.4 min^{-1}) are used as the light source for all the photooxidation experiments reported herein; ozonolysis experiments were carried out in the dark.

4.2.2 Gas and particle analysis

The Agilent 6890 Gas Chromatograph – equipped with a flame ionization detector was used to measure concentrations of precursor hydrocarbons and an inert tracer (perfluorohexane) unless noted otherwise (Table S1). Analytical conditions are described elsewhere (Nakao *et al.*, 2011ab).

Particle effective density was directly measured with an Aerosol Particle Mass Analyzer (APM, Kanomax) (Ehara *et al.*, 1996) coupled to a custom-built Scanning Mobility Particle Sizer (SMPS) (Cocker *et al.*, 2001) in series. A detailed description of the APM-SMPS system and data algorithms are described elsewhere (Malloy *et al.*, 2009;

Nakao *et al.*, 2011c). Chemical composition of SOA was monitored by HR-ToF-AMS (DeCarlo *et al.*, 2006); the elemental ratios (O/C, H/C) of SOA were acquired by the elemental analysis (EA) described by Aiken *et al.* (2008). The ion species list in the high-resolution data analysis toolkit, PIKA (v1.08), was modified to fit all significant ions with *m*/*z* less than 100. The high-resolution fragmentation table was modified to account for different $(H_2O^+)_{org}/(CO_2^+)_{org}$ for different systems as discussed in Section 4.4.1.

4.2.3 Chamber experiments

The reactants used for the chamber experiments are summarized in Figure 4.1. NO (UHP grade, Matheson) was used for NO_x photooxidation experiments. All other chemicals were purchased from Sigma-Aldrich at the highest purity available. All experiments were performed under dry (RH<0.1%) conditions. The experimental procedure has been described elsewhere (Nakao *et al.*, 2011ab; Tang *et al.*, 2012). Reactants were oxidized under the following three conditions: 1) photooxidation in the presence of NO_x, 2) photooxidation using H_2O_2 (50wt% solution in water) as a radical source, or 3) dark ozonolysis. Produced SOA concentrations were typically within 5~150 μg/m^3.

4.3 **Density prediction method**

Previous methods to estimate material density require information on chemical structures (e.g., Girolami, 1994), which is practically infeasible for SOA consisting of many unknown species (Hallquist *et al.*, 2009). Recently, Kuwata *et al.* (2011) proposed a semi-empirical relationship between organic material density (ρ_{org}), O/C, and H/C as follows:

$$\rho_{org} = \frac{12 + H/C + 16 \cdot O/C}{7 + 5 \cdot H/C + 4.15 \cdot O/C} \qquad \text{Eq-1}$$

The relationship was optimized for 31 individual atmospherically relevant organic species with known densities, and was further evaluated against chamber results using two reactants (α-pinene and isoprene) and an Amazon field data set. The stated accuracy of the prediction is within 12% (Kuwata *et al.*, 2011). A Van Krevelen diagram (H/C vs. O/C) with density contour (Figure 4.2) allows visualization of density prediction in terms of elemental ratios. Note that the oxidation state of carbon (OSc) and density isopleth is nearly parallel in the region for typical SOA (around 1.2–1.5 g cm^{-3}), which suggests that chemical processing without change in OSc (e.g., hydrolysis) would have minor impact on density prediction. Two curved lines denote the range of elemental ratios of ambient organic aerosol deconvoluted by PMF (Positive Matric Factorization) (Ng *et al.*, 2011), suggesting that density of low volatility oxygenated organic aerosol (LV-OOA) can reach 1.8 g cm^{-3}.

Uncertainties of elemental analysis of HR-ToF-AMS data includes the quantification of $(H_2O^+)_{org}$ and $(CO^+)_{org}$. Although both ions possibly have significant contribution to bulk elemental ratios, the contribution of organics to H_2O^+ is uncertain due to other sources of H_2O^+ (moisture in the air, unevaporated water, and/or inorganics) while the CO^+ peak is typically overwhelmed by the neighboring N_2^+ peak. The default assumption is that $(CO^+)_{org}$ is equal to $(CO^+)_{org}$ and $(H_2O^+)_{org}$ is 22.5% of $(CO^+)_{org}$ (Aiken *et al.*, 2008; Kuwata *et al.*, 2012) applied calibration factors of $(CO^+)_{org}/(CO_2^+)_{org}$ and $(H_2O^+)_{org}/(CO_2^+)_{org}$ fragment ratios for HR-ToF-AMS measurement determined by Chen *et al.* (2011). The impact of $(CO^+)_{org}$ and $(H_2O^+)_{org}$ on elemental ratios and density prediction is discussed in the following.

4.4 **Results and Discussion**

4.4.1 Measurement of SOA density and elemental ratio

When ambient aerosols are analyzed by a HR-ToF-AMS, a number of sources may contribute H_2O^+ fragment (Aiken *et al.*, 2008); however, since the chamber experiments in this study were carried out under dry conditions without seed particles, measured H_2O^+ is predominantly from organics. Measured $(H_2O^+)_{org}/(CO_2^+)_{org}$ is shown in Figure 4.3 (relative ionization efficiency of H_2O^+ and CO_2^+ is assumed to be 2.0 and 1,4, respectively; Aiken *et al.*, 2008). $(H_2O^+)_{org}$ /$(CO_2^+)_{org}$ values were generally observed to be higher than the default assumption, which significantly affect elemental ratios. $(H_2O^+)_{org}$ /$(CO_2^+)_{org}$ tended to increase as the number of alkyl substituents on aromatic ring increases (trimethylbenzene highest). This trend was due to nearly constant $(H_2O^+)_{org}$ fraction and decreasing $(CO_2^+)_{org}$ fraction as the number of substituent increases (not shown). The decreasing trend of $(CO_2^+)_{org}$ fragment fraction is consistent with higher formation of less reactive ketones than reactive aldehydes (benzene vs. trimethylbenzene; Sato *et al.*, 2012). The observed $(H_2O^+)_{org}$ /$(CO_2^+)_{org}$ was grouped according to the number of alkyl substituents and the average values of each group are applied to elemental analysis. Note that although the higher $(H_2O^+)_{org}$ /$(CO_2^+)_{org}$ values results in higher H/C and O/C, since H_2O^+ does not affect oxidation state of carbon, $(H_2O^+)_{org}/(CO_2^+)_{org}$ calibration has a minor impact on density prediction (Figure 4.2).

Chen *et al.* (2011) quantified $(CO^+)_{org}$ utilizing difference of PToF (Particle Time-of-Flight) of other ions with m/z 28 (N_2 and gas-phase CO). However, since most of the AMS data in this study was acquired without PToF, and Chhabra *et al.* (2011) reported $(CO^+)_{org}/(CO_2^+)_{org}$ for SOA from toluene/*m*-xylene/phenolic compounds were 0.9 ~ 1.3, reasonably close to the default value, 1, this study kept the default value for $(CO^+)_{org}/(CO_2^+)_{org}$ of 1.

Observed SOA density and elemental ratios are shown in Figure 4.4 (literature values under similar experimental conditions are shown for comparison, Kuwata *et al.*, 2012;Chhabra *et al.*, 2010;Ng *et al.*, 2007;Chen *et al.*, 2011a) and Table S1. Results were grouped by each reactant without regard for oxidation conditions in the following discussion. Although different experimental conditions might significantly influence elemental ratios and density, no systematic dependence of density and elemental ratios on oxidation conditions is observed within the data set. Shilling *et al.* (2009) observed loading dependence of density and elemental ratio with particularly stronger loading dependence for <10 mg/m^3, using a steady-state continuous flow chamber that provided large amount of integrated signal at low mass-loading. However, since this study was generally performed under higher mass loading compared to Shilling *et al.*, mass loading effect was observed to be minor.

SOA density ranged between 1.21 and 1.48 g/cm^3, with phenol yielding the highest SOA density (average: 1.42 g/cm^3) and *ß*-caryophyllene the lowest (average: 1.22 g/cm^3). The measured density and O/C followed a similar trend; density (and O/C) decreased slightly as the carbon number of reactants increased, except for isoprene. The different trend for isoprene SOA indicates that bulk composition of isoprene SOA formation is significantly different from aromatic SOA. The trend of H/C was opposite to O/C. These observations support previous findings of the correlation between density and the extent of oxidation of SOA (Katrib *et al.*, 2005).

O/C of aromatic SOA and corresponding phenolic SOA were similar (Figure 4.4). If additional oxygen in reactant (e.g., phenol vs. benzene) results in additional oxygen in condensing species, O/C ratio of phenolic SOA is expected to be higher than corresponding aromatic SOA (e.g., ~17% higher for phenol SOA than benzene SOA assuming condensing products have six carbons). A possible explanation is that aromatic SOA is mostly consisted of multigenerational reaction products (two or more oxidation steps), and hence the presence of additional oxygen in reactants (e.g., phenol) only shortened the reaction steps needed to reach condensing products.

4.4.2 Density prediction vs. measurement

Predicted densities are compared with measured densities in Figure 4.5. The predictions agreed with measurements within 12% except for C6 aromatic/phenolic compounds (benzene, phenol, and catechol). The over prediction of C6 SOA density suggests the lack of structural features that enhances organic density such as hydrogen bonds or ring structures (Girolami, 1994). A characteristic of C6 SOA is its higher CO_2^+ fragment signals in AMS spectra compared to SOA from methylated aromatics, which suggest higher contribution of carboxylic acids and possibly oligoesters (from reactions of carboxylic acids and alcohols) in C6 aromatic SOA (Sato *et al.*, 2012; benzene vs. 1,3,5-trimethylbenzene). Oligoester formation could result in loss of hydrogen bonding, and hence lower density. Further chemical analysis using different techniques would be needed to verify the hypothesis.

As reported by Kuwata *et al.* (2012), the effect of nitrogen or sulfur containing species on the density prediction needs further investigation. For all experiments in this study, the effect of nitrogen is expected to be minor since N/C ratios of SOA were 0.00–0.01 (Table 4.1). No reactant in this study includes sulfur and thus the effect of sulfur is not probed.

4.5 **Conclusion**

A recent study proposed a semi-empirical relationship between organic aerosols density, O/C, and H/C (Kuwata *et al.*, 2012). This study applied the semi-empirical relationship to the extensive data set of elemental compositions and densities of SOA formed by the oxidation of 22 different reactants including terpenes, aromatic hydrocarbons, and phenolic compounds, in an environmental chamber. The semi-empirical relationship successfully predicted density of SOA within 12% error except for over prediction for C6 aromatics (benzene, phenol, and catechol). This study further extended the range of application of the prediction method to include anthropogenic systems.

4.6 References

Aiken, A. C., DeCarlo, P. F., Kroll, J. H., Worsnop, D. R., Huffman, J. A., Docherty, K., Ulbrich, I., Mohr, C., Kimmenl, J. R., Sun, Y., Zhang, Q., Trimborn, A. M., Northway, M., Ziemann, P. J., Canagaratna, M. R., Onasch, T. B., Alfarra, M. R., Prevot, A. S., Dommen, J., Duplissy, J., Metzger, A., Baltensperger, U., Jimenez, J. L.: O/C and OM/OC ratios of primary, secondary, and ambient organic aerosols with High-Resolution Time-of-Flight Aerosol Mass Spectrometry, Environmental Science & Technology, 42, 4487-4485, 2008

Carter, W. P. L., Cocker, D. R., Fitz, D. R., Malkina, I. L., Bumiller, K., Sauer, C. G., Pisano, J. T., Bufalino, C., Song, C.: A new environmental chamber for evaluation of gas-phase chemical mechanisms and secondary aerosol formation, Atmospheric Environment, 39, 7768-7788, 2005

Chen, Q., Liu, Y., Donahue, N. M., Shilling, J. E., Martin, S. T.: Particle-Phase Chemistry of Secondary Organic Material: Modeled Compared to Measured O:C and H:C Elemental Ratios Provide Constraints, Environmental Science & Technology, 45(11), 4763–4770, 2011

Chhabra, P. S., Ng, N. L., Canagaratna, M. R., Corrigan, A. L., Russell, L. M., Worsnop, D. R., Flagan, R. C., Seinfeld, J. H.: Elemental composition and oxidation of chamber organic aerosol, Atmos. Chem. Phys., 11(17), 8827-8845, 2011

Cocker, D. R., Flagan, R. C., Seinfeld, J. H.: State-of the art chamber facility for studying atmospheric aerosol chemistry, Environmental Science & Technology, 35(12), 2594-2601, 2001

DeCarlo, P. F., Kimmel, J. R., Trimborn, A. M., Northway, M., Jayne, J. T., Aiken, A. C., Gonin, M., Fuhrer, K., Horvath, T., Docherty, K., Worsnop, D. R., Jimenez, J. L.: Field-deployable, high-resolution, Time-of-Flight Aerosol Mass Spectrometer, Anal. Chem., 78, 8281-8289, 2006

Ehara, K., Hagwood, C., Coakley, K. J.: Novel method to classify aerosol particles according to their mass-to-charge ratio-Aerosol particle mass analyzer, Journal of Aerosol Science, 27(2), 217-234, 1996

Girolami, G. S.: A simple "back of the envelope" method for estimating the densities and molecular volumes of liquids and solids, Journal of Chemical Education, 71(11), 962-964, 1994

Hallquist, M., Wenger, J. C., Baltensperger, U., Rudich, Y., Simpson, D., Claeys, M., Dommen, J., Donahue, N. M., George, C., Goldstein, A. H., Hamilton, J. F., Herrmann, H., Hoffmann, T., Iinuma, Y., Jang, M., Jenkin, M., Jimenes, J. L., Kiendler-Scharr, A., Maenhaut, W., McFiggans, G., Mentel, T. F., Monod, A., Prevot, A. S., Seinfeld, J. H., Surratt, J. D., Szmigielski, R., Willdt, J.: The formation, properties and impact of secondary organic aerosol: current and emerging issues, Atmospheric Chemistry and Physics, 9, 5155-5236, 2009

Katrib, Y., Martin, S. T., Rudich, Y., Davidovits, P., Jayne, J. T., Worsnop, D. R.: Density changes of aerosol particles as a result of chemical reaction, Atmospheric Chemistry and Physics, 5, 275-291, 2005

Kuwata, M., Zorn, S. R., Martin, S. T.: Using Elemental Ratios to Predict the Density of Organic Material Composed of Carbon, Hydrogen, and Oxygen, Environmental Science & Technology, 46(2), 787-794, 2011

Malloy, Q., Nakao, S., Qi, L., Austin, R. L., Stothers, C., Hagino, H., Cocker, D. R.: Real-time aerosol density determination utilizing a modified Scanning Mobility Particle Sizer - Aerosol Particle Mass Analyzer system, Aerosol Science and Technology, 43, 673-678, 2009

Nakao, S., Clark, C., Tang, P., Sato, K., Cocker III, D.: Secondary organic aerosol formation from phenolic compounds in the absence of NOx, Atmos. Chem. Phys., 11(20), 10649-10660, 2011a

Nakao, S., Liu, Y., Tang, P., Chen, C. L., Zhang, J., Cocker III, D.: Role of glyoxal in SOA formation from aromatic hydrocarbons: gas-phase reaction trumps reactive uptake, Atmos. Chem. Phys. Discuss., 11(11), 30599-30625, 2011b

Nakao, S., Shrivastava, M., Nguyen, A., Jung, H., Cocker, D.: Interpretation of Secondary Organic Aerosol Formation from Diesel Exhaust Photooxidation in an Environmental Chamber, Aerosol Science and Technology, 45(8), 954-962, 2011c

Ng, N. L., Canagaratna, M. R., Jimenez, J. L., Chhabra, P. S., Seinfeld, J. H., Worsnop, D. R.: Changes in organic aerosol composition with aging inferred from aerosol mass spectra, Atmos. Chem. Phys., 11(13), 6465-6474, 2011

Seinfeld, J. H., Pandis, S. N.: Atmospheric Chemistry and Physics: From Air Pollution to Climate Change - 2nd ed. New Jersey, A Wiley-Interscience publication. 2006.

Shilling, J. E., Chen, Q., King, S. M., Rosenoern, T., Kroll, J. H., Worsnop, D. R., DeCarlo, P. F., Aiken, A. C., Sueper, D., Jimenes, J. L., Martin, S. T.: Loading-dependent elemental composition of a-pinene SOA particles, Atmospheric Chemistry and Physics, 9, 771-782, 2009

Tang, X., Cocker III, D. R., Asa-Awuku, A.: Are sesquiterpenes good secondary organic cloud condensation nuclei (CCN)?, Atmospheric Chemistry and Physics Discussions, submitted 2012

4.7 Tables

Table 4.1 Elemental composition, predicted density, and measured density of SOA formed in an environmental chamber

Parent species	Experimental condition[a]	Elemental ratio[b,c]		Effective density (g/cm^3)[c]		Error (%)	n[e]
		O/C	H/C	AMS EA prediction[d]	APM-SMPS measurement		
Isoprene	NO_x; H_2O_2; O_3	0.32 ± 0.13	1.43 ± 0.13	1.20 ± 0.09	1.33 ± 0.02	-10	13
Benzene	NO_x; H_2O_2	0.69 ± 0.04	1.08 ± 0.07	1.58 ± 0.05	1.37 ± 0.06	15	7
Phenol	NO_x; H_2O_2	0.73 ± 0.13	1.08 ± 0.15	1.60 ± 0.13	1.42 ± 0.02	13	5
Catechol	H_2O_2	0.73	1.04	1.62	1.37	18	1
Toluene	NO_x; H_2O_2	0.65 ± 0.05	1.24 ± 0.04	1.49 ± 0.03	1.40 ± 0.02	6	3
o-/m- Cresol	NO_x; H_2O_2	0.55 ± 0.04	1.18 ± 0.03	1.45 ± 0.02	1.34 ± 0.03	8	5
Ethylbenzene	NO_x; H_2O_2	0.52 ± 0.09	1.35 ± 0.14	1.36 ± 0.10	1.39 ± 0.08	-2	3
o-/m-/p- Xylene	NO_x; H_2O_2	0.53 ± 0.08	1.39 ± 0.08	1.35 ± 0.07	1.42 ± 0.03	-5	4
2,4-Dimethylphenol	NO_x; H_2O_2	0.49 ± 0.05	1.26 ± 0.02	1.38 ± 0.03	1.33 ± 0.03	4	3
Trimethylbenzenes[f]	NO_x; H_2O_2	0.42 ± 0.07	1.45 ± 0.12	1.26 ± 0.08	1.32 ± 0.05	-5	10
o-/m-/p- Ethyltoluene	NO_x; H_2O_2	0.44 ± 0.04	1.35 ± 0.05	1.31 ± 0.04	1.28 ± 0.09	2	15
n-Propylbenzene	NO_x	0.48 ± 0.02	1.29 ± 0.09	1.36 ± 0.04	1.31 ± 0.01	4	2
α-Pinene	O_3	0.27	1.44	1.16	1.28	-9	1
2-*tert*-Butylphenol	H_2O_2	0.26	1.60	1.11	1.22	-9	1
4-Octylphenol	H_2O_2	0.17	1.54	1.05	1.06	0	1
β-Caryophyllene	O_3; H_2O_2	0.33 ± 0.09	1.45 ± 0.09	1.20 ± 0.05	1.20 ± 0.04	0	12

a: NO_x: photooxidation with NO_x, H_2O_2: photooxidation using H_2O_2 as a radical source, O_3: ozonolysis

b: molar ratio

c: Average ± standard deviation

d: Density predicted by Eq1

e: Number of chamber experiments

f: 1,2,3-/1,2,4-/1,3,5-Trimethylbenzene isomers

4.8 **Figures**

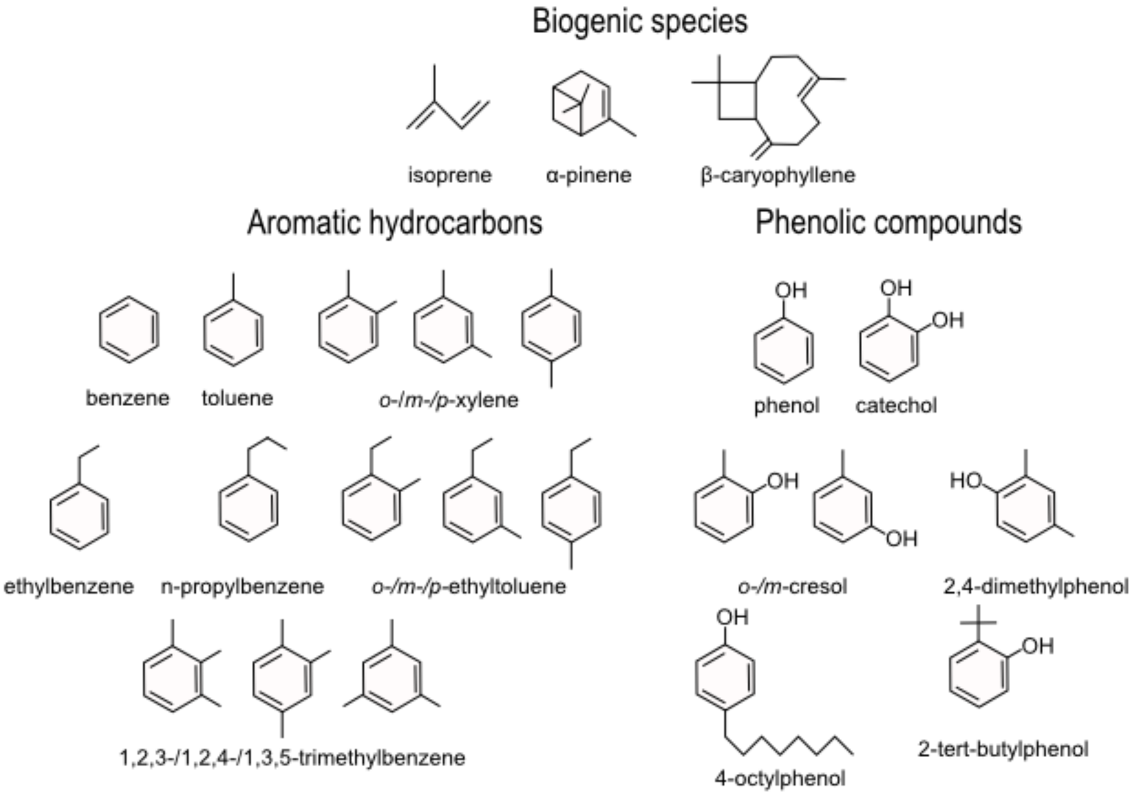

Figure 4.1 Reactants used for chamber experiments.

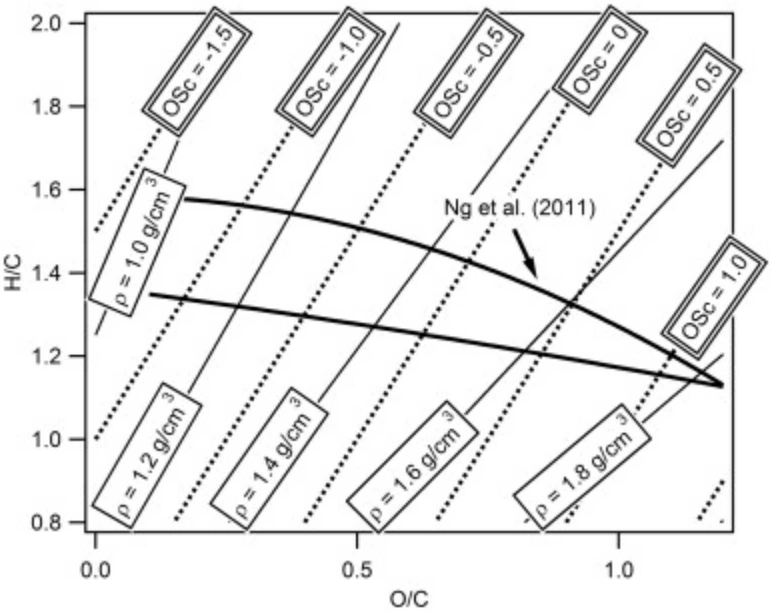

Figure 4.2 Van Krevelen diagram with density and oxidation state of carbon (OSc) contours.

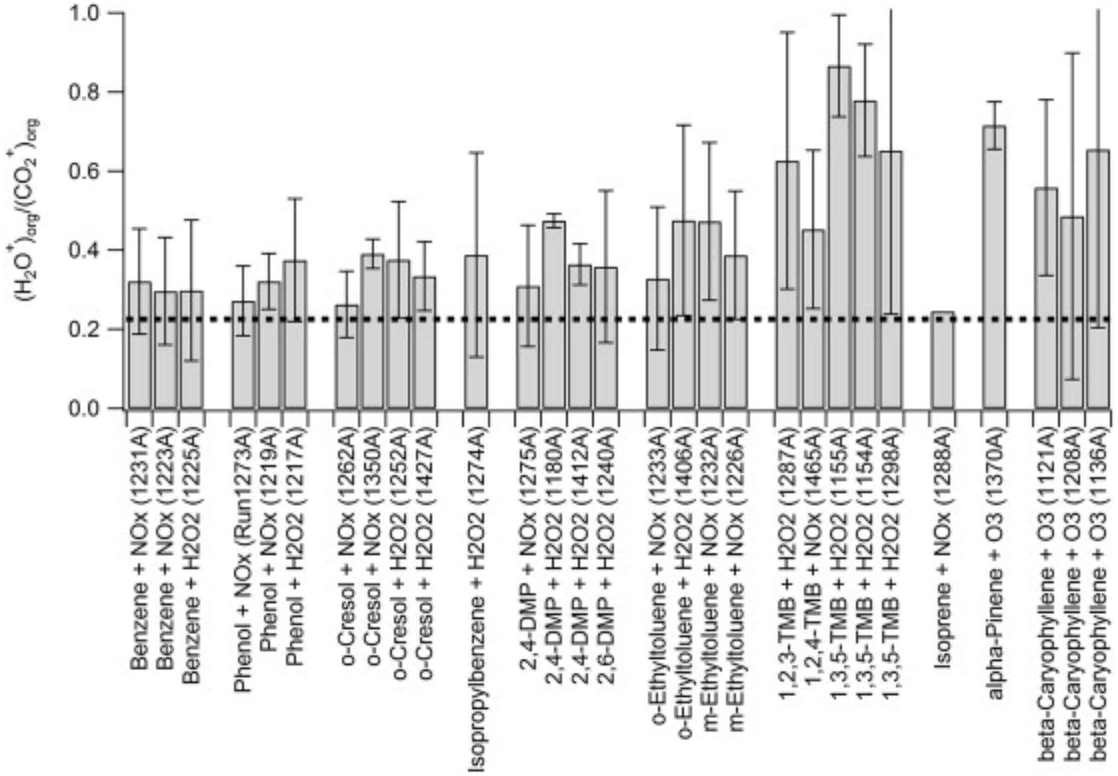

Figure 4.3 $(H_2O^+)_{org}/(CO_2^+)_{org}$ fragment ratio of SOA observed by the HR-ToF-AMS.

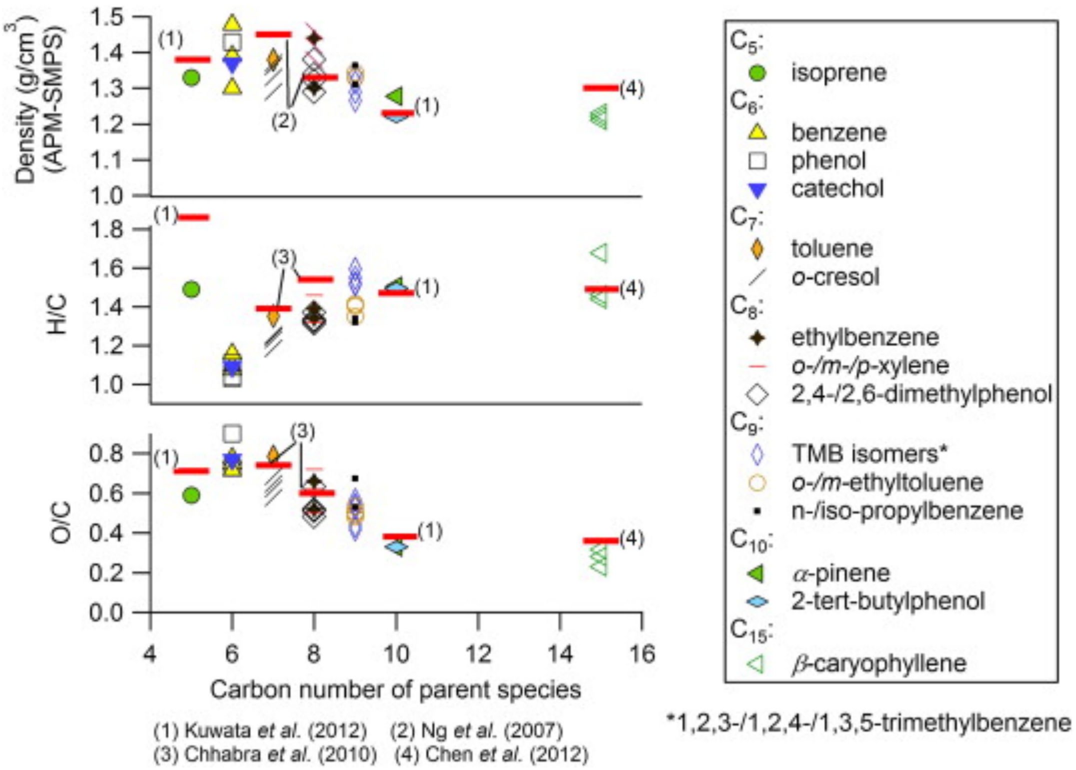

Figure 4.4 Effective density, H/C, and O/C of secondary organic aerosol as function of carbon number of parent species.

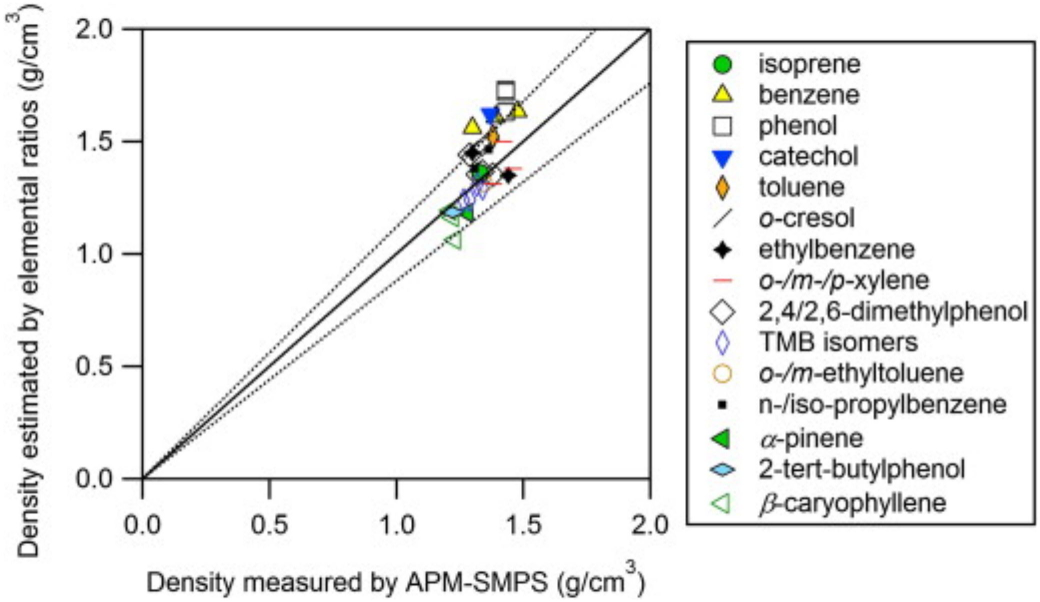

Figure 4.5 Comparison of predicted and measured density of secondary organic aerosol. Dotted lines indicate ±12% lines.

5 Relationship Between OH/HO$_2$ Level and Aerosol Formation Potential for Aromatic Hydrocarbons

5.1 Introduction

Secondary organic aerosol (SOA) accounts for a large fraction of total organic particulate mass based on ambient measurements (e.g., Lanz *et al.*, 2007b; Turpin and Huntzicker, 1995; Turpin and Lim, 2001; Q. Zhang *et al.*, 2005). Environmental simulation chambers are typically employed to simulate controlled atmospheres to quantify SOA formation from individual precursors, and then integrate into atmospheric models to predict aerosol formation in the atmosphere. Basically, models of SOA formation represent gas-phase oxidation reactions that lead to the formation of lower volatility compounds and also the partitioning of semi-volatile species between gas and particle phase. There are two approaches that have been largely used in atmospheric models: empirical models constrained by laboratory data and explicit and semi-explicit models in which gas-phase mechanisms predict formation of semi-volatile products (Hallquist *et al.*, 2009). Recent studies have suggested that current models informed by chamber measurements do not always capture the variability of observed SOA loadings, and often predict far less SOA than is observed (de Gouw *et al.*, 2005; Heald *et al.*, 2005; Kleinman *et al.*, 2008; Volkamer *et al.*, 2006). Factors including incomplete treatment of SOA chemistry, omission of important precursors in models and differences between chamber experiments and the atmosphere are responsible for model and measurement discrepancies (Hallquist *et al.*, 2009; Kroll and Seinfeld, 2008).

SOA formation is highly dependent on a series of experimental conditions, including NO_X conditions, preexisting particles mass and particle acidity. A number of studies (Hurley *et al.*, 2001; Johnson *et al.*, 2004; Kroll *et al.*, 2006; Ng *et al.*, 2007; Song *et al.*, 2005; Chapter 2 and 5) have observed decreasing SOA yield with increasing initial NO_X concentration. NO_X levels were found to influence the initial gas-phase oxidation steps and also determine the fate of RO_2 radicals (Hurley *et al.*, 2001; Kroll *et al.*, 2006; Nøjgaard *et al.*, 2006). Higher NO_X levels favor RO_2 + NO reactions over the RO_2 + HO_2/RO_2 + RO_2 reactions, which are more likely to form lower-volatility organics. However, the correlations between NO_X level and SOA formation are not always clear. Other studies have found a reverse dependence of SOA yield on NO_X levels (Kroll *et al.*, 2006; Pandis *et al.*, 1991; Zhang *et al.*, 1992). Studies by Stroud *et al.* (2004) and Ng *et al.* (2007) observed particle formation from aromatic precursors even when NO was still present. These observations may be attributed to different OH levels in their experiments that affected the formation of semi-volatiles. The role of reactive radicals (OH, HO_2 and RO_2) during gas phase oxidation process is necessary to understand to best predict SOA formation in the atmosphere.

The photooxidaiton of 17 different aromatic compounds was investigated in this study within the UCR/CE-CERT environmental chamber under varying initial NO_X conditions. Hydroxyl radical (OH) constrained by experimental data and hydroperoxyl radical (HO_2) predicted by SAPRC-11 model are used to explain the variation of SOA yield and composition under low-NO_X and no-NO_X conditions for different aromatic photooxidation systems.

5.2 **Experimental Setup**

5.2.1 Chamber Facilities

All the experiments in this paper were carried out in UC Riverside/CE-CERT indoor environmental chamber, which has been described in detail elsewhere (Carter *et al.*, 2005). All experiments were conducted under dry conditions (RH<0.1%), in the absence of inorganic seed aerosol, and at environmental chamber temperatures of 27°C. The UV-radiation is generated by 272 115 W Sylvania 350 Black lights for an overall NO_X photolysis rate of 0.4 min^{-1}. Under no-NO_X condition, H_2O_2 was used as hydroxyl (OH) radical source. Hydrocarbon decay was measured by a Hewlett-Packard 5890 (Palo Alto, CA) gas chromatograph (GC) equipped with a DB-5 column and a flame ionization detector (FID). The size distribution and number concentration of SOA were monitored using an in-house build scanning mobility particle sizer spectrometer (SMPS) located inside the temperature-controlled room. The Aerodyne High Resolution Time-of-Flight Aerosol Mass Spectrometer (HR-ToF-AMS) (Canagaratna *et al.*, 2007; DeCarlo *et al.*, 2006b) is used to provide on-line quantitative measurements of bulk chemical composition.

5.2.2 Model Prediction

A new version of the SAPRC model, SAPRC-11, was utilized to simulate chamber experiments in this study. SAPRC-11 revised the mechanisms of gas-phase atmospheric reactions of aromatic hydrocarbons based on SAPRC-07, including new parameterized mechanisms for phenolic compounds and updates of mechanisms concerning acetylene, glyoxal and acyl peroxy + HO_2 (Carter *et al.*, 2012). The new aromatics mechanism was evaluated against chamber experimental data and gave better simulations of ozone formation in almost all chamber experiments with the exception of higher (> 100 ppb) NO_X benzene and toluene experiments. Details of SAPRC-11 have been described in detail elsewhere (Carter and Heo, 2012; Carter *et al.*, 2012). In this study, OH radical concentration was calculated based on the hydrocarbon decay using SAPRC-11; HO_2 concentration was predicted by SAPRC-11 using OH values constrained by hydrocarbon decay rates.

5.2.3 Experiments Conducted

Table 5.1 and Table 5.2 summarizes the chamber experiments performed and used for this work including hydrocarbon reacted, aerosol formed, m/z 43 to m/z 44 ratio and model error.

5.3 Results and Discussion

SOA yields of different aromatics under low-NO_X (HC (ppbC)/NO_X (ppb) > 7) were explored in Chapter 2 (Figure 5.1 a) and are plotted along with aerosol formation for the no-NO_X H_2O_2 experiments (Figure 5.1 b). It was observed that aerosol formation decreases as the number of carbon atoms of the parent aromatic compound increases for low-NO_X conditions. It is hypothesized that lighter aromatic compounds formed more ring-retaining products with lower vapor pressures than ring-cleavage products produced from heavier aromatics (Odum *et al.*, 1996; Sato *et al.*, 2007; Smith *et al.*, 1999). However, these trends were not observed for H_2O_2 photooxidations without NO_X present.

Aromatic gas-phase oxidation is initiated by reaction of with the OH radical. The OH radical is further expected to be a key factor influencing the oxidation of 1st and later generation products. The OH concentration during each experiment was calculated from the decay of the aromatic precursor using SAPRC-11. The OH radical level for both low-NO_X and no-NO_X conditions is displayed (Figure 5.2) for individual aromatic systems. For the low-NO_X experiments the OH level is highly associated with the reaction rate of aromatic hydrocarbon with OH (k_{OH}). While benzene has the lowest k_{OH}, OH concentrations remained sufficiently high throughout the experiment to allow for further oxidation of later generation oxidation products. On the other hand, heavier compounds like trimethylbenzene decayed at a much faster rates (higher k_{OH}) than benzene, the OH radical levels dropped quickly in the experiment slowing the oxidation rate of later generation oxidation products possibly resulting in the lower observed aerosol yields. However, when H_2O_2 was used as OH source, the OH concentration remained relatively stable throughout the experiments for each of the individual aromatics and the observed trends in aerosol formation with carbon number were not observed (Figure 5.1 b). Therefore, the SOA formation for the different aromatic systems may be partly attributed to variations in OH levels for the different aromatic systems. However, H_2O_2 experiments typically formed considerably more aerosol than NO experiments even though these experiments had lower average OH concentrations. Therefore, we explore the possibility of another important radical, HO_2, in the formation of SOA during aromatic photooxidation.

5.3.1 Relationship Between [OH]/[HO_2] and SOA Formation

Hydroxyl radical chemistry in the atmosphere is closely related to other atmospheric oxidants including HO_2, NO_X and ozone. Monks (2005) reviewed the chemistry of the three main groups of atmospheric radicals (HO_X, NO_X and XO_X (X = Cl, Br, I)) and showed that NO_X controlled the partitioning of HO_X between OH and HO_2--as NO_X increases the HO_2/OH decreases. Urban measurements showed a decreasing of HO_2 at high NO_X. For photooxidation experiments of aromatic hydrocarbons, the NO_X level is known to govern the fate of the RO_2 radical, which in turn controls the volatility of organic products subsequent to the initial hydrocarbon-OH reaction (Ng *et al.*, 2007). When there is NO present, RO_2 reacts entirely with NO; otherwise RO_2 + HO_2 /RO_2 + RO_2 reactions dominate. Since OH and HO_2 radical both play an important role gas phase oxidation process, a new factor, the [OH]/[HO_2] ratio, was used in this study to interpret the SOA formation from individual aromatic phootooxidation systems.

In this work, OH concentration was calculated from hydrocarbon decay rates using SAPRC-11 and HO_2 concentration was directly predicted by SAPRC-11 using the OH data constrained by the hydrocarbon decay rate. Model performance is evaluated by using the rate change of Δ([O_3]-[NO]) (Carter *et al.*, 2012). Therefore, we use the Formation Rate Model Error (Carter *et al.*, 2012) to evaluate HO_2 prediction for NO experiments as

$$Formaiton\ Rate\ Model\ Error$$
$$= \frac{\Delta([O_3]-[NO])Rate^{model} - \Delta([O_3]-[NO])Rate^{expt}}{average\ \{\Delta([O_3]-[NO])Rate^{model}, \Delta([O_3]-[NO])Rate^{expt}\}}$$

For H_2O_2 experiments there was insufficient NO_X to allow for this estimation. Therefore, no error estimate was made for the H_2O_2 experiments. The size of the triangle on the following figures is used to represent the Formation Rate Model Error while the circle symbol size is fixed.

The SOA formation of trimethylbenzene isomers for varying NO_X concentrations are presented in Figure 5.3; the data points are colored by the $[OH]/[HO_2]$ ratio from white to dark blue representing low to high $[OH]/[HO_2]$ ratios. It is observed that for fixed amounts of total hydrocarbon reacted (red rectangular area, Figure 5.3), higher Mo values correspond to lower $[OH]/[HO_2]$ values. For low-NO_X experiments, many previous studies have observed increasing SOA yields with decreasing NO concentration (Hurley *et al.*, 2001; Johnson *et al.*, 2004; Kroll *et al.*, 2006; Ng *et al.*, 2007; Song *et al.*, 2005). However, it is hard to compare H_2O_2 experiments with NO experiments using NO as an indicator. By using $[OH]/[HO_2]$ as an indicator in this study, we found that most trimethylbenzene /H_2O_2 experiments had lower $[OH]/[HO_2]$ value compared to NO experiments, which corresponded to a higher SOA yield than NO experiments, indicating that functionalization may be preferred over fragmentation for decreasing $[OH]/[HO_2]$ ratios.

SOA formation from aromatic systems under low-NO_X and no-NO_X conditions is displayed (Figure 5.4) using the traditional Yield vs. Mo plot to present data. Within Figure 5.4, color shading is used to indicate $[OH]/[HO_2]$ ratio while symbol shape designates experiment type and triangle size represents the estimated model error in predicting $[OH]/[HO_2]$ ratios. Straight dashed lines are used to indicate the expected yield curve for experiments conducted with similar hydrocarbon reacted due to the nature of the aerosol yield curve ($\Delta M_o/\Delta HC$ vs. ΔM_o; the slope of each dashed line shown has a slope of $1/\Delta HC$). Mathematically, any experiment with a given ΔHC must lie upon the $1/\Delta HC$ line shown irregardless of the aerosol produced or aromatic system chosen. Movement on the dashed line toward the origin indicates aerosol systems with lower aerosol formation for a given $1/\Delta HC$. It is further observed that for fixed $1/\Delta HC$, higher SOA yields are observed with decreasing $[OH]/[HO_2]$ values, irregardless of the aromatic compound that the data represents. H_2O_2 experiments were observed to locate on the upper left regime of the plot while NO experiments cluster in the lower right area. This means that photooxidation of aromatics react away less hydrocarbon to form the same amount of particles for H_2O_2 systems than for the low-NO_X systems. Moving from the upper left regime of the plot to the lower right, a decreasing SOA yield is observed with increasing $[OH]/[HO_2]$ values. Decreasing SOA formation is expected in the presence of NO as the NO + HO_2 and NO + RO_2 reactions compete directly with the formation of lower volatility semi-volatile products via the RO_2 + HO_2 reactions. During the H_2O_2 experiments, HO_2 radicals are not consumed by NO, so the RO_2 + HO_2 reactions dominate and products with lower volatility are formed.

To better illustrate the effect of $[OH]/[HO_2]$ ration on SOA formation, Figure 5.5 shows the Mo vs. delta HC plot of all the aromatic experiments. It is clear that data points on the bottom of the plot have higher $[OH]/[HO_2]$ values, which corresponds to smaller amounts of aerosol formed. Therefore, the [OH]/[HO2] may provide an indicator of fragmentation ($[OH]/[HO_2]$ higher; higher vapor pressure products) versus functionalization ([OH]/[HO_2] lower; lower vapor pressure products) of the oxidation products.

5.3.2 Relationship Between [OH]/[HO_2] and Aromatic Structure

Figure 5.6 and Figure 5.7 show the yield vs. [OH]/[HO_2] plot for all aromatic photooxidation experiments. Generally, we found that SOA yield decreased with increasing [OH]/[HO_2] value. However, the amount of aerosol formed also changed even for a certain value of [OH]/[HO_2]. The data is colored with OH concentration in Figure 5.6; SOA yield is found decreased with the OH concentration for a certain [OH]/[HO_2] values. In Figure 5.7 data points of NO experiments are further grouped according to the carbon number of parent aromatics. Aerosol yield is observed to increase with increasing OH concentration even for systems with similar [OH]/[HO_2] ratios. Further, for fixed values of [OH]/[HO_2], aerosol formed from aromatics with lower carbon number is observed to have higher yields than aromatics with higher carbon numbers. Both the effect of parent carbon number and OH radical concentration on SOA yield is mainly due to the availability of the OH radical to react further with aromatic later generation products. When NO is present, compounds with larger carbons numbers react faster with OH resulting in a lower OH level in the system during times when oxidation of later generation oxidation products occur thereby limiting the availability of these multigenerational compounds to produce additional aerosol.

5.3.3 Relationship Between [OH]/[HO_2] and SOA Chemical Composition

Laboratory experiments in this study had lower [OH]/[HO_2] ratios compared to ambient measurements. Figure 5.8 shows the SOA yield vs. [OH]/[HO_2] plot colored by

43/44 ratio, while the red box (Figure 5.8) represents the ambient level of [OH]/[HO_2], which ranges from 0.01 ~ 0.02 (Dusanter *et al.*, 2009; Kanaya *et al.*, 2012; Martinez *et al.*, 2003). The43/44 ratio is observed to decrease with increasing [OH]/[HO_2] ratio indicating that aerosol formed in higher [OH]/[HO_2] environment are more oxidized. Given the importance of the [OH]/[HO_2] ratio observed in this paper, traditional smog chamber experiments will need to be modified so that not only NO_X levels but also [OH]/[HO_2] levels in the environmental chambers are representative of the atmosphere. Given that the [OH]/[HO_2] ratio may be governing the fragmentation versus functionalization of 1st and later generation products, the importance of this ratio should not be overlooked. The observed trends indicate that aerosol formation may be over predicted by H_2O_2 and low-NO_X experiments, despite their more appropriate NO_X levels.

5.4 Conclusion

SOA formation from the photooxidation of 17 different aromatic hydrocarbons was investigated in this study. The [OH]/HO_2] ratio is used to explain the aerosol formation from aromatic photooxidation under both low-NO_X and no-NO_X conditions, presumably by it's effect on fragmentation versus functionalization of the 1st and later generation oxidation products. Generally, more aerosol were formed under no-NO_X condition, consistent with much lower [OH]/[HO_2] conditions. Further, SOA yield was observed to increase with decreasing [OH]/[HO_2] ratio for aromatic experiments regardless of the aromatic compound chosen. However, for similar [OH]/[HO_2] ratios, SOA yield is observed to decrease with increasing OH concentration as well as with increasing aromatic carbon number. The chemical composition of SOA observed in the chamber experiments based on m/z 43/44 indicate a less oxidized aerosol than is typically observed in the environment. The 43/44 ratio decreasing with increasing [OH]/[HO_2] value suggests that more OH radical is needed for further oxidation of later generation organic products. Comparison of the [OH]/[HO_2] levels achieved in typical H_2O_2 and low-NO_X chamber experiments to typical ambient conditions strongly suggests that SOA formation under the chamber conditions may overestimate SOA formation in the atmosphere and that chamber experiments may need modification to better achieve not only the NO_X concentrations but also [OH]/[HO_2] concentrations representative of the atmosphere.

5.5 References

Camredon, M., Aumont, B., Lee-Taylor, J., Madronich, S., 2007. The SOA/VOC/NOx system: an explicit model of secondary organic aerosol formation. Atmos. Chem. Phys. 7, 5599–5610.

Canagaratna, M.R., Jayne, J.T., Jimenez, J.L., Allan, J.D., Alfarra, M.R., Zhang, Q., Onasch, T.B., Drewnick, F., Coe, H., Middlebrook, A., Delia, A., Williams, L.R., Trimborn, A.M., Northway, M.J., DeCarlo, P.F., Kolb, C.E., Davidovits, P., Worsnop, D.R., 2007. Chemical and microphysical characterization of ambient aerosols with the aerodyne aerosol mass spectrometer. Mass Spectrom Rev 26, 185–222.

Carter, W., Cockeriii, D., Fitz, D., Malkina, I., Bumiller, K., Sauer, C., Pisano, J., Bufalino, C., Song, C., 2005. A new environmental chamber for evaluation of gas-phase chemical mechanisms and secondary aerosol formation. Atmospheric Environment 39, 7768–7788.

Carter, W.P.L., Heo, G., 2012. Development of revised SAPRC aromatics mechanisms (No. 07-730).

Carter, W.P.L., Heo, G., Cocker III, D.R., Nakao, S., 2012. SOA fromation: Chamber study and model development (No. 08-326).

De Gouw, J.A., Middlebrook, A.M., Warneke, C., Goldan, P.D., Kuster, W.C., Roberts, J.M., Fehsenfeld, F.C., Worsnop, D.R., Canagaratna, M.R., Pszenny, A. a. P., Keene, W.C., Marchewka, M., Bertman, S.B., Bates, T.S., 2005. Budget of organic carbon in a polluted atmosphere: Results from the New England Air Quality Study in 2002. Journal of Geophysical Research: Atmospheres 110, n/a–n/a.

Dusanter, S., Vimal, D., Stevens, P.S., Volkamer, R., Molina, L.T., Baker, A., Meinardi, S., Blake, D., Sheehy, P., Merten, A., Zhang, R., Zheng, J., Fortner, E.C., Junkermann, W., Dubey, M., Rahn, T., Eichinger, B., Lewandowski, P., Prueger, J., Holder, H., 2009. Measurements of OH and HO_2 concentrations during the MCMA-2006 field campaign – Part 2: Model comparison and radical budget. Atmos. Chem. Phys. 9, 6655–6675.

Hallquist, M., Wenger, J.C., Baltensperger, U., Rudich, Y., Simpson, D., Claeys, M., Dommen, J., Donahue, N.M., George, C., Goldstein, A.H., Hamilton, J.F., Herrmann, H., Hoffmann, T., Iinuma, Y., Jang, M., Jenkin, M.E., Jimenez, J.L., Kiendler-Scharr, A., Maenhaut, W., McFiggans, G., Mentel, T.F., Monod, A., Prévôt, A.S.H., Seinfeld, J.H., Surratt, J.D., Szmigielski, R., Wildt, J., 2009. The formation, properties and impact of secondary organic aerosol: current and emerging issues. Atmos. Chem. Phys. 9, 5155–5236.

Heald, C.L., Jacob, D.J., Park, R.J., Russell, L.M., Huebert, B.J., Seinfeld, J.H., Liao, H., Weber, R.J., 2005. A large organic aerosol source in the free troposphere missing from current models. Geophysical Research Letters 32, n/a–n/a.

Hurley, M.D., Sokolov, O., Wallington, T.J., Takekawa, H., Karasawa, M., Klotz, B., Barnes, I., Becker, K.H., 2001. Organic Aerosol Formation during the Atmospheric Degradation of Toluene. Environ. Sci. Technol. 35, 1358–1366.

Johnson, D., Jenkin, M.E., Wirtz, K., Martin-Reviejo, M., 2004. Simulating the Formation of Secondary Organic Aerosol from the Photooxidation of Toluene. Environ. Chem. 1, 150–165.

Kanakidou, M., Seinfeld, J.H., Pandis, S.N., Barnes, I., Dentener, F.J., Facchini, M.C., Van Dingenen, R., Ervens, B., Nenes, A., Nielsen, C.J., Swietlicki, E., Putaud, J.P., Balkanski, Y., Fuzzi, S., Horth, J., Moortgat, G.K., Winterhalter, R., Myhre, C.E.L., Tsigaridis, K., Vignati, E., Stephanou, E.G., Wilson, J., 2005. Organic aerosol and global climate modelling: a review. Atmos. Chem. Phys. 5, 1053–1123.

Kanaya, Y., Hofzumahaus, A., Dorn, H.-P., Brauers, T., Fuchs, H., Holland, F., Rohrer, F., Bohn, B., Tillmann, R., Wegener, R., Wahner, A., Kajii, Y., Miyamoto, K., Nishida, S., Watanabe, K., Yoshino, A., Kubistin, D., Martinez, M., Rudolf, M., Harder, H., Berresheim, H., Elste, T., Plass-Dülmer, C., Stange, G., Kleffmann, J., Elshorbany, Y., Schurath, U., 2012. Comparisons of observed and modeled OH and HO2 concentrations during the ambient measurement period of the HOxComp field campaign. Atmos. Chem. Phys. 12, 2567–2585.

Kleinman, L.I., Springston, S.R., Daum, P.H., Lee, Y.-N., Nunnermacker, L.J., Senum, G.I., Wang, J., Weinstein-Lloyd, J., Alexander, M.L., Hubbe, J., Ortega, J., Canagaratna, M.R., Jayne, J., 2008. The time evolution of aerosol composition over the Mexico City plateau. Atmos. Chem. Phys. 8, 1559–1575.

Kroll, J.H., Ng, N.L., Murphy, S.M., Flagan, R.C., Seinfeld, J.H., 2006. Secondary Organic Aerosol Formation from Isoprene Photooxidation. Environ. Sci. Technol. 40, 1869–1877.

Kroll, J.H., Seinfeld, J.H., 2008. Chemistry of secondary organic aerosol: Formation and evolution of low-volatility organics in the atmosphere. Atmospheric Environment 42, 3593–3624.

Martinez, M., Harder, H., Kovacs, T.A., Simpas, J.B., Bassis, J., Lesher, R., Brune, W.H., Frost, G.J., Williams, E.J., Stroud, C.A., Jobson, B.T., Roberts, J.M., Hall, S.R., Shetter, R.E., Wert, B., Fried, A., Alicke, B., Stutz, J., Young, V.L., White, A.B., Zamora, R.J., 2003. OH and HO2 concentrations, sources, and loss rates during the

Southern Oxidants Study in Nashville, Tennessee, summer 1999. Journal of Geophysical Research: Atmospheres 108, n/a–n/a.

Monks, P.S., 2005. Gas-phase radical chemistry in the troposphere. Chem. Soc. Rev. 34, 376–395.

Ng, N.L., Kroll, J.H., Chan, A.W.H., Chhabra, P.S., Flagan, R.C., Seinfeld, J.H., 2007. Secondary organic aerosol formation from m-xylene, toluene and benzene. Atmospheric Chemistry and Physics 7, 3909–3922.

Nøjgaard, J.K., Bilde, M., Stenby, C., Nielsen, O.J., Wolkoff, P., 2006. The effect of nitrogen dioxide on particle formation during ozonolysis of two abundant monoterpenes indoors. Atmospheric Environment 40, 1030–1042.

Odum, J.R., Hoffmann, T., Bowman, F., Collins, D., Flagan, R.C., Seinfeld, J.H., 1996. Gas/Particle Partitioning and Secondary Organic Aerosol Yields. Environ. Sci. Technol. 30, 2580–2585.

Pandis, S.N., Paulson, S.E., Seinfeld, J.H., Flagan, R.C., 1991. Aerosol formation in the photooxidation of isoprene and β-pinene. Atmospheric Environment. Part A. General Topics 25, 997–1008.

Smith, D.F., Kleindienst, T.E., McIver, C.D., 1999. Primary Product Distributions from the Reaction of OH with m-, p-Xylene, 1,2,4- and 1,3,5-Trimethylbenzene. Journal of Atmospheric Chemistry 34, 339–364.

Song, C., Na, K., Cocker, D.R., 2005. Impact of the Hydrocarbon to NO_X Ratio on Secondary Organic Aerosol Formation. Environ. Sci. Technol. 39, 3143–3149.

Stroud, C.A., Makar, P.A., Michelangeli, D.V., Mozurkewich, M., Hastie, D.R., Barbu, A., Humble, J., 2004. Simulating organic aerosol formation during the photooxidation of toluene/NO_X mixtures: comparing the equilibrium and kinetic assumption. Environ. Sci. Technol. 38, 1471–1479.

Tang, P., Nakao, S., Chen, J., Qi, L., Cocker, D.R., 2013. Secondary organic aerosol formation from 17 different aromatic hydrocarbons: Yield comparison. In preparation.

Turpin, B.J., Huntzicker, J.J., 1995. Identification of secondary organic aerosol episodes and quantitation of primary and secondary organic aerosol concentrations during SCAQS. Atmospheric Environment 29, 3527–3544.

Turpin, B.J., Lim, H.J., 2001. Species Contributions to PM2.5 Mass Concentrations: Revisiting Common Assumptions for Estimating Organic Mass. Aerosol Science and Technology 35, 602–610.

Volkamer, R., Jimenez, J.L., San Martini, F., Dzepina, K., Zhang, Q., Salcedo, D., Molina, L.T., Worsnop, D.R., Molina, M.J., 2006. Secondary organic aerosol formation from anthropogenic air pollution: Rapid and higher than expected. Geophysical Research Letters 33, n/a–n/a.

Zhang, Q., Worsnop, D.R., Canagaratna, M.R., Jimenez, J.L., 2005. Hydrocarbon-like and oxygenated organic aerosols in Pittsburgh: insights into sources and processes of organic aerosols. Atmos. Chem. Phys. 5, 3289–3311.

Zhang, S.-H., Shaw, M., Seinfeld, J.H., Flagan, R.C., 1992. Photochemical aerosol formation from α-pinene- and β-pinene. Journal of Geophysical Research: Atmospheres 97, 20717–20729.

5.6 **Tables**

Table 5.1 Summary of low-NO_X experiments.

Compound	Run ID	NO ppb	ΔHC $\mu g.m^{-3}$	Mo $\mu g.m^{-3}$	43/44	Model error %
Benzene	EPA1236A	53.58	406.79	106.44	0.13	4
	EPA1236B	154.7	449.68	34.85	N/A	1
	EPA1237A	41.64	265.78	45.93	N/A	-2
	EPA1237B	21.12	252.78	51.39	N/A	-1
	EPA1618A	35.4	354.16	46.25	N/A	-13
	EPA1223A	59.47	397.7	138.73	0.15	N/A
	EPA1223B	119.26	453.26	104.69	N/A	-18
Toluene	EPA1101A	19.24	206.2	30.13	N/A	5
	EPA1101B	9.38	175.54	25.14	N/A	3
	EPA1102A	43.33	222.68	21.76	N/A	-15
	EPA1102B	32.96	238.39	22.19	N/A	-6
	EPA1106A	20.14	126.1	9.8	0.29	-41
	EPA1106B	10.6	111.15	12.42	N/A	-26
	EPA1107A	40.11	121.5	2.8	0.35	-24
	EPA1107B	30.03	118.05	5.89	N/A	-32
Ethylbenzene	EPA1142A	47.37	331.22	21.99	0.27	-5
	EPA1142B	66.56	341.12	4.35	N/A	-2
	EPA1146A	22.22	256.58	35.99	0.3	10
	EPA1146B	34.78	330.78	23.62	N/A	1
	EPA1147A	66.91	845.71	87.49	N/A	13
	EPA1147B	36.51	625.78	88.13	N/A	15
Propylbenzene	EPA1245A	22.12	230.98	11.84	0.33	1
	EPA1246A	68.46	420.46	22.93	0.27	0
Isopropylbenzene	EPA1247A	22.36	300.97	33.24	0.46	-6
	EPA1247B	48.12	299.98	16.55	N/A	-3
	EPA1253A	56.36	537.95	53.09	0.56	0
	EPA1253B	100.07	526.46	16.52	N/A	22
m-Xylene	EPA1193A	36.78	238.9	13.59	1.15	6
	EPA1193B	36.52	236.25	11.23	N/A	0
	EPA1191A	52.24	298.19	15.23	1.19	7
	EPA1191B	45.71	340.46	14.64	N/A	8
	EPA1516A	26.69	357.25	48.71	N/A	N/A

o-Xylene	EPA1315A	49.8	324.13	26.32	0.96	-9
	EPA1315B	22.24	278.21	25.37	N/A	11
	EPA1321A	20.47	263.19	16.16	N/A	N/A
	EPA1321B	10.44	225.66	9.84	N/A	N/A
p-Xylene	EPA1308A	55.55	278.65	6.8	0.66	-4
	EPA1308B	22.93	273.79	11.28	N/A	N/A
m-Ethyltoluene	EPA1151A	62.48	408.97	8.26	N/A	3
	EPA1151B	32.27	414.96	28.69	N/A	N/A
	EPA1199A	45.43	447.46	72.03	1.08	17
	EPA1199B	91.08	482.46	54.63	N/A	-6
	EPA1222A	107.83	493.46	68.91	0.87	-63
	EPA1222B	69.44	483.96	70.88	N/A	-42
	EPA1226A	251.13	982.42	132.82	1.01	-36
	EPA1226B	137.64	895.43	137.91	N/A	-8
	EPA1232A	121.95	900.92	150.09	1.09	-1
	EPA1232B	67.52	751.44	116.62	N/A	N/A
o- Ethyltoluene	EPA1179A	52.85	399.47	86.49	0.96	13
	EPA1179B	52.92	415.46	75.33	N/A	7
	EPA1202A	60.31	421.96	69.89	1.00	-9
	EPA1202B	107.86	453.46	34.1	N/A	-15
	EPA1215A	107.85	637.45	150.91	1.09	9
	EPA1215B	56.47	581.45	97.71	N/A	7
	EPA1233A	197.48	925.92	157.98	0.75	-5
	EPA1233B	259.1	896.92	120.69	N/A	13
	EPA1413A	21.33	370.97	64.47	0.81	-35
	EPA1413B	45.83	455.46	64.37	N/A	-40
	EPA1421A	22.08	409.46	46.2	N/A	13
	EPA1421B	44.88	477.46	54.6	N/A	-1
p- Ethyltoluene	EPA1194A	90.69	741.44	90.43	0.94	15
	EPA1194B	88.4	760.94	72.99	N/A	N/A
	EPA1197A	56.36	653.44	66.43	1.02	25
	EPA1197B	98.54	710.44	58.35	N/A	19
	EPA1214A	103.9	455.96	19.17	0.61	-51
	EPA1214B	53.41	417.96	29.06	N/A	-34
	EPA1229A	192.1	888.43	87.56	0.76	-35
	EPA1229B	258.21	819.93	37.41	N/A	-47
1,2,3-Trimethylbenzene	EPA1158A	10.27	295.97	22.18	2.2	-1
	EPA1158B	22.37	378.97	32.28	N/A	15

	EPA1162A	33.39	390.97	46.52	2.08	-1
	EPA1162B	N/A	398.46	46.59	N/A	-15
	EPA1330A	150	416.96	14.13	0.58	N/A
	EPA1330B	100	394.97	17.37	N/A	N/A
1,2,4-Trimethylbenzene	EPA1117A	10.31	334.97	16.8	1.24	-22
	EPA1117B	20.71	367.97	18.2	N/A	-15
	EPA1119A	49.78	384.97	19.6	1.25	-11
	EPA1119B	41.57	389.97	25.48	N/A	8
	EPA1123A	10.14	299.98	11.2	1.2	N/A
	EPA1123B	22.09	344.97	15.4	N/A	N/A
	EPA1126A	10.07	286.48	12.6	1.26	-2
	EPA1126B	24.3	332.97	15.4	N/A	-4
	EPA1129A	41.64	200.48	4.2	0.45	-17
	EPA1129B	15.63	200.98	5.6	N/A	7
	EPA1352A	186.06	394.97	5.71	N/A	-50
	EPA1352B	132.44	394.96	8.9	N/A	-47
	EPA1354A	200.17	387.47	5.77	0.43	-51
	EPA1354B	152.7	385.97	9.25	N/A	-55
	EPA1356A	120.61	389.97	14.66	0.86	-44
	EPA1356B	100.2	388.97	11	N/A	-47
1,3,5-Trimethylbenzene	EPA1153A	10.98	309.47	12.36	1.93	1
	EPA1153B	20.38	381.47	19.63	N/A	15
	EPA1156A	32.31	379.47	24.77	2.46	14
	EPA1156B	46.11	390.47	19	N/A	-3
	EPA1329A	86.18	388.97	0.6	0.14	N/A
	EPA1329B	64.78	296.47	3.01	N/A	N/A
1,2,4,5-Tetramethylbenzene	EPA1529A	70	274.69	3.17	2.83	N/A
Pentamethylbenzene	EPA1488A	25.14	834.93	165.07	4.55	N/A
Hexamethylbenzene	EPA1557A	28	999	15.28	1.25	N/A

N/A: not applicable

Table 5.2 Summary of no-NO_X experiments.

Compound	Run ID	H_2O_2 ppm	ΔHC µg.m^{-3}	Mo µg.m^{-3}	43/44
Benzene	EPA1161A	5	330.76	90.82	0.24
	EPA1161B	5	161.16	30.27	N/A
	EPA1149A	5	187.48	35.97	N/A
Toluene	EPA1149B	5	103.67	20.38	N/A
	EPA1477A	1	239.5	62.22	0.88
	EPA1477B	1	415.1	104.4	N/A
Ethylbenzene	EPA1296A	2	220.37	54.31	N/A
	EPA1296B	2	220.81	30.84	N/A
	EPA1294A	1	317.53	34.02	0.25
	EPA1294B	1	142.2	21.73	N/A
Propylbenzene	EPA1256A	1	189.48	42.48	0.46
	EPA1256B	1	325.97	69.94	N/A
	EPA1269A	2	150.99	43.45	0.44
	EPA1269B	2	262.98	72.32	N/A
	EPA1426A	1	330.47	60.95	N/A
	EPA1426B	1	227.98	26.56	N/A
Isopropylbenzene	EPA1265A	1	129.99	24.39	0.56
	EPA1265B	1	255.98	47.14	N/A
	EPA1274A	2	117.99	46.16	0.52
	EPA1274B	2	309.97	62.76	N/A
m-Xylene	EPA1209A	2	671.23	190.33	2.48
	EPA1209B	2	600.57	140.55	N/A
	EPA1212A	1	557.73	137.27	N/A
	EPA1212B	1	208.87	72.27	N/A
	EPA1523A	1	1488.18	279.25	N/A
p-Xylene	EPA1304A	1	328.55	59.62	1.61
	EPA1304B	1	185.78	43.23	N/A
	EPA1301A	1	299.97	29.30	1.51
	EPA1301B	1	124.99	19.73	N/A
o-Xylene	EPA1310A	1	287.04	39.01	N/A
	EPA1310B	1	177.08	30.82	N/A
	EPA1313A	1	264.96	67.98	1.57
	EPA1313B	1	249.26	46.89	N/A
	EPA1389A	1	240.67	25.1	1.07

	EPA1389B	1	137.78	34.87	N/A
m-Ethyltoluene	EPA1205A	1	309.97	128.87	1.39
	EPA1205B	1	337.97	118.23	N/A
	EPA1211A	1	285.48	92.08	1.46
	EPA1211B	1	351.97	78.08	N/A
	EPA1218A	1	330.47	151.62	1.18
	EPA1218B	1	556.45	197.19	N/A
	EPA1416A	1	590.95	203	N/A
	EPA1416B	1	408.97	27.4	N/A
o- Ethyltoluene	EPA1242A	1	552.95	137.02	N/A
	EPA1242B	1	166.49	34.29	N/A
	EPA1326A	1	293.97	69.2	0.78
	EPA1326B	1	387.97	82.91	N/A
	EPA1406A	1	257.48	53.49	0.71
	EPA1406B	1	287.48	59.74	N/A
p- Ethyltoluene	EPA1227A	1	535.45	146.8	1.08
	EPA1227B	1	345.47	67.17	N/A
	EPA1235A	1	346.47	62.22	0.95
	EPA1235B	1	476.46	110.29	N/A
	EPA1239A	1	137.49	86.79	1.01
	EPA1239B	1	241.48	99.65	N/A
	EPA1597A	1	269.98	65.41	N/A
	EPA1597B	1	259.98	55.02	N/A
1,2,3-Trimethylbenzene	EPA1287A	1	343.97	103.88	2.55
	EPA1287B	1	194.48	62.08	N/A
1,2,4-Trimethylbenzene	EPA1135A	2	369.97	88.91	2.21
	EPA1135B	2	384.74	61.82	N/A
	EPA1278A	1	263.98	50.54	1.88
	EPA1278B	1	238.48	35.8	N/A
	EPA1292A	1	277.48	59.88	2.01
	EPA1292B	1	171.48	53.98	N/A
1,3,5-Trimethylbenzene	EPA1154A	1	359.47	77.7	3.64
	EPA1154B	1	191.48	47.38	N/A
	EPA1155A	1	604.95	85.44	3.91
	EPA1155B	1	453.46	88.48	N/A
	EPA1298A	1	311.97	89.7	2.75
	EPA1298B	1	195.48	59.17	N/A

1,2,4,5-Tetramethylbenzene	EPA1494A	1	541.57	126.72	3.23
Pentamethylbenzene	EPA1492A	1	747.98	261.61	4.55
	EPA1564A	1	837.39	115.9	3.82
	EPA1564B	1	748.16	168.81	N/A
Hexamethylbenzene	EPA1558A	1	376	89.86	4.84
	EPA1558B	1	450.9	74.88	N/A

N/A: not applicable

5.7 Figures

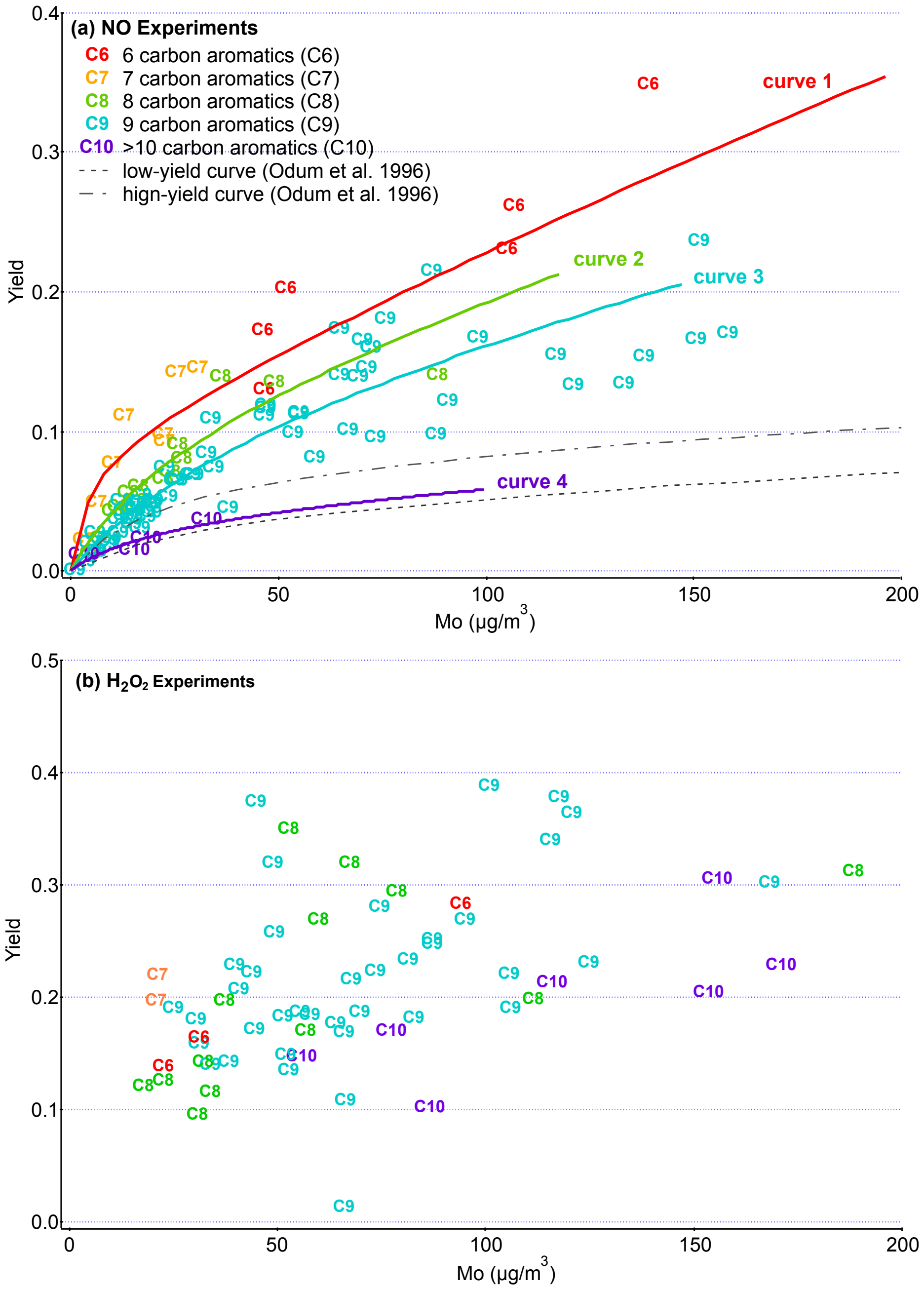

Figure 5.1 Secondary organic aerosol yield as a function of total organic aerosol mass concentration (M_o) for 17 individual aromatic species. Each point represents an individual experiment. (a) aromatic/NO experiments, (b) aromatic/H_2O_2 experiments.

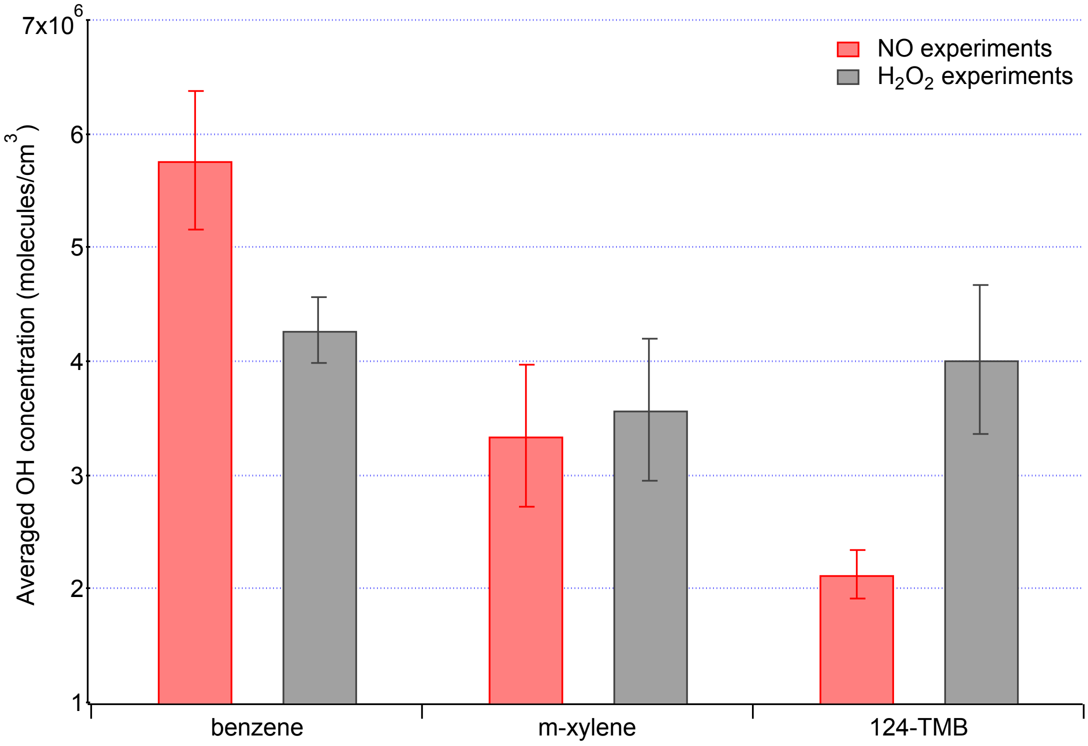

Figure 5.2 Comparison of averaged OH level between aromatic/NO and aromatic/H_2O_2 experiments of benzene, m-xylene and 124-trimethylbenzene photooxidation.

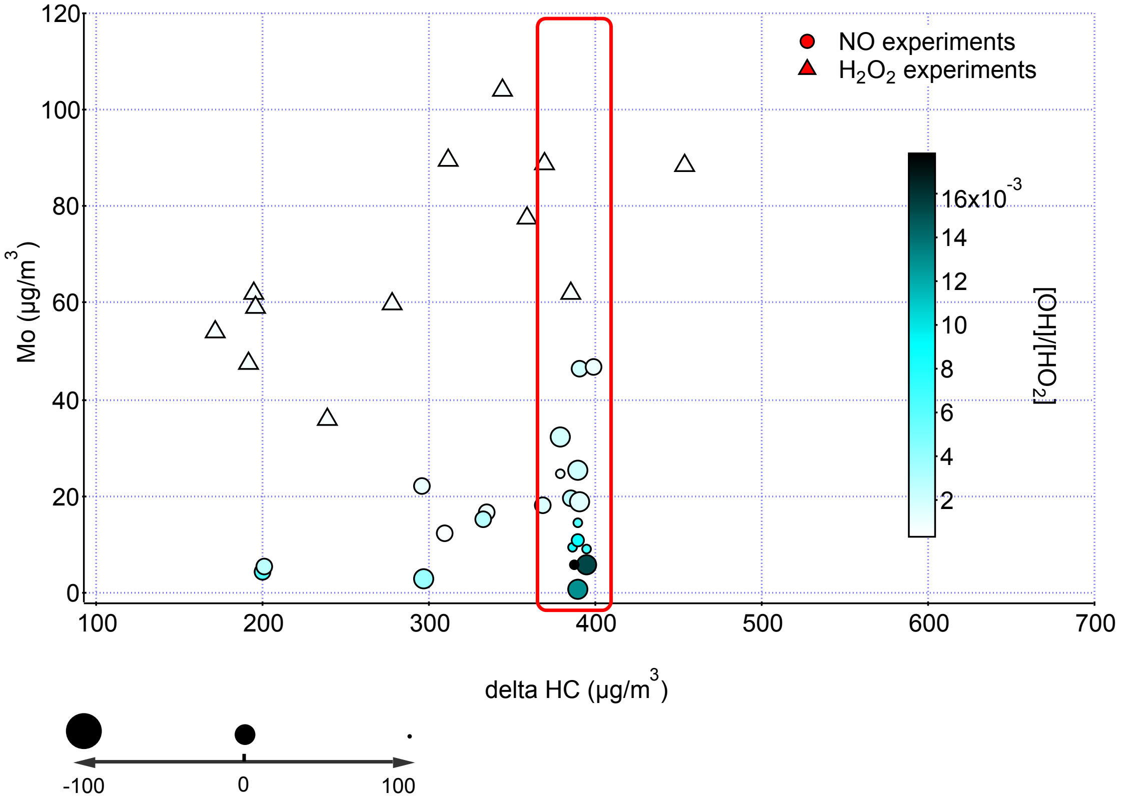

Figure 5.3 Secondary organic aerosol formation from trimethylbenzene isomers. For NO experiments, size of the circle represents model error of SAPRC-11. A middle size circle means a model error of 0; a larger size and smaller size mean an over-prediction and under-prediction of HO_2 concentration, respectively. For H_2O_2 experiments, no indicator is used to evaluate the model performance, the size of all triangles are fixed.

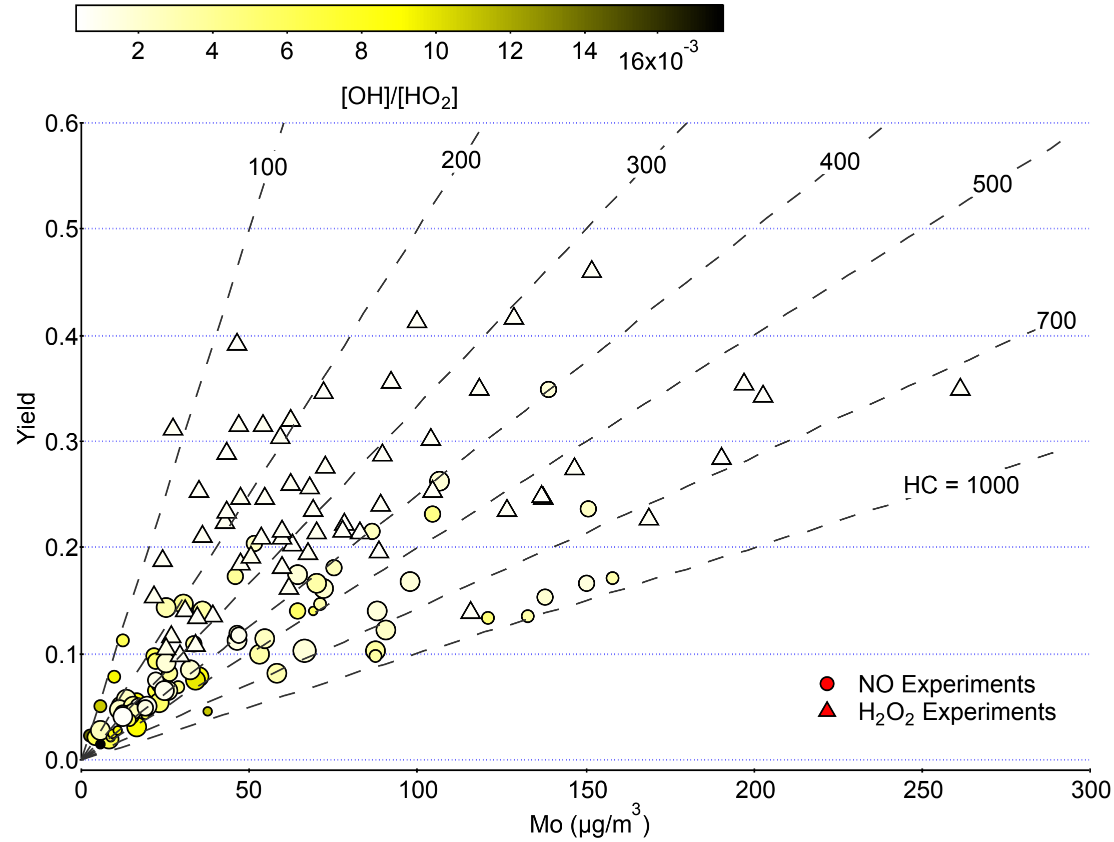

Figure 5.4 Secondary organic aerosol yield as a function of M_o for both aromatic/NO and aromatic/H_2O_2 experiments. Straight dashed lines are used to indicate the expected yield curve for experiments conducted with similar hydrocarbon reacted (the slope of each dashed line shown has a slope of $1/\Delta HC$).

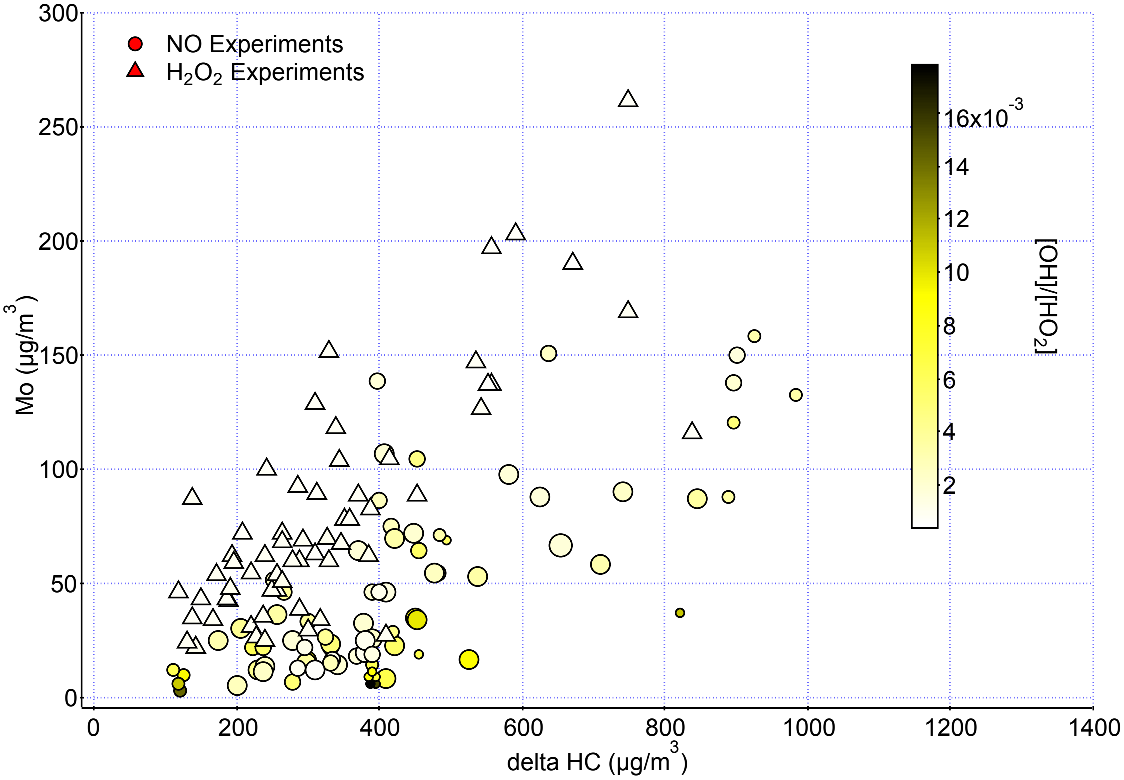

Figure 5.5 Secondary organic aerosol mass M_o as a function of hydrocarbon reacted for low-NO_X and no-NO_X experiments.

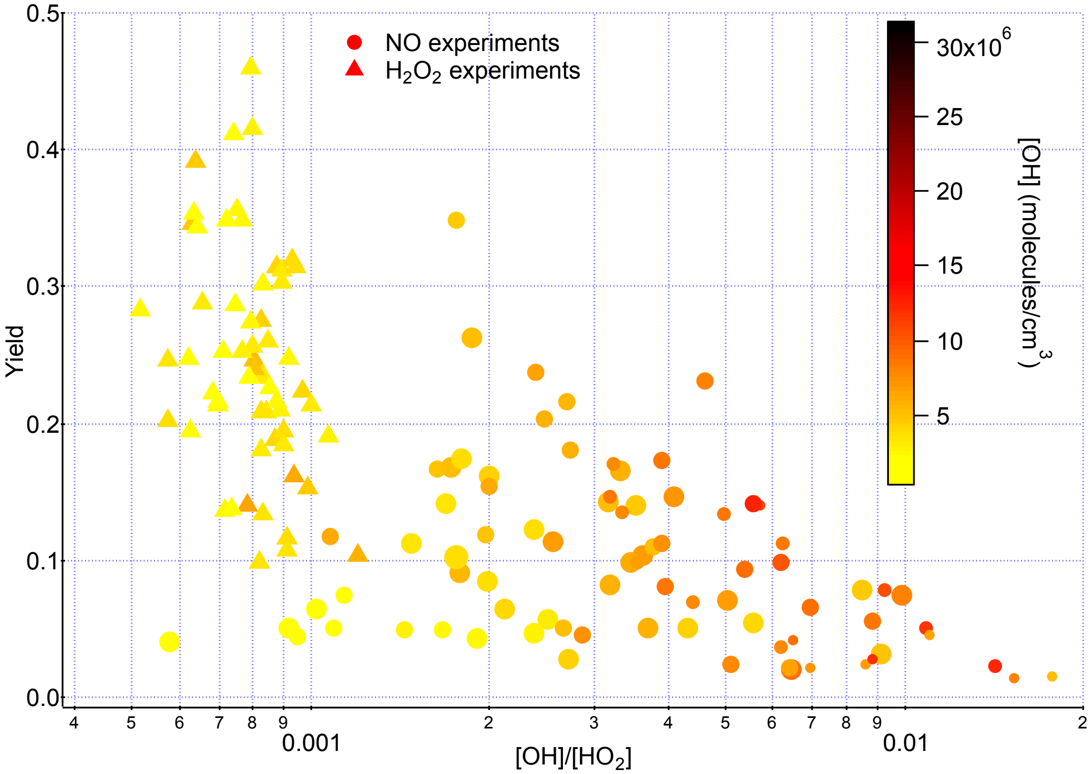

Figure 5.6 Secondary organic aerosol yield as a function of $[OH]/[HO_2]$ ratio for both aromatic/NO and aromatic/H_2O_2 experiments. Data points are colored with OH concentration in each experiment.

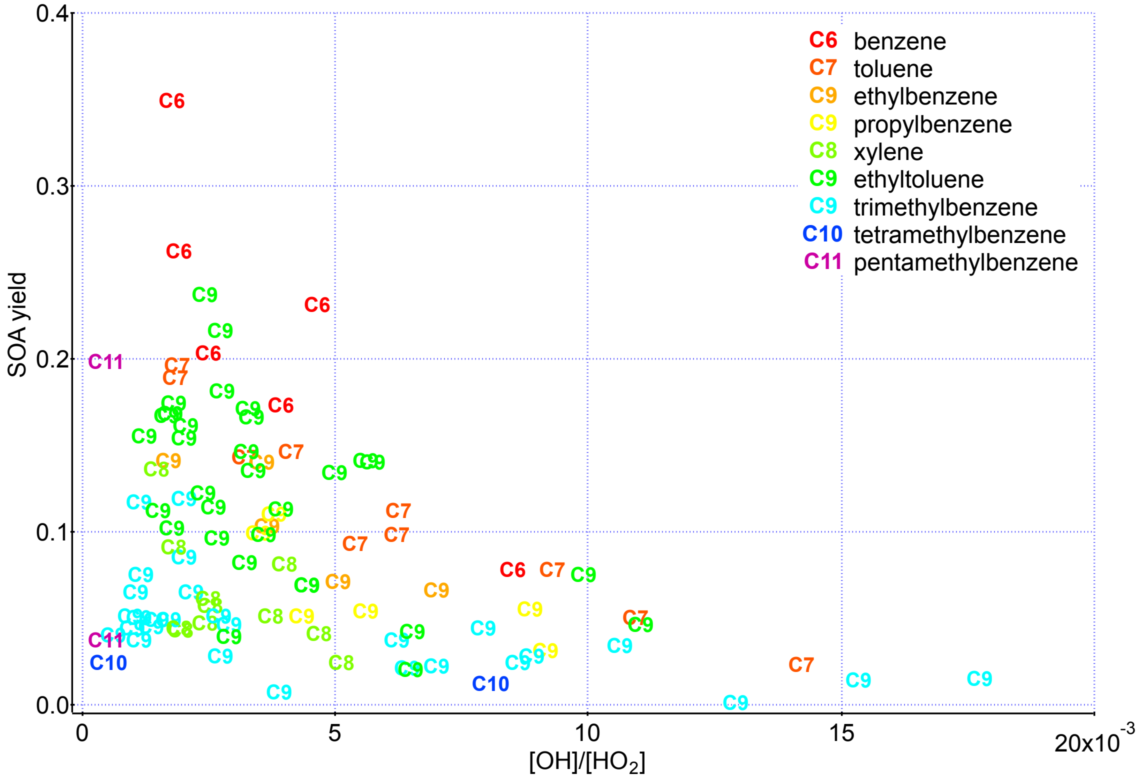

Figure 5.7 Secondary organic aerosol yield as a function of $[OH]/[HO_2]$ ratio for aromatic/NO experiments. Data points are grouped according to the carbon number of aromatic precursors.

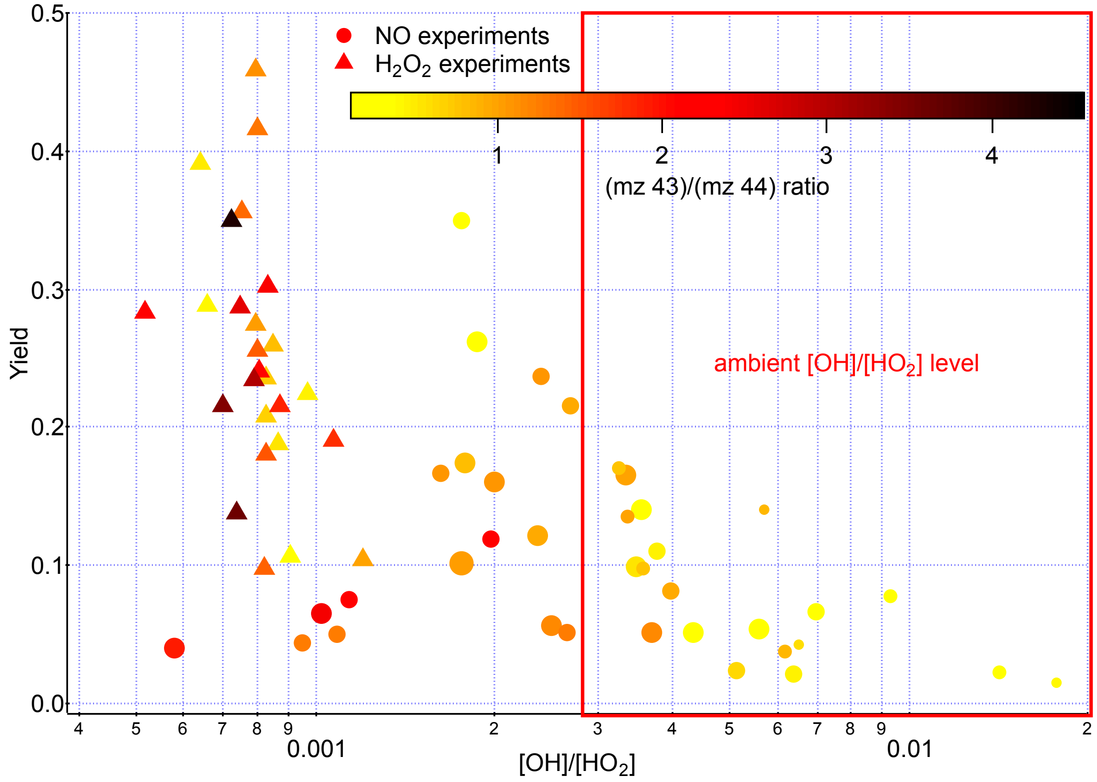

Figure 5.8 Secondary organic aerosol yield as a function of [OH]/[HO_2] ratio for aromatic/NO and aromatic/H_2O_2 experiments. Data points are colored by mz 43/ mz 44 ratio measured by HR-ToF-AMS. Rectangular area represent ambient level of [OH]/[HO_2].

6 Summary of Dissertation

The overall objective of this study was to advance our understanding of SOA formation from aromatic hydrocarbons while improving our ability to accurately predict SOA formation from aromatic precursors. This work utilized careful experimental chamber photooxidation simulations under a variety of conditions (e.g., hydrocarbon to NO_X ratio, OH and HO_2 radical levels) for 17 aromatic hydrocarbons including: benzene, toluene, ethylbenzene, propylbenzenes, xylenes, ethyltoluenes, trimethylbenzenes, tetramethylbenzene, pentamethylbenzene and hexamenthylbenzene. A series of online techniques were employed allowing for the comparison of SOA formation potential as well as comparison of the chemical and physical properties of SOA formed from different aromatic precursors. The gas-phase reaction model SAPRC 11 was further utilized to help predict radical levels present during these experiments.

Chapter 2 investigated the aerosol formation potential of different aromatic hydrocarbons under low-NO_X conditions; SOA yields in our study were also compared with aerosol formation from aromatics of previous studies. It is observed that aerosol formed from aromatic hydrocarbon with more carbon atoms had lower yields, generally consistent with Odum's definition of high-yield and low-yield aromatics (Odum, 1996). Four yield curves (one for C6 and C7 aromatics, one for C8 aromatics, one for C9 aromatics, and one for C10 aromatics) were provided as best estimates of SOA formation under low-NO_X conditions for aromatic species. A possible explanation for this trend is that lighter compounds such as benzene and toluene are more likely to form low vapor pressure ring-retaining products. It is also found that para-substituent aromatics have lower SOA yield than their isomers. Many studies reported similar trends and pointed out that more unsaturated diketones and less aldehydes were produced. Experimental differences between this study and earlier studies are used to explain differences in observed yields for these aromatic precursors.

Chapter 3 compared the chemical composition of secondary aerosol formed from aromatic hydrocarbons investigated in Chapter 2 under both low-NO_X and no-NO_X conditions. Triangle plots (f44 vs. f43) and Van Krevelen (O/C vs. H/C) diagrams were used as aids to evaluate similarities and differences in chemical properties. With respect to the triangle plot for ambient OOA, SOA formed in this study were located in the lower right area outside the triangle indicating that less oxidized aerosol are formed from aromatic precursors in the environmental chamber than is observed for bulk ambient OOA. Decreased in f44 and increases of f43 were observed as the number of alkyl substituents on the aromatic ring increased; the trend is attributed to because the formation of more low-reactive ketones and less reactive aldehydes with the presence of more substituents. This trend was also observed on Van Krevelen diagram with a higher O/C ratio and lower H/C ratio observed for the lighter aromatics. Additionally, SOA volatility was correlated with chemical composition with lower aerosol volatility observed for SOA generated from photooxidation of lighter aromatics.

Chapter 4 is an extension of Chapter 3 and evaluates a recently proposed semi-empirical relationship between SOA elemental ratios (O/C and H/C) and aerosol density. An extensive dataset of density and elemental ratios of SOA formed by the oxidation of 23 different reactants including terpenes, aromatic hydrocarbons, and phenolic compounds within an environmental chamber was investigated. Experimental results suggest that SOA density was found to be nearly independent of oxidants used in chamber experiments. The semi-empirical relationship successfully predicted density of SOA within 20% error for more than 90% of experiments; therefore, the range of the application has been extended to include SOA from anthropogenic systems. The density estimation method has a potential to be applied to a number of predictive models. This study provided a fundamental dataset to support the applicability of the method to SOA formation from aromatic hydrocarbons. Future studies need to address the uncertainty due to the presence of nitrogen and sulfur in SOA.

Chapter 5 further explored the radical (OH and HO_2) levels generated from different aromatic oxidation systems using SAPRC-11. [OH]/HO_2] ratio is used to explain aerosol formation trends from aromatic photooxidation experiments. Generally, more aerosol were formed under no-NO_X conditions, corresponding to a much lower [OH]/[HO_2] generated for the no-NO_X conditions. Furthermore, SOA yield was observed with the increasing of [OH]/[HO_2] ratio for all aromatic experiments. It was hypothesized that the SOA formation trends can be explained by decomposition of intermediate products to form organics with higher volatility in the more OH radical abundant environment. A decreasing SOA yield trend with OH concentration for fixed [OH]/[HO_2] ratios is also observed. It is hypothesized that the heavier aromatic systems have insufficient OH to further oxidize later generation products thus limiting overall SOA formation. The 43/44 ratio increased with decreasing [OH]/[HO_2] value suggesting that more HO_2 radicals are available for the oxidation of organic products.

In the future, the impact of temperature, humidity and light intensity on SOA formation from aromatic hydrocarbons can be investigated to further our understanding of aerosol formation similar to ambient conditions. Controlled experiments are needed to simulate ambient [OH]/[HO_2] levels. To achieve this goal, NO_2 or CO could be added to aromatic photooxidation systems to lower OH and raise HO_2 concentrations in the system. Moreover, a direct measurement of OH and HO_2 radicals in aromatic photooxidation system is necessary to evaluate SAPRC prediction. A more complete understanding of the radicals' level in aromatic system under various conditions is important to improve future predictions of SOA formation and improve extrapolations of chamber data to the ambient environment.